TESIS TESIS TESIS TESIS TESIS

UNIVERSIDAD AUTÓNOMA DE AGUASCALIENTES
CENTRO DE CIENCIAS BÁSICAS
DEPARTAMENTO DE MATEMÁTICAS Y FÍSICA

A dissipative space-fractional 2D sine-Gordon equation and its efficient numerical solution

TESIS QUE PRESENTA:

Dagoberto Raziel Mares Rincón

para optar por el grado de:

Maestro en Ciencias con orientación en Matemáticas Aplicadas

TUTORES:
Dr. José Antonio Guerrero Díaz de León
Dr. Jorge Sigfrido Macías Medina

INTEGRANTES DEL COMITÉ TUTORAL:
Dr. Jorge Eduardo Macías Díaz

Aguascalientes, Ags., junio de 2026

TESIS TESIS TESIS TESIS TESIS

TESIS TESIS TESIS TESIS TESIS

UNIVERSIDAD AUTÓNOMA DE AGUASCALIENTES

Centro de Ciencias Básicas

Departamento de Matemáticas y Física

Este apartado contiene las copias oficiales de los documentos de autorización debidamente firmados que validan la culminación del trabajo recepcional:

1. **Carta de voto aprobatorio del Comité Tutoral**
2. **Dictamen de Liberación Académica**

TESIS TESIS TESIS TESIS TESIS

TESIS TESIS TESIS TESIS TESIS

MTRO. GUILLERMO DOMÍNGUEZ AGUILAR
DECANO (A) DEL CENTRO DE CIENCIAS BÁSICAS

PRESENTE

Por medio del presente como ***DIRECTOR*** designado del estudiante ***DAGOBERTO RAZIEL MARES RINCÓN*** con ID *235284* quien realizó *la tesis* titulado/a: ***A DISSIPATIVE SPACE-FRACTIONAL 2D SINE-GORDON EQUATION AND ITS EFFICIENT NUMERICAL SOLUTION***, un trabajo propio, innovador, relevante e inédito y con fundamento en la fracción IX del Artículo 43 del Reglamento General de Posgrados, doy mi consentimiento de que la versión final del documento ha sido revisada y las correcciones se han incorporado apropiadamente, por lo que me permito emitir el **VOTO APROBATORIO**, para que *él* pueda continuar con el procedimiento administrativo para la obtención del grado.

Pongo lo anterior a su digna consideración y sin otro particular por el momento, me permito enviarle un cordial saludo.

ATENTAMENTE
"Se Lumen Proferre"
Aguascalientes, Ags., a 22 de junio de 2026.

Dr. José Antonio Guerrero Díaz de León
Director

c.c.p.- Interesado
c.c.p.- Coordinación del Programa de Posgrado

TESIS TESIS TESIS TESIS TESIS

TESIS TESIS TESIS TESIS TESIS

MTRO. GUILLERMO DOMÍNGUEZ AGUILAR
DECANO (A) DEL CENTRO DE CIENCIAS BÁSICAS

P R E S E N T E

Por medio del presente como ***CODIRECTOR*** designado del estudiante ***DAGOBERTO RAZIEL MARES RINCÓN*** con ID *235284* quien realizó *la tesis* titulado/a: ***A DISSIPATIVE SPACE-FRACTIONAL 2D SINE-GORDON EQUATION AND ITS EFFICIENT NUMERICAL SOLUTION***, un trabajo propio, innovador, relevante e inédito y con fundamento en la fracción IX del Artículo 43 del Reglamento General de Posgrados, doy mi consentimiento de que la versión final del documento ha sido revisada y las correcciones se han incorporado apropiadamente, por lo que me permito emitir el **VOTO APROBATORIO**, para que *él* pueda continuar con el procedimiento administrativo para la obtención del grado.

Pongo lo anterior a su digna consideración y sin otro particular por el momento, me permito enviarle un cordial saludo.

A T E N T A M E N T E
"Se Lumen Proferre"
Aguascalientes, Ags., a *22* de junio de 2026.

Sigfrido Macias
Dr. Jorge Sigfrido Macías Medina
Co director

c.c.p.- Interesado
c.c.p.- Coordinación del Programa de Posgrado

TESIS TESIS TESIS TESIS TESIS

TESIS TESIS TESIS TESIS TESIS

MTRO. GUILLERMO DOMÍNGUEZ AGUILAR
DECANO (A) DEL CENTRO DE CIENCIAS BÁSICAS

PRESENTE

Por medio del presente como ***ASESOR*** designado del estudiante ***DAGOBERTO RAZIEL MARES RINCÓN*** con ID *235284* quien realizó *la tesis* titulado/a: ***A DISSIPATIVE SPACE-FRACTIONAL 2D SINE-GORDON EQUATION AND ITS EFFICIENT NUMERICAL SOLUTION***, un trabajo propio, innovador, relevante e inédito y con fundamento en la fracción IX del Artículo 43 del Reglamento General de Posgrados, doy mi consentimiento de que la versión final del documento ha sido revisada y las correcciones se han incorporado apropiadamente, por lo que me permito emitir el **VOTO APROBATORIO**, para que *él* pueda continuar con el procedimiento administrativo para la obtención del grado.

Pongo lo anterior a su digna consideración y sin otro particular por el momento, me permito enviarle un cordial saludo.

ATENTAMENTE
"Se Lumen Proferre"
Aguascalientes, Ags., a *22* de junio de 2026.

Dr. Jorge Eduardo Macías Díaz
Asesor de *tesis*

c.c.p.- Interesado
c.c.p.- Coordinación del Programa de Posgrado

TESIS TESIS TESIS TESIS TESIS

TESIS TESIS TESIS TESIS TESIS

UNIVERSIDAD AUTÓNOMA DE AGUASCALIENTES

DICTAMEN DE LIBERACIÓN ACADÉMICA PARA INICIAR LOS TRÁMITES DEL EXAMEN DE GRADO

POSGRADOS UAA

Fecha de dictaminación (dd/mm/aaaa): 22/06/2026

NOMBRE: DAGOBERTO RAZIEL MARES RINCÓN **ID** 235284

PROGRAMA: MAESTRÍA EN CIENCAS CON OPCIONES EN COMPUTACIÓN, MATEMÁTICAS APLICADAS **LGAC (del posgrado):** Matemáticas Aplicadas

MODALIDAD DEL PROYECTO DE GRADO: Tesis Tradicional ( ) *Tesis por artículos científicos (X) **Tesis por Patente ( ) Trabajo Práctico ( )

TITULO: A dissipative space-fractional 2D sine-Gordon equation and its efficient numerical solution

IMPACTO SOCIAL (señalar el impacto logrado): El trabajo desarrolla métodos matemáticos precisos y códigos abiertos para simular fenómenos físicos complejos. Al garantizar un cálculo fiel de la energía cinética K y potencial U, entrega a la comunidad científica herramientas confiables para impulsar nuevas tecnologías en superconductores y metamateriales.

INDICAR SEGÚN CORRESPONDA: SI, NO, NA (No Aplica)

	Elementos para la revisión académica del trabajo de tesis o trabajo práctico:
SI	El trabajo es congruente con las LGAC del programa de posgrado
SI	La problemática fue abordada desde un enfoque multidisciplinario
SI	Existe coherencia, continuidad y orden lógico del tema central con cada apartado
SI	Los resultados del trabajo dan respuesta a las preguntas de investigación o a la problemática que aborda
SI	Los resultados presentados en el trabajo son de gran relevancia científica, tecnologíca o profesional según el área
SI	El trabajo demuestra más de una aportación original al conocimiento de su área
SI	Las aportaciones responden a los problemas prioritarios del país
NA	Generó transferencia del conocimiento o tecnológica
SI	Cumple con la ética para la investigación (reporte de la herramienta antiplagio)
	El egresado cumple con lo siguiente:
SI	Cumple con lo señalado por el Reglamento General de Posgrados
SI	Cumple con los requisitos señalados en el plan de estudios (créditos curriculares, optativos, actividades complementarias, estancia, predoctoral, etc.)
SI	Cuenta con los votos aprobatorios del comité tutorial
NA	Cuenta con la carta de satisfacción del Usuario (En caso de que corresponda)
SI	Coincide con el título y objetivo registrado
SI	Tiene congruencia con cuerpos académicos
SI	Tiene el CVU de la SECIHTI actualizado
SI	Tiene el o los artículos aceptados o publicados y cumple con los requisitos institucionales (en caso de que proceda)
	****En caso de Tesis por artículos científicos publicados** (completar solo si la tesis fue por artículos)*
SI	Aceptación o Publicación de los artículos en revistas indexadas de alto impacto según el nivel del programa
SI	El (la) estudiante es el primer autor(a)
SI	El (la) autor(a) de correspondencia es el Director (a) del Núcleo Académico
SI	En los artículos se ven reflejados los objetivos de la tesis, ya que son producto de este trabajo de investigación.
SI	Los artículos integran los capítulos de la tesis y se presentan en el idioma en que fueron publicados
	*****En caso de Tesis por Patente***
NA	Cuenta con la evidencia de solicitud de patente en el Departamento de Investigación (anexarla al presente formato)

Con base en estos criterios, se autoriza continuar con los trámites de titulación y programación del examen de grado: Sí X No ____

FIRMAS

Elaboró:

*NOMBRE Y FIRMA DEL(LA) CONSEJERO(A) SEGÚN LA LGAC DE ADSCRIPCION: Dra. Mariana Alfaro Gomez

** En caso de conflicto de intereses, firmará un revisor miembro del NA de la LGAC correspondiente distinto al director o miembro del comité tutorial, asignado por el Decano.*

NOMBRE Y FIRMA DEL COORDINADOR DE POSGRADO: Dra. Mariana Alfaro Gomez

Revisó:

NOMBRE Y FIRMA DEL SECRETARIO DE INVESTIGACIÓN Y POSGRADO: Dr. Iliana Ernestina Medina Ramírez

Autorizó:

NOMBRE Y FIRMA DEL DECANO: Mtro. Guillermo Domínguez Aguilar

Nota: procede el trámite para el Depto. de Apoyo al Posgrado

En cumplimiento con el Art. 24 fracción V del Reglamento General de Posgrado, que a la letra señala entre las funciones del Consejo Académico: Proponer criterios y mecanismos de selección, permanencia, egreso y titulación de estudiantes para asegurar la eficiencia terminal y la titulación y el Art. 28 fracción IX, atender, asesorar y dar el seguimiento del estudiantado desde su ingreso hasta su titulación.

TESIS TESIS TESIS TESIS TESIS

TESIS TESIS TESIS TESIS TESIS

Evidencias de publicación

fractal and fractional

an Open Access Journal by MDPI

IMPACT FACTOR 3.3

CITESCORE 6.0

CERTIFICATE OF PUBLICATION

The certificate of publication for the article titled:

A Discrete Model to Solve a Bifractional Dissipative Sine-Gordon Equation: Theoretical Analysis and Simulations

Authored by:

Dagoberto Mares-Rincón; Siegfried Macías; Jorge E. Macías-Díaz; José A. Guerrero-Díaz-de-León; Tassos Bountis

Published in:

Fractal Fract. **2025**, Volume 9, Issue 8, 498

MDPI

Basel, March 2026

Prof. Dr. Carlo Cattani
Editor-in-Chief

DOI: `https://doi.org/10.3390/fractalfract9080498`

Evidencia de publicación del artículo en *Fractal and Fractional* (MDPI).

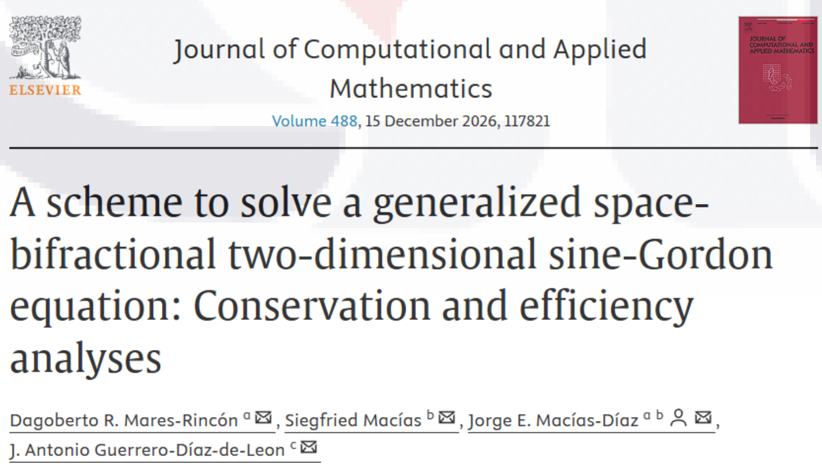

ELSEVIER

Journal of Computational and Applied Mathematics

Volume 488, 15 December 2026, 117821

A scheme to solve a generalized space-bifractional two-dimensional sine-Gordon equation: Conservation and efficiency analyses

Dagoberto R. Mares-Rincón [a], Siegfried Macías [b], Jorge E. Macías-Díaz [a b], J. Antonio Guerrero-Díaz-de-Leon [c]

DOI: `https://doi.org/10.1016/j.cam.2026.117821`

Evidencia de publicación del artículo en *Journal of Computational and Applied Mathematics* (JCAM).

TESIS TESIS TESIS TESIS TESIS

TESIS TESIS TESIS TESIS TESIS

Contents

TESIS TESIS TESIS TESIS TESIS

TESIS TESIS TESIS TESIS TESIS

TESIS TESIS TESIS TESIS TESIS

TESIS TESIS TESIS TESIS TESIS

List of Tables

TESIS TESIS TESIS TESIS TESIS

TESIS TESIS TESIS TESIS TESIS

List of Figures

TESIS TESIS TESIS TESIS TESIS

TESIS TESIS TESIS TESIS TESIS

TESIS TESIS TESIS TESIS TESIS

TESIS TESIS TESIS TESIS TESIS

Resumen

Esta tesis desarrolla, analiza y valida esquemas numéricos de diferencias finitas que preservan la estructura energética para la ecuación de sine-Gordon bifraccionaria en dos dimensiones espaciales, con derivadas de Riesz de órdenes $\alpha, \beta \in (1, 2]$ y coeficientes de dispersión posiblemente anisotrópicos. El modelo continuo incluye amortiguamiento, forzamiento externo y potenciales generalizados; se demuestra que la energía total se conserva en ausencia de disipación y decae monótonamente cuando $\eta > 0$.

La contribución central es doble. Por un lado, se propone un esquema de tres niveles centrados directamente sobre la ecuación de segundo orden, que discretiza los operadores de Riesz mediante diferencias centradas fraccionarias de Ortigueira y linealiza el término no lineal mediante un derivado discreto consistente que cierra el balance de energía sin resto. La solvabilidad de cada paso se garantiza por un argumento de punto fijo bajo una condición explícita sobre el paso temporal. Por otro lado, se presenta un esquema Crank-Nicolson sobre un sistema de primer orden, que también satisface una identidad energética discreta. Ambos esquemas son consistentes de segundo orden en espacio y tiempo, y mediante métodos de energía y la desigualdad discreta de Gronwall se prueba su estabilidad condicional y convergencia con orden $\mathcal{O}(\tau^2 + h^2)$ bajo hipótesis de regularidad realistas.

Los experimentos numéricos confirman las tasas de convergencia, conservación/disipación de la energía y el efecto de los órdenes fraccionarios sobre la amplitud y la fase de solitones anulares. El análisis cruzado de los dos enfoques revela que el carácter conservativo o disipativo depende exclusivamente del coeficiente de amortiguamiento η, no de α ni β. Se discuten las limitaciones (complejidad computacional, condiciones de contorno homogéneas, regularidad requerida) y se señalan direcciones futuras (solvers rápidos, mallado graduado, extensión a condiciones no homogéneas y a ecuaciones relacionadas). Los códigos MATLAB completos se incluyen en apéndices.

TESIS TESIS TESIS TESIS TESIS

TESIS TESIS TESIS TESIS TESIS

Abstract

This thesis develops, analyzes, and validates energy-preserving finite-difference schemes for the two-dimensional bifractional sine-Gordon equation with Riesz space derivatives of orders $\alpha, \beta \in (1, 2]$ and possibly anisotropic dispersion coefficients. The continuous model includes damping, external forcing, and generalized potentials; the total energy is shown to be conserved in the absence of dissipation and to decay monotonically when $\eta > 0$.

The main contribution is twofold. On one hand, a three-level centered scheme directly on the second-order equation discretizes the Riesz operators via Ortigueira's fractional centered differences and linearizes the nonlinear term with a consistent discrete derivative that closes the energy balance without remainder. Solvability at each time step is guaranteed by a fixed-point argument under an explicit time-step restriction. On the other hand, a Crank–Nicolson scheme on a first-order system is proposed, which also satisfies a discrete energy identity. Both schemes are second-order consistent in space and time; using energy methods and a discrete Gronwall inequality, conditional stability and convergence of order $\mathcal{O}(\tau^2 + h^2)$ are proved under realistic regularity assumptions.

Numerical experiments confirm the convergence rates, the energy conservation/dissipation properties, and the influence of the fractional orders on the amplitude and phase of ring solitons. A cross-analysis of the two approaches reveals that the conservative or dissipative character depends exclusively on the damping coefficient η, not on α nor β. Limitations (computational complexity, homogeneous Dirichlet conditions, required regularity) are discussed, and future directions (fast solvers, graded meshes, extension to non-homogeneous boundary conditions and related equations) are outlined. Complete MATLAB codes are provided in the appendices.

TESIS TESIS TESIS TESIS TESIS

TESIS TESIS TESIS TESIS TESIS

The mathematical modeling of wave phenomena in complex media has evolved substantially over the past century, driven by both theoretical curiosity and practical necessity. From the initial formulation of the classical wave equation to the introduction of nonlinear terms in the Klein-Gordon family, and ultimately to fractional generalizations incorporating spatial non-locality, each advance has broadened our capacity to describe increasingly sophisticated physical systems. Among the most emblematic equations in this progression stands the sine-Gordon equation, a nonlinear integrable system originally derived from differential geometry principles [1] whose soliton solutions exhibit remarkable stability properties. These localized wave packets, termed topological solitons or kinks, propagate without dissipation and undergo purely elastic collisions in the classical setting a consequence of the equation's complete integrability and infinite hierarchy of conservation laws [2, 3].

The sine-Gordon equation is more than a mathematical curiosity. It predicts the motion of quantized magnetic flux—fluxons—in long Josephson junctions, a central topic in superconducting electronics and quantum information processing [4]. In nonlinear optics, the equation describes the propagation of certain optical pulse structures in photonic media [5], and recent experiments have even realized sine-Gordon-like dynamics in active mechanical metamaterials that support non-reciprocal solitons [6]. All of these applications share a common assumption: the spatial coupling is strictly local. The Laplacian operator $\Delta = \frac{\partial^2}{\partial x^2} + \frac{\partial^2}{\partial y^2}$ links each point only to its immediate neighbors. This assumption breaks down as soon as the medium exhibits anomalous dispersion, long-range interactions, or heterogeneity that spans multiple scales.

Fractional calculus extends classical derivatives to non-integer orders, providing a rigorous language for spatial non-locality and temporal memory [7, 8]. While ordinary derivatives are local, fractional derivatives integrate over the entire history or domain, encoding long-range interactions directly into the operator [9]. For systems that remain isotropic, the Riesz fractional derivative is the most natural choice. Its Fourier symbol is $-|\xi|^\alpha$, a direct extension of the Laplacian's $-|\xi|^2$, and it remains self-adjoint under suitable boundary conditions [10, 11]. Replacing the Laplacian in the sine-Gordon equation with Riesz derivatives produces the space-fractional sine-Gordon equation.

TESIS TESIS TESIS TESIS TESIS

TESIS TESIS TESIS TESIS TESIS

This single modification brings within reach a wide range of phenomena: anomalous wave propagation in heterogeneous superconductors, non-local effects in crystal dislocations, and dispersion engineering in optical waveguides with extended nonlinear response.

The model becomes even richer when the fractional orders in each direction are allowed to differ. In this bifractional regime, the Riesz derivative has order α and β along the x and y, so the equation can capture directionally anisotropic media. This is physically relevant for layered superconductors with orientation-dependent pinning, optical waveguides with asymmetric index profiles, and materials whose microstructure breaks isotropy. The gains in modeling power, however, come with serious computational challenges. The classical Laplacian uses three-point stencils and couples each grid point only to its neighbors; the Riesz derivative is fundamentally non-local. Every point feels every other point through a power-law kernel, which produces dense linear system with a computational cost that grows rapidly with grid size [12]. Moreover, the nonlinear term $\sin u$ introduces oscillatory behavior that demands robust time-stepping strategies to prevent spurious growth or numerical instability.

A critical design principle for numerical schemes addressing wave equations is the preservation of structural invariants—most notably, energy. The undamped sine-Gordon equation conserves a continuous energy functional composed of kinetic, gradient, and potential contributions. When damping or dissipation is present (parametrized by $\eta > 0$), the energy monotonically decreases along the system trajectory. Numerical methods that fail to respect these energy properties may exhibit artificial energy drift, leading to unphysical solutions, instability, or failure to capture the correct long-time asymptotic behavior. Structure-preserving schemes—those that exactly conserve or appropriately dissipate a discrete energy functional analogous to the continuous one—offer superior performance in long-duration simulations and provide rigorous guarantees on solution boundedness and stability [13]. Such schemes bridge the gap between theoretical analysis and practical simulation, ensuring that computational models faithfully reproduce the underlying physics encoded in the continuous equations.

Numerical methods for the classical two-dimensional sine-Gordon equation are well developed, and energy-preserving schemes have recently appeared for one-dimensional fractional variants [14, 15]. Still, the bifractional 2D problem—with possibly different orders $\alpha \neq \beta$—has no fully discrete scheme that is simultaneously structure-preserving, provably convergent, and backed by a complete stability analysis. High-order proposals exist, but their analysis usually stops at numerical experiments. Filling this gap requires

TESIS TESIS TESIS TESIS TESIS

TESIS TESIS TESIS TESIS TESIS

three ingredients: (1) a spatial discretization of the Riesz operators that retains their self-adjointness, (2) a time integrator that respects the discrete energy balance, and (3) rigorous proofs of consistency, stability, and convergence under realistic regularity hypotheses.

This thesis addresses this gap by developing, analyzing, and validating structure-preserving finite-difference schemes for the two-dimensional bifractional sine-Gordon equation with Riesz spatial derivatives. The work synthesizes theoretical foundations from fractional calculus, numerical analysis of partial differential equations, and energy methods, culminating in schemes that provably conserve or dissipate energy at the discrete level while achieving second-order convergence to the continuous solution. The contributions of this research advance both the theoretical understanding of fractional wave equations and the practical computational treatment of anomalous wave phenomena in directionally heterogeneous media.

1.1 Problem Statement

This thesis studies the two-dimensional bifractional sine-Gordon equation for a scalar field $u(x,y,t)$ on a bounded square $\Omega = (a,b)^2$ over a finite time interval $(0,T)$:

$$\frac{\partial^2 u}{\partial t^2} + \eta \frac{\partial u}{\partial t} - \lambda_1 \frac{\partial^\alpha u}{\partial |x|^\alpha} - \lambda_2 \frac{\partial^\beta u}{\partial |y|^\beta} = -\varphi(x,y)\sin u + F(x,y,t) - G'(u), \qquad (1.1.1)$$

subject to homogeneous Dirichlet boundary conditions:

$$u(x,y,t) = 0 \quad \text{for } (x,y) \in \partial\Omega \text{ and } t \in (0,T], \qquad (1.1.2)$$

and initial data:

$$u(x,y,0) = u_0(x,y), \quad \frac{\partial u}{\partial t}(x,y,0) = v_0(x,y) \quad \text{for } (x,y) \in \Omega. \qquad (1.1.3)$$

Here $\alpha, \beta \in (1,2]$ are the Riesz fractional orders along x and y; $\lambda_1, \lambda_2 \geq 0$ set the strength of fractional dispersion in each direction; $\eta \geq 0$ is a damping coefficient; $\phi(x,y) \geq 0$ is a spatially varying potential; $F(x,y,t)$ is a continuous forcing; and $G : \mathbb{R} \to \mathbb{R}$ is a continuously differentiable nonlinear potential satisfying $G' \geq 0$.

The Riesz derivative of order α with respect to x is the symmetric combination of left-

TESIS TESIS TESIS TESIS TESIS

TESIS TESIS TESIS TESIS TESIS

and right-sided Riemann-Liouville derivatives [7]:

$$\frac{\partial^\alpha u}{\partial|x|^\alpha} = -\frac{1}{2\cos(\pi\alpha/2)}\left({}_{-\infty}D_x^\alpha u + {}_xD_\infty^\alpha u\right), \tag{1.1.4}$$

and analogously for y. Its Fourier symbol is $-|\xi|^\alpha$, which directly generalizes the Laplacian's $-|\xi|^2$. Hence the Riesz operator is the fractional counterpart of the second derivative. When $\alpha = \beta = 2$, equation (1.1.1) reduces to the classical generalized sine-Gordon equation; when $\alpha \neq \beta$, it captures directional anisotropy in non-local interactions.

The boundary conditions $u = 0$ on $\partial\Omega$ are physically natural for systems with rigid edges—a clamped crystal sample or a fixed junction boundary. For the Riesz operator, homogeneous Dirichlet data must be supplemented with zero extension outside Ω so that the non-local integrals are well defined and the solution remains sufficiently regular [11].Under these conditions, the Riesz operator satisfies a fractional integration-by-parts identity that underpins all the energy estimates that follow.

The energy functional associated with equation (1.1.1) plays a central role in both the continuous and discrete theories. For the undamped case ($\eta = 0$, $G' = 0$, $F = 0$), the total energy is defined as:

$$E(t) = \frac{1}{2}\int_\Omega \left[\left(\frac{\partial u}{\partial t}\right)^2 + \lambda_1\left(\frac{\partial^{\alpha/2} u}{\partial|x|^{\alpha/2}}\right)^2 + \lambda_2\left(\frac{\partial^{\beta/2} u}{\partial|y|^{\beta/2}}\right)^2\right] dx\,dy + \int_\Omega H(x,y,u)\,dx\,dy, \tag{1.1.5}$$

where $H(x,y,u) = \varphi(x,y)\cos u$ represents the effective potential. This energy is exactly conserved in time for the undamped system. When damping or nonlinear dissipation is present ($\eta > 0$ or $G' > 0$), the energy dissipates at a rate proportional to the damping terms:

$$\frac{dE}{dt} = -\eta\int_\Omega \left(\frac{\partial u}{\partial t}\right)^2 dx\,dy - \int_\Omega G'(u)\frac{\partial u}{\partial t}\,dx\,dy \leq 0. \tag{1.1.6}$$

This monotonic decrease in energy provides fundamental *a priori* bounds on the solution and forms the basis for proving long-time existence and stability.

The primary numerical challenges posed by equation (1.1.1) are threefold. First, the non-local nature of the Riesz fractional derivatives requires coupling each grid point to all other points via power-law kernels, resulting in dense matrix systems that are

TESIS TESIS TESIS TESIS TESIS

TESIS TESIS TESIS TESIS TESIS

computationally expensive to invert. Classical finite-difference approximations to the Laplacian involve only nearest-neighbor coupling (three-point stencils in one dimension, five-point in two dimensions), whereas fractional derivatives require global stencils with entries decaying algebraically with distance. This non-locality fundamentally alters the computational cost and numerical stability considerations. Second, the nonlinear term $\sin u$ introduces oscillatory behavior and necessitates robust time integration strategies to prevent spurious growth or numerical instability. Standard explicit methods may suffer from severe time-step restrictions or fail to preserve boundedness, while implicit methods require iterative solvers for the resulting nonlinear algebraic systems. Third, and most critically, the preservation of the energy structure (1.1.5)–(1.1.6) at the discrete level is non-trivial. Naive discretizations may introduce artificial energy drift—either spurious growth leading to blow-up or incorrect dissipation rates—that destroys the qualitative behavior of the solution over long time intervals.

Existing numerical methods for fractional partial differential equations offer partial solutions but do not fully address this combination of challenges. Finite-difference schemes for Riesz fractional derivatives have been developed and analyzed [10, 12], achieving high-order accuracy and, in some cases, preserving discrete energy for linear or weakly nonlinear problems. Spectral and pseudospectral methods, which leverage the simple Fourier symbol of the Riesz operator, can achieve exponential convergence for smooth solutions but typically require periodic or homogeneous boundary conditions and may struggle with the strong nonlinearity of $\sin u$. Structure-preserving schemes for classical (non-fractional) sine-Gordon equations have been extensively studied [13], demonstrating that energy-conserving or dissipative time integrators can dramatically improve long-time accuracy and stability. Recent research on one-dimensional space-fractional sine-Gordon equations has produced energy-preserving schemes of fourth-order accuracy [14], and fast solvers for related fractional wave systems have been developed [16]. However, these advances largely remain confined to one spatial dimension or assume isotropic fractional orders ($\alpha = \beta$). The extension to two dimensions with distinct fractional orders $\alpha \neq \beta$—the bifractional case—introduces additional complexity in both the discretization of the anisotropic Riesz operators and the formulation of energy-preserving time integrators.

A comprehensive structure-preserving numerical scheme for the 2D bifractional sine-Gordon equation must therefore satisfy the following requirements: (i) the spatial discretization of the Riesz fractional derivatives must preserve the self-adjoint property and yield a discrete fractional integration-by-parts formula; (ii) the time integration

TESIS TESIS TESIS TESIS TESIS

TESIS TESIS TESIS TESIS TESIS

method must be compatible with the discrete energy balance, exactly conserving energy in the undamped case and correctly dissipating energy at the prescribed rate when damping is present; (iii) the fully discrete scheme must be provably consistent, stable, and convergent under realistic regularity assumptions; and (iv) the computational cost must be manageable for practical simulations, ideally through efficient matrix-vector products or fast transform techniques. Existing methods in the literature do not simultaneously meet all these criteria for the general two-dimensional bifractional problem. This gap in the theoretical and computational framework motivates the present research.

1.2 Objectives

The overall aim of this thesis is to design, analyze, and validate structure-preserving finite-difference schemes for the 2D bifractional sine-Gordon equation with Riesz derivatives. The work is organized around five concrete objectives:

1. Spatial discretization of the Riesz operators. Construct centered finite-difference approximations of $\partial^{\alpha}_{|x|}$ and $\partial^{\beta}_{|y|}$ on bounded domains with homogeneous Dirichlet data. Prove that the discrete operators are self-adjoint and satisfy a discrete fractional integration-by-parts identity. Establish the truncation error as $O(h^2)$ and quantify it in terms of grid spacing and solution regularity.

2. Energy-preserving time integrators. Design second-order time-stepping schemes (explicit and implicit) that, when coupled with the spatial discretization from Objective 1, satisfy a discrete energy balance. In the undamped case, the scheme must conserve a discrete energy exactly; with damping, it must obey a dissipation inequality that mirrors the continuous one.

3. Stability analysis. Prove unconditional or conditional stability using energy methods. For the linear or weakly nonlinear regime, derive explicit stability conditions linking τ, h, and the fractional orders. For the fully nonlinear case, use discrete energy estimates to obtain *a priori* bounds that guarantee non-blow-up and support the convergence proof.

4. Convergence and error estimates. Establish rigorous second-order convergence to the exact solution under suitable smoothness assumptions. Combine the consistency bounds from Objectives 1–2, the stability results from Objective 3, and a discrete Grönwall inequality to obtain optimal error bounds that depend explicitly on α, β, λ_1, λ_2, and η.

5. Numerical validation. Implement both schemes and verify their theoretical prop-

TESIS TESIS TESIS TESIS TESIS

TESIS TESIS TESIS TESIS TESIS

erties through systematic experiments: convergence tests against manufactured solutions, simulations of ring solitons, long-time runs that demonstrate energy conservation or dissipation and measure observed convergence rates.

1.2.1 Scope and Delimitations

The work is deliberately focused. The spatial dimension is two; extensions to three dimensions are conceptually straightforward but computationally demanding and lie outside the present scope. The Riesz orders stay within $(1, 2]$, where centered differences provide a unified treatment; orders outside this range would require different analytical tools. Only homogeneous Dirichlet boundary conditions are considered; Neumann or periodic conditions introduce additional boundary terms that are not analyzed here. The numerical experiments concentrate on single-soliton evolution, ring solitons, and small-amplitude perturbations, leaving complex multi-soliton collisions and chaotic regimes to future work. Finally, the emphasis is on the mathematical correctness and structure-preserving properties of the schemes rather than on the development of fast solvers; algorithmic acceleration (FFT, multigrid, preconditioners) is discussed as a natural next step but is not the primary focus.

1.3 Thesis Organization

Chapter 2 develops the theoretical background shared by both articles. It covers the principal fractional operators and their properties, with particular attention to the Riesz derivative and its Fourier symbol; the self-adjoint structure of the fractional Laplacian on bounded domains and the integration-by-parts identity that drives every energy argument; the sine-Gordon equation and its physical realizations; the extension to bifractional and dissipative settings; and the energy methods and structure-preserving discretization principles that motivate the numerical schemes.

Chapter 3 reproduces the article “A Discrete Model to Solve a Bifractional Dissipative Sine–Gordon Equation: Theoretical Analysis and Simulations”, published in *Fractal and Fractional* (MDPI, 2025). It presents a two-step Crank–Nicolson scheme on a first-order reformulation of the equation, establishes a discrete energy balance, and validates the scheme through convergence tables and ring-soliton simulations.

Chapter 4 reproduces the article “A Scheme to Solve a Generalized Space-Bifractional 2D Sine–Gordon Equation: Conservation and Efficiency Analysis”, submitted to the *Journal of Computational and Applied Mathematics*. It develops a three-level centered scheme directly on the second-order equation, proves solvability via Banach’s fixed-point

TESIS TESIS TESIS TESIS TESIS

TESIS TESIS TESIS TESIS TESIS

theorem, and provides a rigorous second-order convergence analysis.

Chapter 5 steps outside each article to compare the two approaches on equal footing. It identifies the shared spatial discretization as a common foundation, contrasts the two temporal integrators and their stability regimes, and draws a conclusion that neither article could reach independently: the qualitative conservative or dissipative character of the dynamics is governed exclusively by the damping coefficient η and is insensitive to the fractional orders α and β.

Chapter 6 synthesizes the contributions, states the methodological observations that emerge from the joint body of work, acknowledges the limitations of the present results, and outlines the most pressing directions for future research. The MATLAB codes used to produce the numerical experiments are collected in Appendices A and B.

TESIS TESIS TESIS TESIS TESIS

TESIS TESIS TESIS TESIS TESIS

Chapter 2. Theoretical Framework

2.1 Fundamentals of Fractional Calculus

Fractional calculus extends differentiation and integration to arbitrary non-integer orders, replacing the classical operator d^n/dx^n by d^α/dx^α for α real or complex. The theory rests on integral representations and special functions, and its distinguishing feature is that the resulting operators are non-local: evaluating a fractional derivative of f at a point x requires knowledge of f over an entire interval. This section introduces the three principal formulations—Riemann–Liouville, Caputo, and Grünwald–Letnikov—and explains why spatial non-locality calls for a different operator altogether.

The conceptual foundation dates to 1695, when l'Hôpital asked Leibniz about the meaning of a half-order derivative. Lacroix (1819) deduced the first explicit fractional derivative, and Abel (1823) provided the first physical application through a fractional-order integral equation arising in the tautochrone problem. These early results catalyzed subsequent formalizations by Liouville, Riemann, and Grünwald [7, 8]. Fractional operators are motivated by their ability to capture non-local phenomena, memory effects, and multiscale dynamics. Unlike classical derivatives, which are strictly local, fractional derivatives integrate over the entire history or domain, directly encoding long-range interactions [9, 7]. This non-local character yields more realistic descriptions of anomalous diffusion, scaling behavior in continuous-time random walks, and viscoelasticity [17].

Unlike classical calculus, the formulation of fractional operators is not unique. Multiple definitions coexist and must be selected based on the physical and boundary properties of the system under study. The Riemann–Liouville formulation evaluates the fractional integral prior to integer-order differentiation. For an order $\alpha \in (n-1, n]$, this operator is defined as [7]:

$$D_t^\alpha f(t) = \frac{1}{\Gamma(n-\alpha)} \frac{d^n}{dt^n} \int_0^t (t-\zeta)^{n-\alpha-1} f(\zeta)\, d\zeta. \tag{2.1.1}$$

A notable feature is that the fractional derivative of a constant is non-zero, and initial conditions must be expressed in terms of fractional-order limits, which frequently lack direct physical meaning [8].

The Caputo approach resolves these difficulties by reversing the operational sequence—

TESIS TESIS TESIS TESIS TESIS

TESIS TESIS TESIS TESIS TESIS

applying the integer derivative before fractional integration [7, 8]:

$$ {}^{C}D^{\alpha} f(t) = \frac{1}{\Gamma(n-\alpha)} \int_0^t (t-\zeta)^{n-1-\alpha} f^{(n)}(\zeta)\, d\zeta. \tag{2.1.2}$$

The Caputo derivative of a constant evaluates to zero, and initial value problems utilize standard integer-order initial data (position, velocity). This consistency makes the Caputo formalism prevalent in applied physics and engineering.

The Grünwald–Letnikov formulation approximates fractional derivatives through the limit of finite differences, offering direct advantages for numerical implementation [7]:

$$ D^{\nu} f(x) = \lim_{h\to 0} \frac{1}{h^{\nu}} \sum_{k=0}^{\infty} (-1)^k \binom{\nu}{k} f(x-kh). \tag{2.1.3}$$

The explicit summation over previous states makes historical memory transparent, facilitating numerical discretization of complex media. While other formalisms—Weyl, Marchaud, Hadamard, Katugampola, and conformable derivatives—have been developed for periodic functions or specific scaling behaviors, the three operators above remain the standard for modeling temporal memory. Certain physical systems are dominated by spatial non-locality: anomalous diffusion, turbulent transport, and Lévy flights are governed by spatial fractional operators [17] that require a symmetric treatment of spatial coordinates. Capturing those isotropic, non-local interactions calls for the Riesz fractional derivative, introduced in the next section.

2.2 The Riesz Fractional Derivative

The temporal operators of the previous section are inherently one-sided: they accumulate information from the past but not the future. For spatial operators, physical isotropy demands that both directions contribute equally. The Riesz derivative achieves this by symmetrically combining the left- and right-sided Riemann–Liouville operators, and its spectral properties make it the natural fractional generalization of the Laplacian.

For a function $v(x)$ defined on $\mathbb{R}$ and a fractional order $\alpha \in (1, 2]$, the Riesz derivative is [7, 8]:

$$ \frac{\partial^{\alpha} v}{\partial |x|^{\alpha}} = -\frac{1}{2\cos(\pi\alpha/2)} \left({}_{-\infty}D_x^{\alpha} v(x) + {}_{x}D_{\infty}^{\alpha} v(x) \right), \tag{2.2.1}$$

where ${}_{-\infty}D_x^{\alpha}$ and ${}_{x}D_{\infty}^{\alpha}$ denote the left and right Riemann–Liouville fractional derivatives. The linear combination accumulates influence symmetrically from both $-\infty$ and $+\infty$, and the normalization constant ensures consistency with the standard Laplacian when

TESIS TESIS TESIS TESIS TESIS

TESIS TESIS TESIS TESIS TESIS

$\alpha \to 2$, rendering the Riesz derivative a fractional generalization of $\partial^2/\partial x^2$.

The symmetric nature of the Riesz derivative becomes transparent in the frequency domain. Applying the Fourier transform yields a purely algebraic multiplier [11]:

$$\mathcal{F}\left\{\frac{\partial^\alpha v}{\partial |x|^\alpha}\right\}(\xi) = -|\xi|^\alpha \hat{v}(\xi), \tag{2.2.2}$$

where $\hat{v}(\xi)$ is the Fourier transform of v and ξ the wavenumber. This symbol is structurally identical to that of the classical Laplacian, whose multiplier is $-|\xi|^2$. Consequently, the Riesz derivative is equivalent to the one-dimensional fractional Laplacian $-(-\Delta)^{\alpha/2}$, and this spectral equivalence is precisely why it serves as the natural spatial operator for modeling non-local dispersion.

To solve fractional PDEs numerically, one must analyze the Riesz operator on a bounded interval $I \subset \mathbb{R}$. Functions are assumed to satisfy homogeneous Dirichlet conditions and are extended by zero outside I [11]. Under this framework, the Riesz derivative exhibits a self-adjoint property yielding the fractional integration-by-parts identity: for sufficiently smooth functions u and w vanishing outside I,

$$\int_I \frac{\partial^\alpha u}{\partial |x|^\alpha}\, w \, dx = \int_I u \, \frac{\partial^\alpha w}{\partial |x|^\alpha}\, dx = -\int_I \frac{\partial^{\alpha/2} u}{\partial |x|^{\alpha/2}} \frac{\partial^{\alpha/2} w}{\partial |x|^{\alpha/2}}\, dx. \tag{2.2.3}$$

This identity underpins weak formulations of fractional boundary value problems [11, 12] and provides the theoretical basis for the energy estimates and stability analysis used throughout this thesis.

2.3 The Sine-Gordon Equation

The sine-Gordon equation emerges from the nonlinear Klein-Gordon family as the preeminent integrable case, distinguished by a periodic potential that supports topological solitons. This section traces the equation's origins in the classical wave hierarchy, describes its exact solutions, and surveys the physical settings where it governs observable phenomena—applications that motivate both the two-dimensional generalization and the fractional extension treated in the remainder of the thesis.

The classical wave equation constitutes the foundational linear hyperbolic framework from which nonlinear and relativistic models are formulated. In $(1+n)$ dimensions, the d'Alembertian is $\partial_\mu \partial^\mu \equiv \partial_{tt} - \sum_{i=1}^n \partial_{x_i x_i}$. The structural simplicity of this linear operator motivates the introduction of nonlinear terms to model dispersive and subatomic

TESIS TESIS TESIS TESIS TESIS

TESIS TESIS TESIS TESIS TESIS

phenomena. The Klein-Gordon equation incorporates restoring and nonlinear force terms, fundamentally altering wave dynamics. Formulated in 1927, it describes spinless particles and remains central to quantum mechanics and special relativity [3]. In $(1+1)$ dimensions, a general nonlinear Klein-Gordon equation takes the form $u_{tt} - u_{xx} + f(u) = 0$, where the choice of f determines the specific model. The ϕ^4 model, $u_{tt} = u_{xx} + 2(u - u^3)$, arises in structural phase transitions and cosmological domain walls. This family provides the mathematical foundation for representing localized wave packets known as solitons.

Within the Klein-Gordon family, the sine-Gordon equation stands out as a prominent integrable subclass, replacing polynomial nonlinearities with a periodic potential. In $(1+1)$ dimensions [3, 2]:

$$\frac{\partial^2 \phi}{\partial t^2} - \frac{\partial^2 \phi}{\partial x^2} + \sin \phi = 0. \tag{2.3.1}$$

This equation is completely integrable in one spatial dimension and supports topological solitons. Through the Inverse Scattering Transform [18], Bäcklund transformations, and the Hirota method, it admits exact solutions: topological kinks (traveling fronts), anti-kinks, and breathers—bound, time-periodic states of a kink–anti-kink pair [19]. The remarkable stability of these solitary waves guarantees purely elastic collisions, a property linked to the infinite conservation laws inherent to the system's integrability. The nexus with the Klein-Gordon family is evident when expanding $\sin u$ in a Taylor series, which yields the cubic nonlinearity as the leading-order correction.

The sine-Gordon equation models complex physical phenomena across condensed matter physics and engineering, and its exact soliton solutions serve as analytical baselines that motivate extensions into more complex, non-local media. In superconductivity, long Josephson junctions—two superconducting layers separated by a thin insulating barrier—provide a physical laboratory for sine-Gordon dynamics [1, 4]. The phase difference of the macroscopic wave functions across the junction obeys the sine-Gordon equation, with topological kinks manifesting as magnetic flux quanta (fluxons) propagating along the transmission line. In nonlinear optics, the equation describes self-induced transparency [5]: an ultra-short coherent pulse propagating through a resonant two-level medium passes unattenuated by locally inverting the atomic population and subsequently extracting the energy back, a process mirrored by the elastic propagation of a 2π-kink. Mechanical metamaterials provide macroscopic demonstrations of sine-Gordon solitons [6]: arrays of coupled pendula connected via torsional springs supply both the periodic $\sin \phi$ potential (gravity) and the spatial coupling (torsion), allowing direct visual observation of kink propagation, breather oscillations, and topological conservation. When

TESIS TESIS TESIS TESIS TESIS

TESIS TESIS TESIS TESIS TESIS

the standard model is generalized to two spatial dimensions, the equation incorporates the 2D Laplacian alongside phenomenological dissipation, adopting the form:

$$\partial_{tt} v + \eta\, \partial_t v - \lambda \Delta v = -\varphi(x, y) \sin v, \tag{2.3.2}$$

where η represents damping and λ governs spatial diffusion. While the 2D equation generally lacks complete integrability, the topological defect solutions of the 1D case continue to inform the analysis.

2.4 Fractional Generalizations of the Sine-Gordon Equation

Replacing the classical Laplacian with fractional spatial operators extends the sine-Gordon model to media where the spatial coupling decays according to a power law rather than exponentially. This section describes the space-fractional and bifractional variants, explains the modeling motivation for the anisotropic (α, β) setting, and discusses how boundary conditions are handled on bounded domains.

Fractional generalizations replace integer-order derivatives with fractional operators, extending the model to capture non-local spatial interactions and temporal memory effects. In the spatial domain, the space-fractional sine-Gordon equation incorporates the Riesz derivative or fractional Laplacian:

$$\partial_{tt} v - (-\Delta)^{\alpha/2} v + \sin v = 0. \tag{2.4.1}$$

This operator bridges the classical wave equation ($\alpha = 2$) and the non-local Hilbert-transform limit ($\alpha = 1$). Spatial non-locality modifies kink profiles, replacing exponential decay with power-law tails and enabling non-monotonic structures for $\alpha > 2$ [14]. These models capture non-local dynamics in atomic lattices, crystal dislocations, and Josephson junction arrays. Conversely, the time-fractional sine-Gordon equation replaces ∂_{tt} with a Caputo operator of order $\gamma \in (1, 2)$, which breaks Hamiltonian conservation by imposing intrinsic dissipation even without explicit damping [20]; kinks that propagate at constant velocity in the classical model undergo exponential deceleration under time-fractionality.

Generalized frameworks combine fractional derivatives in both spatial directions to create bifractional sine-Gordon models [14, 16, 15]. In two-dimensional media, wave propagation is not necessarily isotropic: a system may exhibit non-locality of order α along x and a different order β along y. This anisotropic framework is formalized

TESIS TESIS TESIS TESIS TESIS

TESIS TESIS TESIS TESIS TESIS

through the bifractional Laplacian $\Delta_{\alpha,\beta}$, defined as:

$$\Delta_{\alpha,\beta}\, v = \frac{\partial^\alpha v}{\partial |x|^\alpha} + \frac{\partial^\beta v}{\partial |y|^\beta}, \tag{2.4.2}$$

which enables direction-dependent tuning of spatial dispersion relations. This operator is critical for modeling stratified materials, asymmetric crystal lattices, and engineered metamaterials with directional properties [21]. It is within this anisotropic (α, β) setting that the numerical schemes developed in the subsequent chapters operate.

The formulation of fractional models on bounded domains requires appropriate boundary conditions. Dirichlet conditions arise naturally when modeling lattice defects and crystal dislocations, where boundary atoms are rigidly constrained. For the Riesz-based sine-Gordon equation, homogeneous Dirichlet conditions ($v = 0$) are imposed both on ∂I^2 and in the exterior domain [11]. This zero extension simplifies the non-local integrals, ensuring they vanish outside the physical region, and satisfies the regularity assumptions required for the theoretical analysis.

2.5 Energy Methods and Structure-Preserving Discretizations

Numerical stability for long-time wave simulations is most reliably achieved by schemes that exactly mirror a continuous energy law at the discrete level. This section introduces the continuous energy functional, characterizes its dissipative or conservative behavior, and explains how the Summation-By-Parts property transfers this structure to the discrete setting.

The analysis of nonlinear fractional wave equations relies on energy functionals [13, 12]. For the bifractional sine-Gordon equation on I^2 with damping coefficient $\eta \geq 0$, the total energy $E(t) = K(t) + U(t)$ splits into kinetic and potential components. Taking the $L^2(I^2)$ inner product of the governing equation with $\partial_t v$ and applying the integration-by-parts identity (2.2.3) yields:

$$K(t) = \tfrac{1}{2}\|\partial_t v\|^2_{L^2(I^2)}, \tag{2.5.1}$$

$$U(t) = \tfrac{1}{2}\Lambda\|\nabla_{\alpha/2,\beta/2} v\|^2_{L^2(I^2)} + \|\varphi(1-\cos v)\|_{L^1(I^2)} + \|G(v)\|_{L^1(I^2)}, \tag{2.5.2}$$

where the first term of U is the anisotropic fractional strain energy, the second the periodic nonlinear potential, and the third the auxiliary potential G. The energy rate is:

$$\frac{dE}{dt} = -\eta\|\partial_t v\|^2_{L^2(I^2)}. \tag{2.5.3}$$

TESIS TESIS TESIS TESIS TESIS

TESIS TESIS TESIS TESIS TESIS

When $\eta = 0$ the system is conservative ($E(t) = E(0)$ for all $t > 0$); when $\eta > 0$ it is dissipative [21].

Standard numerical methods introduce spurious dissipation that, in long-time simulations of conservative systems, causes unphysical amplitude attenuation and phase errors [13]. Structure-preserving discretizations circumvent this by obeying a discrete analogue of the integration-by-parts identity—the Summation-By-Parts (SBP) property—so that the scheme exactly mimics the continuous energy transfer between K and U [12]. To handle the nonlinear potential without destroying energy preservation, the nonlinear term is discretized via a consistent discrete derivative $\delta_{v,t}$ that preserves the telescoping structure of the energy identity. This approach, employed in both articles of this thesis [21], guarantees that the discrete energy balance mirrors (2.5.3) at every time step.

For the classical sine-Gordon equation, conservative finite-difference schemes and high-order integrators have been developed to maintain geometric profiles during multi-soliton collisions [13]. Fractional variants demand different paradigms because the non-local operators produce dense matrices. For time-fractional models, the Alikhanov $L2\text{-}1_\sigma$ scheme achieves second-order temporal convergence for the Caputo derivative while preserving energy decay [16]. For the space-fractional equations central to this thesis, shifted finite-difference schemes based on fractional centered differences are predominantly used [14, 15]; these methods handle the Toeplitz structure of the discrete Riesz operator and form the computational foundation of the subsequent chapters.

2.6 Fractional Centered Differences and Discrete Operators

The passage from continuous Riesz operators to computable matrices requires a discretization that preserves self-adjointness. This section presents the fractional centered differences of Ortigueira, derives the Summation-By-Parts identity they satisfy, and introduces the discrete Gronwall inequality that closes the convergence proofs.

Standard Grünwald–Letnikov approximations exhibit asymmetric $\mathcal{O}(h)$ truncation errors, unsuitable for the symmetric Riesz operator. The fractional centered difference framework of Ortigueira [10] achieves $\mathcal{O}(h^2)$ accuracy via the operator:

$$\Delta_h^\alpha v(x) = \sum_{k=-\infty}^{\infty} g_k^{(\alpha)}\, v(x - kh), \tag{2.6.1}$$

with weights:

$$g_k^{(\alpha)} = \frac{(-1)^k\,\Gamma(\alpha+1)}{\Gamma(\alpha/2 - k + 1)\,\Gamma(\alpha/2 + k + 1)}, \quad k \in \mathbb{Z}. \tag{2.6.2}$$

TESIS TESIS TESIS TESIS TESIS

TESIS TESIS TESIS TESIS TESIS

For sufficiently smooth v and $\alpha \in (0,1) \cup (1,2]$, the Riesz derivative is approximated as [10]:

$$\frac{\partial^\alpha v(x)}{\partial |x|^\alpha} = -\frac{\Delta_h^\alpha v(x)}{h^\alpha} + \mathcal{O}(h^2). \tag{2.6.3}$$

Under the zero-extension convention on the bounded grid I^2, the discrete Riesz operators $\delta_x^{(\alpha)}$ and $\delta_y^{(\beta)}$ are obtained by truncating the sum to the interior nodes [11].

The symmetric Toeplitz matrix of $\delta_x^{(\alpha)}$ satisfies the Summation-By-Parts property [12, 11]. For discrete grid functions V and W with homogeneous Dirichlet boundaries:

$$\langle -\delta_x^{(\alpha)} V, W \rangle_h = \langle \delta_x^{(\alpha/2)} V,\, \delta_x^{(\alpha/2)} W \rangle_h. \tag{2.6.4}$$

This is the exact discrete analogue of (2.2.3). It guarantees positive-definiteness of the discrete potential energy and rigorous energy stability of the proposed schemes [21].

Convergence proofs require bounding the discrete error over successive time steps. The discrete Gronwall inequality [22] states that if a non-negative sequence $\{y_n\}$ satisfies:

$$y_n \le C + h \sum_{k=0}^{n-1} \lambda_k \, y_k, \tag{2.6.5}$$

with $C \ge 0$ constant and $\lambda_k \ge 0$, then:

$$y_n \le C \exp\left(h \sum_{k=0}^{n-1} \lambda_k \right). \tag{2.6.6}$$

Combined with the SBP-based energy estimates and the Ortigueira discretization bounds, this inequality closes the convergence analysis at second order in both space and time.

2.7 Time Integration and Treatment of Nonlinear Terms

The transition from a semi-discrete system to a fully discrete model requires a temporal strategy that preserves the energy structure of the continuous problem.

Explicit time-stepping methods impose severe restrictions on τ and introduce numerical dissipation or growth that compromises long-time soliton simulations. The Crank–Nicolson (CN) scheme provides $\mathcal{O}(\tau^2)$ accuracy with unconditional stability for linear problems [13, 21]. In the bifractional framework, the fully discrete scheme reads:

$$\delta_t^{(2)} V_{i,j}^n + \eta \, \delta_t^{(1)} V_{i,j}^n - \Lambda \cdot \Delta_h^{\alpha,\beta} \, \mu_t V_{i,j}^n - \delta_{v,t} H(V_{i,j}^n) - F_{i,j}^n = 0, \tag{2.7.1}$$

TESIS TESIS TESIS TESIS TESIS

TESIS TESIS TESIS TESIS TESIS

where $\mu_t V^n = (V^{n+1} + V^{n-1})/2$ and $\delta_{v,t} H$ is the consistent discrete derivative preserving the energy's telescoping structure. In the conservative limit ($\eta = 0$), the CN discretization ensures $E^n = K^n + U^n$ remains constant over the discrete time [21].

The CN scheme yields an implicit nonlinear system at each time step. A fixed-point iteration resolves this efficiently [21]: starting from $V^{n+1,0} = V^{n-1}$, one solves the sequence of linear systems:

$$\delta_t^{(2)} V^{n,s+1} + \eta\, \delta_t^{(1)} V^{n,s+1} - \Lambda \cdot \Delta_h^{\alpha,\beta}\, \mu_t V^{n,s+1} = \delta_{v,t} H(V^{n,s}) + F^n, \tag{2.7.2}$$

iterating until $\|V^{n,s+1} - V^{n,s}\|_\infty < \varepsilon$. Convergence is guaranteed by Banach's theorem under $\tau < \tau_*$, where τ_* depends on the Lipschitz constant of H' [21]. In practice, the iteration converges in few steps, and the energy properties of the scheme are guaranteed by its design; they do not depend on the iteration count.

The theoretical elements developed in this chapter form the methodological scaffolding of the entire thesis. The Riesz fractional derivative, with its Fourier symbol $-|\xi|^\alpha$ and its self-adjoint discretization via Ortigueira's centered differences, provides the spatial foundation. The summation-by-parts identity (Lemma 4.6) guarantees that the discrete operators inherit the fractional integration-by-parts property, which is the algebraic engine of every energy argument that follows. The variational linearization $\delta_{v,t}^{(1)} H$ of the nonlinear potential closes the discrete energy balance without remainder, ensuring that the fully discrete schemes respect the conservative or dissipative character of the continuous model. Finally, the fixed-point framework guarantees that the implicit nonlinear step is well posed under a mild time-step restriction. The next two chapters materialize these abstract principles into two concrete, fully discrete numerical schemes for the bifractional sine-Gordon equation.

TESIS TESIS TESIS TESIS TESIS

TESIS TESIS TESIS TESIS TESIS

Chapter 3. A Discrete Model to Solve a Bifractional Dissipative Sine-Gordon Equation: Theoretical Analysis and Simulations

3.1 Introduction

Fractional calculus, or more precisely, arbitrary-order calculus, has seen enormous development within the mathematical community in recent years due to its ability to model phenomena with complex behavior [23]. Amongst these complex phenomena, we can cite long-term memory dynamic effects and randomness or stochasticity with changing distributions, which in many cases result in simpler fractional models compared to their integer-order counterparts [24, 25, 26, 27, 28, 29]. There is also evidence that fractional models provide equally good (or even better) descriptions for real-world processes than classical models in the sense of a closer match between modeled data and experimental measurements [30]. Some examples of the applications of fractional calculus can be found in the field of biological sciences, where fractional-order models have been used to describe the spread of infectious diseases such as dengue [31], as well as pharmacokinetic and pharmacodynamic processes [32], and even technological processes like fermentation [33]. In material engineering, there are also interesting applications, such as modeling viscoelasticity through the use of fractional derivatives [34, 35]. Similarly, in physics, the use of fractional calculus can be observed in the investigation of Stefan problems with fractional time [36], in fractional Bloch–Torrey equations [37], in fluid mechanics [17], in quantum mechanics [38], and in some non-homogeneous Div-Curl systems [39], to mention just a few examples.

On the other hand, in recent times, numerical methods in fractional calculus have seen substantial advances [22]. This is partly due to the fact that fractional differential equations (FDEs) have gained prominence in modeling various real-world phenomena [8]. Indeed, various models have been extended to the fractional case, like Schrödinger's equation [40], the Klein–Gordon equation [41], some reaction–diffusion equations [42, 43], and Havriliak–Negami models [44], among other systems. One commonly employed method for solving these types of problems is the finite-difference method and its variations. These methods are particularly useful for FDEs with Caputo or Riemann–Liouville derivatives [45, 12, 46]. However, these methods can be computationally intensive, especially for high-dimensional problems, due to their global nature. Also, we can find spectral and pseudospectral methods for solving FDEs. Spectral methods have

TESIS TESIS TESIS TESIS TESIS

TESIS TESIS TESIS TESIS TESIS

proven valuable for solving FDEs with high accuracy. The application of these methods includes the use of Chebyshev or Legendre polynomials, which convert fractional problems into systems of algebraic equations [47, 48, 49]. In turn, pseudospectral methods further enhance computational efficiency by reducing the number of function evaluations needed during simulations, albeit with a reduction in precision. Periodic conditions at the boundary are also needed [50]. We can also find the fractional version of the finite-element method. This method is of great interest due to its generality, convergence, and ease with which it allows the introduction of complex domains [51]. While this approach is a staple in classical areas like heat transfer, fluid dynamics, and electromagnetic modeling, its versatility does not end there. Surprisingly, it has also emerged as a key tool for unraveling fractional equations in quantum mechanics and statistical mechanics, as recent studies highlight [52, 53, 54, 55].

One of the models that has been extensively studied in the literature (both analytically and numerically) is the sine-Gordon equation (SGE). This model is a well-known nonlinear partial differential equation. As an extended two-dimensional and integer-order model, the SGE takes the following form:

$$\begin{aligned}\frac{\partial^2 u\left(x,y,t\right)}{\partial t^2}+\gamma\frac{\partial u\left(x,y,t\right)}{\partial t}-\lambda\Delta u(x,y,t)&=-\phi(x,y)\sin u(x,y,t)\\&\quad+F\left(x,y,t\right)+G'(u(x,y,t)).\end{aligned}\tag{3.1.1}$$

Here,$u:\mathbb{R}^2\times\mathbb{R}^{\geq 0}\to\mathbb{R}$ represents a sufficiently smooth function dependent on (x,y,t), where $(x,y)\in\mathbb{R}^2$ are spatial coordinates and $t\in\mathbb{R}^{\geq 0}$ denotes time. The function $\phi(x,y)$ is continuous and varies over space with (x,y), while $F(x,y,t)$ is also a continuous function that depends on both space and time. Additionally, $G:\mathbb{R}\to\mathbb{R}$ is a continuously differentiable function. The parameters γ and λ, both real constants, have direct physical interpretations: γ corresponds to a damping coefficient and λ quantifies constant spatial diffusion. Here, Δ represents the two-dimensional Laplacian operator acting over x and y.

Originally emerging from differential geometry and surface theory, the sine-Gordon equation has become a cornerstone of nonlinear science due to its mathematical depth and wide range of applications across physics [3, 2]. A defining feature of this equation is its ability to support soliton solutions and localized, stable waveforms that retain their shape and velocity over time, even during interactions with other solitons. This property classifies the sine-Gordon equation as an integrable system, solvable via advanced

TESIS TESIS TESIS TESIS TESIS

TESIS TESIS TESIS TESIS TESIS

methods such as Bäcklund transformations and the inverse scattering technique [19, 18]. The equation's relevance spans multiple domains of applied physics. In solid-state physics, for instance, it models magnetic flux dynamics in long Josephson junctions, where solitons manifest as "fluxons" (quantized magnetic flux units) [4]. Similarly, in nonlinear optics, it describes specific light pulse behaviors, offering critical insights into optical soliton propagation in fiber optics [5]. The equation also serves as a foundational model in quantum field theory for studying $(1 + 1)$-dimensional field theories [56, 57].

In this work, we introduce a second-order finite difference model for the dissipative 2D sine-Gordon equation with bifractional damping using Riesz operators in space (3.3.13). Two main contributions are presented in this manuscript. The first one is a structure-preserving formulation that satisfies a discrete energy-dissipation (conservation for the undamped case) law (3.4). The second one is a fully discrete numerical scheme with proven consistency, stability, and convergence in two dimensions (3.10)–(3.14). These developments extend existing 1D or non-dissipative models and offer a solid, efficient tool for exploring the interplay of nonlinearity and fractional damping.

The rest of this paper is organized as follows. In Section 3.2, we introduce the notation and basic properties of Riesz space-fractional derivatives and set up the framework for the problem. Section 3.3 presents the discrete finite-difference scheme: we define the temporal Crank–Nicolson two-step method, the centered-difference approximation of Riesz operators, and the discrete energy. In Section 3.4, we analyze the scheme's numerical properties, proving its consistency (second order in space and time), conditional stability via a discrete Gronwall argument, and convergence to the exact solution. Section 3.5 offers a suite of MATLAB simulations, first validating against a known analytic solution, then exploring the effects of varying fractional orders on the analytic solution and in soliton profiles, and finally demonstrating both conservative and dissipative dynamics of a circular ring soliton. Section 3.6 summarizes our main findings, highlights the practical advantages of the method, and outlines potential directions for future work. Appendix A presents a collection of the full MATLAB code used to generate all numerical experiments.

3.2 Preliminaries

In this work, we consider $T > 0$ as a fixed temporal period. For convenience, we take a fixed one-dimensional spatial domain of the form $D = (a, b)$, with $a < b$ and $D^2 = D \times D$. Let $\Omega = D^2 \times (0, T) \subseteq \mathbb{R}^3$ represent the space–time domain, and agree that $\overline{\Omega}$ represents

TESIS TESIS TESIS TESIS TESIS

TESIS TESIS TESIS TESIS TESIS

the closure of Ω in $\mathbb{R}^3$ under the standard topology. It is obvious that $\overline{D^2} = [a,b] \times [a,b]$. For the remainder of this work, we will let $u : \overline{\Omega} \to \mathbb{R}$ be sufficiently smooth. Motivated by the form of the SGE described in Equation (3.1.1), we will let $\phi : \overline{D^2} \to \mathbb{R}$ and $F : \overline{\Omega} \to \mathbb{R}$ be continuous functions, and let $G : \Omega \to \mathbb{R}$ be continuously differentiable. Throughout, we will suppose that ϕ and G are non-negative functions. As expected, λ and γ will be non-negative real numbers with the property that $\gamma > 0$. Moreover, α and β will denote real numbers in $(1,2]$. These conventions will be observed throughout this work.

Definition 3.1 (Podlubny [7]). Suppose that $n \in \mathbb{N}$ and $\alpha \in \mathbb{R}$ satisfy $n-1 < \alpha < n$. Let us recall now that the Riesz fractional derivative of order α of the function u at the point $(x,y,t) \in \Omega$ with respect to x is provided by the following:

$$\frac{\partial^\alpha u(x,y,t)}{\partial |x|^\alpha} = \frac{-1}{2\cos(\frac{\pi\alpha}{2})\Gamma(n-\alpha)} \frac{\partial^n}{\partial x^n} \int_{-\infty}^{\infty} \frac{u(\xi,y,t)}{|x-\xi|^{\alpha-n+1}} d\xi. \tag{3.2.1}$$

Here, Γ denotes the usual gamma function. In the case that $\alpha = n$, let us agree that the Riesz fractional derivative of u with respect to x coincides with the usual integer-order nth derivative of u with respect to x. In a similar fashion, if $n-1 < \beta < n$, then we define the Riesz fractional derivative of order β of u with respect to y at the point $(x,y,t) \in \Omega$ as follows:

$$\frac{\partial^\beta u(x,y,t)}{\partial |y|^\beta} = \frac{-1}{2\cos(\frac{\pi\beta}{2})\Gamma(n-\beta)} \frac{\partial^n}{\partial y^n} \int_{-\infty}^{\infty} \frac{u(x,\xi,t)}{|y-\xi|^{\beta-n+1}} d\xi. \tag{3.2.2}$$

As expected, we define the Riesz derivative of order $\beta = 2$ of u with respect to y as the classical second-order derivative of u with respect to y. For the sake of commodity, we introduce the fractional Laplacian operator of order (α,β) of u at the point (x,y,t) as follows:

$$\Delta^{\alpha,\beta} u(x,y,t) = \frac{\partial^\alpha u(x,y,t)}{\partial |x|^\alpha} + \frac{\partial^\beta u(x,y,t)}{\partial |y|^\beta}. \tag{3.2.3}$$

Finally, we define the fractional gradient operator of order (α,β) of u at (x,y,t) as the following vector:

$$\nabla^{\alpha,\beta} u(x,y,t) = \left(\frac{\partial^\alpha u(x,y,t)}{\partial |x|^\alpha}, \frac{\partial^\beta u(x,y,t)}{\partial |y|^\beta} \right). \tag{3.2.4}$$

With these conventions, the fractional form of the two-dimensional SGE investigated in

TESIS TESIS TESIS TESIS TESIS

TESIS TESIS TESIS TESIS TESIS

the present work is the nonlinear partial differential equation provided by the following:

$$\begin{aligned}\frac{\partial^2 u(x,y,t)}{\partial t^2} + \gamma \frac{\partial u(x,y,t)}{\partial t} - \lambda \Delta^{\alpha,\beta} u(x,y,t) = -\phi(x,y) \sin u(x,y,t) \\ + F(x,y,t) - G'(u(x,y,t))\end{aligned} \tag{3.2.5}$$

for each $(x,y,t) \in \Omega$. For the remainder of this work, we will let $\psi_1, \psi_2 \colon \overline{D^2} \to \mathbb{R}$ be sufficiently smooth functions that are equal to zero at the boundary of $\overline{D^2}$. We will also consider the following initial and boundary conditions:

$$\begin{aligned} u(x,y,0) &= \psi_1(x,y), \qquad \forall (x,y) \in D^2, \\ \frac{\partial u}{\partial t}(x,y,0) &= \psi_2(x,y), \qquad \forall (x,y) \in D^2, \\ u(x,y,t) &= 0, \qquad \forall (x,y,t) \in \partial D^2 \times (0,T). \end{aligned} \tag{3.2.6}$$

Here, we observe that the functions ψ_1 and ψ_2 describe the initial position and velocity of the problem, respectively. For the remainder of the present manuscript, Equation (3.2.5) will be called the *fractional 2D sine-Gordon equation* (FSG). It is worthwhile noticing that, when $\alpha = \beta = 2$, this equation is equal to the mathematical model (3.1.1).

In implementing the Riesz fractional derivative discretely on a bounded grid, we adopt homogeneous Dirichlet boundary conditions $u = 0$ outside and on $\partial\Omega$. This zero-extension simplifies the non-local integral to vanish outside the domain. Our finite-difference scheme respects summation-by-parts identities, mirroring integration-by-parts in the continuous case, and supports discrete energy-dissipation properties [12]. Additionally, truncation error of far-field contributions is controlled via domain size and mesh resolution, following established bounds for finite-difference and quadrature approximations of the fractional Laplacian [11].

In some real physical systems, a sine-Gordon equation with a space-fractional (Riesz) derivative offers a more realistic model than its classical (integer-order) form. For example, in crystal dislocations and lattice defects, long-range interactions in the atomic lattice can be captured more accurately by a spatial fractional model. These nonlocal interactions justify the use of the Riesz operator in space, while the displacement of atoms at the boundary can be fixed at the edges of a finite crystal sample [15]. In nonlocal Josephson junctions, the phase dynamics along junction arrays with nonlocal coupling correspond to a space-fractional sine-Gordon form [58]. In nonlinear supratransmission problems in continuum media, a spatial fractional sine-Gordon equation better

TESIS TESIS TESIS TESIS TESIS

TESIS TESIS TESIS TESIS TESIS

reproduces wave propagation through media with long-range dispersion [59].

Definition 3.2. Let $p \in [1, \infty)$. In what follows, we use $L^p(D^2)$ to represent the space of all p-integrable functions on $\overline{D^2}$. We will use $L^p(\Omega)$ to denote the set of all functions $v : \overline{\Omega} \to \mathbb{R}$ that vanish at the boundary of D^2 at all times, and for which $v(\cdot, \cdot, t) \in L^p(D^2)$, for each $t \in [0, T]$. In particular, if $v, w \in L^2(\Omega)$, then we define

$$\langle v, w \rangle_{L^2(\Omega)} = \int_{\overline{D^2}} v(x, y, t) w(x, y, t) dxdy, \quad \forall t \in [0, T]. \tag{3.2.7}$$

Here, place emphasis on the fact that $\langle v, w \rangle_{L^2(\Omega)}$ is a function of t. It is well known that $\langle \cdot, \cdot \rangle$ is an inner product in $L^2(\Omega)$. For the remainder of this section, we will use $\| \cdot \|_{L^2(\Omega)}$ to denote the Euclidean norm induced by $\langle \cdot, \cdot \rangle$. Moreover, for each $v \in L^1(\Omega)$, we let

$$\|v\|_{L^1(\Omega)} = \int_{\overline{D^2}} |v(x, y, t)| dxdy, \quad \forall t \in [0, T]. \tag{3.2.8}$$

Finally, we agree that

$$\left\| \nabla^{\alpha/2, \beta/2} u \right\|_{L^2(\Omega)}^2 = \left\| \frac{\partial^{\alpha/2} u}{\partial |x|^{\alpha/2}} \right\|_{L^2(\Omega)}^2 + \left\| \frac{\partial^{\beta/2} u}{\partial |y|^{\beta/2}} \right\|_{L^2(\Omega)}^2, \quad \forall t \in [0, T]. \tag{3.2.9}$$

Definition 3.3. Let u be a solution of Equation (3.2.5) subject to the initial boundary conditions (3.2.6). Then, the *total energy* of the system at time $t \in [0, T]$ is provided by the following:

$$E(t) = \frac{1}{2} \left\| \frac{\partial u}{\partial t} \right\|_{L^2(\Omega)}^2 + \frac{\lambda}{2} \left\| \nabla^{\alpha/2, \beta/2} u \right\|_{L^2(\Omega)}^2 + \| \phi (1 - \cos u) \|_{L^1(\Omega)} + \| G(u) \|_{L^1(\Omega)}. \tag{3.2.10}$$

One of the well-known properties of the classical integer-order SGE is the conservation of energy over time in the undamped case [60, 12]. Motivated by this fact, we wish to prove a similar result for our fractional extension of the SGE. To that end, we will use the fact that Riesz spatial derivatives satisfy a generalization of the formula for integration by parts [61]. More precisely, if $\alpha, \beta \in (1, 2)$, then the following formulas

TESIS TESIS TESIS TESIS TESIS

TESIS TESIS TESIS TESIS TESIS

hold for all $u, v \in L^2(D^2)$:

$$\left\langle -\frac{\partial^\alpha u}{\partial|x|^\alpha}, v \right\rangle_{L^2(\Omega)} = \left\langle u, -\frac{\partial^\alpha v}{\partial|x|^\alpha} \right\rangle_{L^2(\Omega)} = \left\langle \frac{\partial^{\frac{\alpha}{2}} u}{\partial|x|^{\frac{\alpha}{2}}}, \frac{\partial^{\frac{\alpha}{2}} v}{\partial|x|^{\frac{\alpha}{2}}} \right\rangle_{L^2(\Omega)}, \tag{3.2.11}$$

$$\left\langle -\frac{\partial^\beta u}{\partial|y|^\beta}, v \right\rangle_{L^2(\Omega)} = \left\langle u, -\frac{\partial^\beta v}{\partial|y|^\beta} \right\rangle_{L^2(\Omega)} = \left\langle \frac{\partial^{\frac{\beta}{2}} u}{\partial|y|^{\frac{\beta}{2}}}, \frac{\partial^{\frac{\beta}{2}} v}{\partial|y|^{\frac{\beta}{2}}} \right\rangle_{L^2(\Omega)}. \tag{3.2.12}$$

Theorem 3.4. *If u is a solution to (3.2.5) subject to the conditions (3.2.6), then*

$$E'(t) = -\gamma \left\| \frac{\partial u}{\partial t} \right\|^2 + \left\langle F, \frac{\partial u}{\partial t} \right\rangle_{L^2(\Omega)}, \quad \forall t \in [0, T]. \tag{3.2.13}$$

The system is conservative in case $\gamma = 0$ and $F \equiv 0$.

Proof. In the first step, we will take the derivative of E with respect to t. Next, we will exchange the derivative operator with the integral sign and apply the chain rule. The property of integration by parts for Riesz fractional operators will be applied next, and Equation (3.2.5) will be substituted. In addition, recall that ϕ and G are non-negative functions. As a consequence, we obtain the following chain of identities:

$$\begin{aligned} E'(t) = & \left\langle \frac{\partial^2 u}{\partial t^2}, \frac{\partial u}{\partial t} \right\rangle_{L^2(\Omega)} + \lambda \left\langle \frac{\partial^{\alpha/2}}{\partial|x|^{\alpha/2}} \frac{\partial u}{\partial t}, \frac{\partial^{\alpha/2} u}{\partial|x|^{\alpha/2}} \right\rangle_{L^2(\Omega)}, \\ & + \lambda \left\langle \frac{\partial^{\beta/2}}{\partial|y|^{\beta/2}} \frac{\partial u}{\partial t}, \frac{\partial^{\beta/2} u}{\partial|y|^{\beta/2}} \right\rangle_{L^2(\Omega)} + \left\langle \phi \sin u, \frac{\partial u}{\partial t} \right\rangle_{L^2(\Omega)} + \left\langle G'(u), \frac{\partial u}{\partial t} \right\rangle_{L^2(\Omega)}, \\ = & \left\langle \frac{\partial^2 u}{\partial t^2}, \frac{\partial u}{\partial t} \right\rangle_{L^2(\Omega)} - \lambda \left\langle \frac{\partial^\alpha u}{\partial|x|^\alpha}, \frac{\partial u}{\partial t} \right\rangle_{L^2(\Omega)} - \lambda \left\langle \frac{\partial^\beta u}{\partial|y|^\beta}, \frac{\partial u}{\partial t} \right\rangle_{L^2(\Omega)}, \\ & + \left\langle \phi \sin u, \frac{\partial u}{\partial t} \right\rangle_{L^2(\Omega)} + \left\langle G'(u), \frac{\partial u}{\partial t} \right\rangle_{L^2(\Omega)}, \\ = & \left\langle \frac{\partial^2 u}{\partial t^2} - \lambda \nabla^{\alpha,\beta} u + \phi \sin u + G'(u), \frac{\partial u}{\partial t} \right\rangle_{L^2(\Omega)}, \\ = & -\gamma \left\| \frac{\partial u}{\partial t} \right\|^2_{L^2(\Omega)} + \left\langle F, \frac{\partial u}{\partial t} \right\rangle_{L^2(\Omega)}, \quad \forall t \in [0, T]. \end{aligned} \tag{3.2.14}$$

This is what we wanted to prove. From here, if $\gamma = 0$ and $F \equiv 0$, then the energy is preserved over time. In another case, the energy will dissipate. ■

TESIS TESIS TESIS TESIS TESIS

TESIS TESIS TESIS TESIS TESIS

The following is a straightforward consequence of Theorem 3.4.

Corollary 3.5. *Suppose that $F \equiv 0$ and u is a solution of (3.2.5) subject to conditions (3.2.6). Then, both $\frac{\partial u}{\partial t}$ and $\nabla^{\alpha/2,\beta/2}u$ belong to $L^2(\Omega)$.* ■

Before closing this stage of our investigation, we wish to rewrite the partial differential Equation (3.2.5) as a system of two first-order differential equations. More precisely, notice that Equation (3.2.5) is equivalent to the following system:

$$\begin{cases} \dfrac{\partial u(x,y,t)}{\partial t} = v(x,y,t), \quad \forall (x,y,t) \in \Omega, \\ \dfrac{\partial v(x,y,t)}{\partial t} = -\gamma v(x,y,t) + \lambda \Delta^{\alpha,\beta} u(x,y,t) - \phi(x,y)\sin u(x,y,t) \\ \qquad\qquad\qquad + F(x,y,t) - G'(u(x,y,t)), \quad \forall (x,y,t) \in \Omega. \end{cases} \tag{3.2.15}$$

As a consequence, the energy of the system can be rewritten as follows:

$$E(t) = \frac{1}{2}\|v\|^2_{L^2(\Omega)} + \frac{\lambda}{2}\left\|\nabla^{\alpha/2,\beta/2}u\right\|^2_{L^2(\Omega)} + \|\phi(1-\cos u)\|_{L^1(\Omega)} + \|G(u)\|_{L^1(\Omega)}. \tag{3.2.16}$$

Convenient discretization of this system of temporally first-order partial differential equations will be provided and analyzed in the following sections.

3.3 Numerical Model

In the present section, we propose the finite-difference discretization of the mathematical model (3.2.15). To that end, we will consider regular partitions of the interval $\overline{D}$ in both the x- and y-directions, as well as a regular partition of $[0,T]$. Spatially, we will fix partition norms Δx and Δy in the x and y directions, respectively, which satisfy $\Delta x = \Delta y = h$. Moreover, we will temporally fix a partition norm $\Delta t = \tau$. We define $M = (b-a)/h$ and $N = T/\tau$ as positive integers. The spatial and temporal domains are divided into uniform partitions: $x_i = a + ih$, $y_j = a + jh$, and $t_k = k\tau$, where $0 \leq i,j \leq M$ and $0 \leq k \leq N$. For clarity, we define $u^k_{i,j} = u(x_i, y_j, t_k)$ as the exact solution at grid point x_i, y_j, t_k, while $U^k_{i,j}$ will represent its numerical approximation at the same point.

Next, let R_h denote the *spatial mesh*, which consists of all points (x_i, y_j) generated by $x_i = a + ih$ and $y_j = a + jh$. We also define $\mathcal{V}_h$ as the linear space over $\mathbb{R}$ of all real-valued functions defined on the grid R_h that vanish at the grid's boundary. For any two functions $f, g \in \mathcal{V}_h$, the discrete inner product $\langle \cdot, \cdot \rangle : \mathcal{V}_h \times \mathcal{V}_h \to \mathbb{R}$ and discrete

TESIS TESIS TESIS TESIS TESIS

TESIS TESIS TESIS TESIS TESIS

norms $\|\cdot\|_1, \|\cdot\|_2 : \mathcal{V}_h \to \mathbb{R}$ are defined as follows:

$$\langle f, g\rangle = h^2 \sum_{i,j=0}^{M-1} f_{i,j} g_{i,j}, \tag{3.3.1}$$

$$\|f\|_1 = h^2 \sum_{i,j=1}^{M-1} |f_{i,j}|, \tag{3.3.2}$$

$$\|f\|_2 = \sqrt{\langle f, f\rangle}. \tag{3.3.3}$$

In what follows, let us assume that $(U^k)_{k=0}^K$ is a sequence of $\mathcal{V}_h$. For the remainder of this work, we will employ the following discrete operators:

$$\delta_t U_{i,j}^{k+\frac{1}{2}} = \frac{U_{i,j}^{k+1} - U_{i,j}^k}{\tau}, \tag{3.3.4}$$

$$\mu_t U_{i,j}^{k+\frac{1}{2}} = \frac{U_{i,j}^{k+1} + U_{i,j}^k}{2}. \tag{3.3.5}$$

Similarly, we will employ the following nonlinear difference operator to consistently approximate the derivative of $F(u)$ with respect to u:

$$\delta_{u,t} F(U_{i,j}^{k+\frac{1}{2}}) = \begin{cases} \dfrac{F(U_{i,j}^{k+1}) - F(U_{i,j}^k)}{U_{i,j}^{k+1} - U_{i,j}^k} & \text{if } U_{i,j}^{k+1} \neq U_{i,j}^k, \\ F'(U_{i,j}^{k+\frac{1}{2}}) & \text{if } U_{i,j}^{k+1} = U_{i,j}^k. \end{cases} \tag{3.3.6}$$

In order to approximate the space fractional derivatives of our mathematical model, we require the following definition from the literature.

Definition 3.6 (Ortigueira [10])**.** For function $f : \mathbb{R} \to \mathbb{R}$, $h > 0$, and $\alpha > -1$, whenever it exists, the *fractional centered difference* of order α of f at x is provided by the following:

$$\Delta_h^\alpha f(x) = \sum_{l=-\infty}^{\infty} g_l^{(\alpha)} f(x - lh), \quad \forall x \in \mathbb{R}, \tag{3.3.7}$$

where

$$g_l^{(\alpha)} = \frac{(-1)^l\, \Gamma(\alpha+1)}{\Gamma\left(\frac{\alpha}{2} + l + 1\right) \Gamma\left(\frac{\alpha}{2} - l + 1\right)}, \quad \forall k \in \mathbb{Z}. \tag{3.3.8}$$

It is worth recalling that if f is sufficiently smooth at on its domain and $\alpha \in (0,1) \cup (1,2]$,

TESIS TESIS TESIS TESIS TESIS

TESIS TESIS TESIS TESIS TESIS

then we obtain the following:

$$\frac{\partial^\alpha f(x)}{\partial |x|^\alpha} = -\frac{\Delta_h^\alpha f(x)}{h^\alpha} + \mathcal{O}(h^2), \quad \forall x \in \mathbb{R}. \tag{3.3.9}$$

Motivated by these properties and the definition above, we define the discrete finite-difference operators for the space fractional derivatives as follows:

$$\delta_x^{(\alpha)} U_{i,j}^k = -\frac{1}{h^\alpha} \sum_{l=0}^{M} g_{i-l}^{(\alpha)} U_{l,j}^k, \tag{3.3.10}$$

$$\delta_y^{(\beta)} U_{i,j}^k = -\frac{1}{h^\beta} \sum_{l=0}^{M} g_{j-l}^{(\beta)} U_{i,l}^k. \tag{3.3.11}$$

In turn, the fractional Laplacian and gradient of order (α, β) will be estimated using the operators $\delta_{x,y}^{\alpha,\beta} = \delta_x^{(\alpha)} + \delta_y^{(\beta)}$ and $\widetilde{\nabla}^{\alpha,\beta} = (\delta_x^{(\alpha)}, \delta_y^{(\beta)})$, respectively. Finally, as in the continuous-case scenario, we will agree that

$$\|\widetilde{\nabla}^{\alpha/2,\beta/2} U^k\|_2^2 = \|\delta_x^{(\alpha/2)} U^k\|_2^2 + \|\delta_y^{(\beta/2)} U^k\|_2^2, \quad \forall k \in \{0, 1, \ldots, K\}. \tag{3.3.12}$$

As a consequence of the previous discussion, we will approximate the solutions of (3.2.15) over the space–time domain Ω using the nonlinear finite-difference scheme:

$$\begin{cases} \delta_t U_{i,j}^{k+\frac{1}{2}} = \mu_t V_{i,j}^{k+\frac{1}{2}}, \\ \delta_t V_{i,j}^{k+\frac{1}{2}} = -\gamma \mu_t V_{i,j}^{k+\frac{1}{2}} + \lambda \delta_{x,y}^{\alpha,\beta} \mu_t U_{i,j}^{k+\frac{1}{2}} - \phi_{i,j} \delta_{u,t} \cos U_{i,j}^{k+\frac{1}{2}}, \\ \qquad\qquad + F_{i,j}^{k+\frac{1}{2}} - \delta_{u,t} G(U_{i,j}^{k+\frac{1}{2}}), \end{cases} \tag{3.3.13}$$

with the following discrete initial-boundary conditions:

$$\begin{aligned} \mu_t U_{i,j}^{\frac{1}{2}} &= \psi_1(x_i, y_j), \quad \forall i, j \in \{1, \ldots, M-1\}, \\ \mu_t V_{i,j}^{\frac{1}{2}} &= \psi_2(x_i, y_j), \quad \forall i, j \in \{1, \ldots, M-1\}, \\ U_{i,j}^k = V_{i,j}^k &= 0, \quad \forall k \in \{0, 1, \ldots, K\}, \ \forall (i,j) \in \partial D^2. \end{aligned} \tag{3.3.14}$$

Here, we use ∂D^2 to represent the points of the grid on the boundary of D^2. Moreover, we agree that $F_{i,j}^{k+\frac{1}{2}} = F(x_i, y_j, t_{k+\frac{1}{2}})$ and $t_{k+\frac{1}{2}} = \mu_t t_k$ for each $k = 0, 1, \ldots, K-1$.

Definition 3.7. Let (U, V) be a solution of the finite-difference model (3.3.13). Then,

TESIS TESIS TESIS TESIS TESIS

TESIS TESIS TESIS TESIS TESIS

the *total energy* of the system at time $k \in \{0, 1, \dots, K\}$ is provided by the following:

$$E^k = \frac{1}{2}\|V^k\|_2^2 + \frac{\lambda}{2}\|\widetilde{\nabla}^{\alpha/2,\beta/2}U^k\|_2^2 + \|\phi(1-\cos U^k)\|_1 + \|G(U^k)\|_1. \tag{3.3.15}$$

The next lemma is necessary to demonstrate the energy conservation property of the discrete system (3.3.13). For briefness, we will use U and V to represent sequences $(U^k)_{k=0}^K$ and $(V^k)_{k=0}^K$, respectively, in $\mathcal{V}_h$.

Lemma 3.8 (Macías-Díaz [12]). *If $\alpha, \beta \in (1, 2]$ and $U, V \in \mathcal{V}_h$, then*

$$\begin{aligned} \langle -\delta_x^{(\alpha)}U, V\rangle &= \left\langle \delta_x^{(\alpha/2)}U, \delta_x^{(\alpha/2)}V \right\rangle = \langle U, -\delta_x^{(\alpha)}V\rangle, \\ \langle -\delta_y^{(\beta)}U, V\rangle &= \left\langle \delta_y^{(\beta/2)}U, \delta_y^{(\beta/2)}V \right\rangle = \langle U, -\delta_y^{(\beta)}V\rangle. \end{aligned} \tag{3.3.16}$$

Theorem 3.9. *Let (U, V) be a solution of the discrete system (3.3.13) subject to the initial-boundary conditions (3.3.14). Then,*

$$\delta_t E^k = -\gamma\|\delta_t u^k\|_2^2 + \left\langle F^{k+\frac{1}{2}}, \delta_t U^{k+\frac{1}{2}} \right\rangle. \tag{3.3.17}$$

As a consequence, the discrete system is conservative when $\gamma = 0$ and $F \equiv 0$.

Proof. We start the proof by taking the inner product on both sides of the second equation in (3.3.13) with $\delta_t U^k$ and substitute the first equation in the term multiplied by γ. In this way, we obtain the following expression:

$$\begin{aligned} \left\langle \delta_t V^{k+\frac{1}{2}}, \delta_t U^{k+\frac{1}{2}} \right\rangle &= -\gamma\|\delta_t U^{k+\frac{1}{2}}\|_2^2 + \lambda\left\langle \delta_x^{(\alpha)}\mu_t U^{k+\frac{1}{2}} + \delta_y^{(\beta)}\mu_t U^{k+\frac{1}{2}}, \delta_t U^{k+\frac{1}{2}} \right\rangle, \\ &- \left\langle \phi\delta_{u,t}\left[1-\cos U^{k+\frac{1}{2}}\right], \delta_t U^{k+\frac{1}{2}} \right\rangle - \left\langle \delta_{u,t}G(U^{k+\frac{1}{2}}), \delta_t U^{k+\frac{1}{2}} \right\rangle, \\ &+ \left\langle F^{k+\frac{1}{2}}, \delta_t U^{k+\frac{1}{2}} \right\rangle \end{aligned} \tag{3.3.18}$$

for each $k = 0, 1, \dots, K-1$. Next, we will calculate each of the terms appearing in Equation (3.3.18). First, notice that the term on the left-hand side can be simplified using the first identity of the finite-difference scheme. In that way, obtain the following:

$$\begin{aligned} \left\langle \delta_t V^{k+\frac{1}{2}}, \delta_t U^{k+\frac{1}{2}} \right\rangle &= \left\langle \delta_t V^{k+\frac{1}{2}}, \mu_t V^{k+\frac{1}{2}} \right\rangle = \frac{1}{2\tau}\left\langle V^{k+1} - V^k, V^{k+1} + V^k \right\rangle, \\ &= \frac{1}{2\tau}\left(\|V^{k+1}\|_2^2 - \|V^k\|_2^2\right) = \frac{1}{2}\delta_t\|V^{k+\frac{1}{2}}\|_2^2, \quad \forall k = 0, 1, \dots, K-1. \end{aligned} \tag{3.3.19}$$

TESIS TESIS TESIS TESIS TESIS

TESIS TESIS TESIS TESIS TESIS

We proceed to calculate the second term on the right-hand side of Equation (3.3.18). In this case, we employ the properties of fractional-centered differences to obtain the following:

$$\begin{aligned}\left\langle \delta_x^{(\alpha)} \mu_t U^{k+\frac{1}{2}}, \delta_t U^{k+\frac{1}{2}} \right\rangle &= \frac{1}{2\tau} \left\langle \delta_x^{(\alpha)} \left(U^{k+1} + U^k \right), U^{k+1} - U^k \right\rangle, \\ &= -\frac{1}{2\tau} \left(\|\delta_x^{(\alpha/2)} U^{k+1}\|_2^2 - \|\delta_x^{(\alpha/2)} U^k\|_2^2 \right), \\ &= -\frac{1}{2} \delta_t \|\delta_x^{(\alpha/2)} U^{k+\frac{1}{2}}\|_2^2 \end{aligned} \tag{3.3.20}$$

for each $k = 0, 1, \ldots, K-1$. In a similar way, we can obtain an equivalent expression for the term $\left\langle \delta_x^{(\alpha)} \mu_t U^{k+\frac{1}{2}}, \delta_t U^{k+\frac{1}{2}} \right\rangle$. Next, we simplify the third and fourth terms on the right-hand side of (3.3.18). As a consequence, we obtain the following formulas:

$$\left\langle \phi \delta_t \left[1 - \cos U^{k+\frac{1}{2}} \right], \delta_t U^{k+\frac{1}{2}} \right\rangle = \delta_t \|\phi(1 - \cos U^k)\|_1, \tag{3.3.21}$$

$$\left\langle \delta_{u,t} G(U^{k+\frac{1}{2}}), \delta_t U^{k+\frac{1}{2}} \right\rangle = \delta_t \|G(U^k)\|_1. \tag{3.3.22}$$

Using (3.3.19), (3.3.20), and these last identities, together with some algebraic manipulations, we reach the conclusion of this theorem. ■

3.4 Numerical Properties

The purpose of this section is to establish the most important numerical properties of the discrete model presented in this work. More precisely, we will establish the second-order consistency of the scheme, the property of conditional stability, and the convergence os the second order in both space and time.

To prove the consistency, numerical stability, and convergence of the method we define the continuous operators $\mathcal{L}_1$ and $\mathcal{L}_2$ as follows:

$$\mathcal{L}_1(u, v) = \frac{\partial v}{\partial t} + \gamma \frac{\partial u}{\partial t} - \lambda \Delta^{\alpha,\beta} u + \phi(\mathbf{x}) \sin u - F(\mathbf{x}, t) - G'(u), \tag{3.4.1}$$

$$\mathcal{L}_2(u, v) = \frac{\partial u}{\partial t} - v, \tag{3.4.2}$$

where $\mathbf{x} = (x, y)$. These operators correspond to the residual forms of the first and second equations in (3.2.15). For the numerical approximations $U_{i,j}^k$ and $V_{i,j}^k$, the discrete

TESIS TESIS TESIS TESIS TESIS

TESIS TESIS TESIS TESIS TESIS

operators L_1 and L_2 are defined as follows:

$$L_1(U_{i,j}^k, V_{i,j}^k) = \delta_t V_{i,j}^k + \gamma \mu_t V_{i,j}^k - \lambda \delta_{x,y}^{\alpha,\beta} \mu_t U_{i,j}^k - \phi_{i,j} \delta_{u,t} \cos U_{i,j}^k - \delta_{u,t} G(U_{i,j}^k) - F_{i,j}^{k+\frac{1}{2}}, \tag{3.4.3}$$

$$L_2(U_{i,j}^k, V_{i,j}^k) = \delta_t U_{i,j}^k - \mu_t V_{i,j}^k. \tag{3.4.4}$$

These operators mirror the structure of (3.4.1) and (3.4.2), representing the residuals of the equations in the discretized system (3.3.13).

The following result summarizes the consistency properties of the finite-difference scheme (3.3.13) under suitable regularity assumptions.

Theorem 3.10 (Consistency)**.** *Assume $u \in \mathcal{C}_{x,y,t}^{4,4,3}\left(\overline{\Omega}\right)$ and $v \in \mathcal{C}_{x,y,t}^{3,3,2}\left(\overline{\Omega}\right)$. Then, there exists a constant $C > 0$, independent of h and τ, such that for all $i, j \in \{0, \ldots, M\}$ and $k \in \{0, \ldots, N\}$,*

$$\left|\left(\mathcal{L}_1 + \mathcal{L}_2\right)(u, v) - \left(L_1 + L_2\right)\left(U_{i,j}^k, V_{i,j}^k\right)\right| \leq C\left(h^2 + \tau^2\right). \tag{3.4.5}$$

Proof. Applying Taylor's theorem to u and v at $(x_i, y_j, t_{k+\frac{1}{2}})$, we derive the following truncation error bounds for the discrete operators, where $C_1, \ldots, C_7$ depend on the maximum norms of the fourth-order spatial and third-order temporal derivatives of u and v:

$$\begin{aligned}
\left|\delta_t U_{i,j}^k - \partial_t u(x_i, y_j, t_{k+\frac{1}{2}})\right| &\leq C_1 \tau^2, \\
\left|\delta_t V_{i,j}^k - \partial_t v(x_i, y_j, t_{k+\frac{1}{2}})\right| &\leq C_2 \tau^2, \\
\left|\mu_t V_{i,j}^k - v(x_i, y_j, t_{k+\frac{1}{2}})\right| &\leq C_3 \tau^2, \\
\left|\delta_{u,t} \cos U_{i,j}^k - \sin u(x_i, y_j, t_{k+\frac{1}{2}})\right| &\leq C_4 \tau^2, \\
\left|\delta_{u,t} G(U_{i,j}^k) - G'(u(x_i, y_j, t_{k+\frac{1}{2}}))\right| &\leq C_5 \tau^2, \\
\left|F_{i,j}^{k+\frac{1}{2}} - F(x_i, y_j, t_{k+\frac{1}{2}})\right| &\leq C_6 \tau^2, \\
\left|\delta_{x,y}^{\alpha,\beta} \mu_t U_{i,j}^k - \Delta^{\alpha,\beta} u(x_i, y_j, t_{k+\frac{1}{2}})\right| &\leq C_7 (h^2 + \tau^2).
\end{aligned} \tag{3.4.6}$$

Summing these inequalities via the triangle inequality and defining

$$C = \sum_{i=1}^{7} C_i + (\gamma - 1) C_3 + (\lambda - 1) C_7, \tag{3.4.7}$$

we obtain (3.4.5). Under the regularity assumptions of this theorem, it is obvious that

TESIS TESIS TESIS TESIS TESIS

TESIS TESIS TESIS TESIS TESIS

the constant C is independent of both h and τ. ■

The goal of the following discussion is to establish the properties of stability and convergence. To that end, several lemmas will be required.

Lemma 3.11. *Let $G \in \mathcal{C}^2(\mathbb{R})$ with $G'' \in \mathcal{L}^\infty(\mathbb{R})$. Suppose that sequences $(U_a^k)_{k=0}^N$, $(U_b^k)_{k=0}^N$, and $(V_a^k)_{k=0}^N$, $(V_b^k)_{k=0}^N \subseteq \mathbb{R}^{(M-1)\times(M-1)}$ satisfy*

$$\begin{aligned} \delta_t U_a^{k+\frac{1}{2}} &= \mu_t V_a^{k+\frac{1}{2}}, \\ \delta_t U_b^{k+\frac{1}{2}} &= \mu_t V_b^{k+\frac{1}{2}}. \end{aligned} \tag{3.4.8}$$

Define the error quantities as $\varepsilon_u^k = U_a^k - U_b^k$, $\varepsilon_v^k = V_a^k - V_b^k$, and $\widetilde{G}^k = \delta_{u_a,t}G(U_a^k) - \delta_{u_b,t}G(U_b^k)$. Then, there exist positive constants C_1, C_2, C_3 depending only on G, such that

$$\left|\langle \widetilde{G}^k, \delta_t \varepsilon_u^k \rangle\right| \leq C_1 \left(\|\varepsilon_u^{k+1}\|_2^2 + \|\varepsilon_u^k\|_2^2 + \|\varepsilon_v^{k+1}\|_2^2 + \|\varepsilon_v^k\|_2^2 \right), \tag{3.4.9}$$

$$\left| 2\tau \sum_{k=0}^{n-1} \langle \widetilde{G}^k, \delta_t \varepsilon_u^k \rangle \right| \leq C_2 \|\varepsilon_u^0\|_2^2 + C_3 \tau \sum_{k=0}^{n} \|\varepsilon_v^k\|_2^2. \tag{3.4.10}$$

Proof. Let $C_0 = \|G''\|_\infty$. Using the mean value theorem, we readily establish that

$$|\widetilde{G}_{i,j}^k| \leq C_0 \left(|(\varepsilon_u^{k+1})_{i,j}| + |(\varepsilon_u^k)_{i,j}| \right) \quad \forall (i,j) \in \{1, \ldots, M-1\}. \tag{3.4.11}$$

Applying the Cauchy–Schwarz inequality, we obtain the following:

$$|\langle \widetilde{G}^k, \delta_t \varepsilon_u^{k+\frac{1}{2}} \rangle| \leq \frac{C_0}{4} \left(\|\varepsilon_u^{k+1}\|_2^2 + \|\varepsilon_u^k\|_2^2 + \|\varepsilon_v^{k+1}\|_2^2 + \|\varepsilon_v^k\|_2^2 \right). \tag{3.4.12}$$

Now, inequality (3.4.9) readily follows with $C_1 = \frac{C_0}{4}$. To derive the cumulative bound (3.4.10), observe that the relationship $\delta_t \varepsilon_u^{k+\frac{1}{2}} = \mu_t \varepsilon_v^{k+\frac{1}{2}}$ implies the following:

$$\varepsilon_u^n = \varepsilon_u^0 + \frac{\tau}{2} \sum_{k=0}^{n-1} \left(\varepsilon_v^{k+1} + \varepsilon_v^k \right). \tag{3.4.13}$$

Applying the Cauchy–Schwarz inequality again to (3.4.13) and using $(a+b)^2 \leq 2a^2 + 2b^2$,

TESIS TESIS TESIS TESIS TESIS

TESIS TESIS TESIS TESIS TESIS

we obtain the following inequality:

$$\|\varepsilon_u^n\|_2^2 \leq 2\|\varepsilon_u^0\|_2^2 + 2T\tau \sum_{k=0}^{n} \|\varepsilon_v^k\|_2^2. \tag{3.4.14}$$

Substitute (3.4.14) into (3.4.9), multiply it by 2τ, and sum over $k = 0, \ldots, n-1$. In that way, we can readily derive the inequality as follows:

$$\begin{aligned} 2\tau C_1 \sum_{k=0}^{n-1} \Big(\|\varepsilon_u^{k+1}\|_2^2 + \|\varepsilon_u^k\|_2^2 + \|\varepsilon_v^{k+1}\|_2^2 + \|\varepsilon_v^k\|_2^2 \Big), \\ \leq C_1 \sum_{k=0}^{n-1} \Bigg[8T\|\varepsilon_u^0\|_2^2 + 8T\tau^2 \sum_{i=0}^{k+1} \|\varepsilon_v^i\|_2^2, \\ + 2\tau \left(\|\varepsilon_v^{k+1}\|_2^2 + \|\varepsilon_v^k\|_2^2 \right) \Bigg]. \end{aligned} \tag{3.4.15}$$

Realizing that $\tau^2 \sum_{i=0}^{n+1} \|\varepsilon_v^i\|_2^2 \leq T\tau \sum_{i=0}^{n+1} \|\varepsilon_v^i\|_2^2$ and combining like terms yields, we derive (3.4.10) by letting $C_2 = 8NTC_1$ and $C_3 = (8T^2 + 4)C_1$. ■

The following technical result was taken from the literature. It is a discrete form of the well-known Gronwall inequality.

Lemma 3.12 (Pen-Yu [62]). *Let $(\omega^n)_{n=0}^N$, $(\rho^n)_{n=0}^N$ be non-negative sequences satisfying the following:*

$$\omega^n \leq \rho^n + C\tau \sum_{k=0}^{n-1} \omega^k \quad \forall n \in \{0, \ldots, N\} \tag{3.4.16}$$

for some $C \geq 0$. Then, $\omega^n \leq \rho^n e^{Cn\tau}$ for all $n \in \{0, \ldots, N\}$.

In the next result, constants C_2 and C_3 are the same as in Lemma 3.11, while C_1 is redefined as $C_1 = \max\{\|\phi\|_\infty, \|G''\|_\infty\}$. In the following result, we let $\psi_a = ((\psi_1)_a, (\psi_2)_a)$ and $\psi_b = ((\psi_1)_b, (\psi_2)_b)$ denote two distinct sets of initial conditions for the system (3.3.13).

Theorem 3.13 (Numerical Stability). *Let $G \in \mathcal{C}^2(\mathbb{R})$ with $G'' \in \mathcal{L}^\infty(\mathbb{R})$, and assume the temporal step size $\tau > 0$ satisfies the following condition:*

$$(2T + C_3)\tau < 1. \tag{3.4.17}$$

For the two sets of initial conditions ψ_a, ψ_b, we let $(U_a^k, V_a^k)_{k=0}^N$ and $(U_b^k, V_b^k)_{k=0}^N$ be the corresponding solutions of the system (3.3.13). Define $\widetilde{\cos}^k = \delta_{u_a,t} \cos(U_a^k) - \delta_{u_b,t} \cos(U_b^k)$.

TESIS TESIS TESIS TESIS TESIS

TESIS TESIS TESIS TESIS TESIS

Then, there exist constants $C_4, C_5 > 0$, such that

$$\|\varepsilon_u^n\|_2^2 + \|\varepsilon_v^n\|_2^2 + \lambda\|\widetilde{\nabla}^{\alpha/2,\beta/2}\varepsilon_u^n\|_2^2 \leq C_4\left(\|\varepsilon_u^0\|_2^2 + \|\varepsilon_v^0\|_2^2 + \lambda\|\widetilde{\nabla}^{\alpha/2,\beta/2}\varepsilon_u^0\|_2^2\right)e^{C_5 n\tau}. \quad (3.4.18)$$

Proof. Note that ε_u^k and ε_v^k satisfy the following:

$$\delta_t\varepsilon_u^k = \mu_t\varepsilon_v^k, \quad (3.4.19)$$

$$\delta_t\varepsilon_v^k = -\gamma\delta_t\varepsilon_u^k + \lambda\delta_{x,y}^{\alpha,\beta}\mu_t\varepsilon_u^k + \phi\widetilde{\cos}^k + \widetilde{G}^k. \quad (3.4.20)$$

Taking the inner product of $\delta_t\varepsilon_u^k$ with both sides of (3.4.20), summing from 0 to n, and applying the discrete energy identities from Theorem 3.9 along with Lemma 3.11 we obtain the following:

$$\begin{aligned}&\|\varepsilon_v^n\|_2^2 + \lambda\|\widetilde{\nabla}^{\alpha/2,\beta/2}\varepsilon_u^n\|_2^2 \\ &\qquad \leq \|\varepsilon_v^0\|_2^2 + \lambda\|\widetilde{\nabla}^{\alpha/2,\beta/2}\varepsilon_u^0\|_2^2 + C_2\|\varepsilon_u^0\|_2^2 + C_3\tau\sum_{k=0}^{n}\|\varepsilon_v^k\|_2^2.\end{aligned} \quad (3.4.21)$$

Defining the composite error $\varepsilon^k = \|\varepsilon_u^k\|_2^2 + \|\varepsilon_v^k\|_2^2 + \lambda\|\widetilde{\nabla}^{\alpha/2,\beta/2}\varepsilon_u^k\|_2^2$, we obtain the following:

$$\varepsilon^n \leq (2 + C_2)\varepsilon^0 + (2T + C_3)\tau\sum_{k=0}^{n}\varepsilon^k. \quad (3.4.22)$$

We apply Lemma 3.12 with

$$\begin{aligned}C_4 &= \frac{2 + C_2}{1 - (2T + C_3)\tau}, \\ C_5 &= \frac{2T + C_3}{1 - (2T + C_3)\tau}.\end{aligned} \quad (3.4.23)$$

This completes the proof. ∎

Finally, we establish the property of convergence.

Theorem 3.14 (Convergence). *Let $u \in \mathcal{C}^{4,4,3}(\overline{\Omega})$ and $v \in \mathcal{C}^{3,3,2}(\overline{\Omega})$ be exact solutions of system (3.2.15), with $G \in \mathcal{C}^2(\mathbb{R})$ satisfying $G'' \in L^\infty(\mathbb{R})$. Let $(U^k)_{k=0}^n$ and $(V^k)_{k=0}^N$ denote the numerical solutions of system (3.3.13) with initial boundary conditions ψ.*

TESIS TESIS TESIS TESIS TESIS

TESIS TESIS TESIS TESIS TESIS

We define the approximation errors as follows:

$$\begin{aligned} \varepsilon_u^k &= u(t_k) - U^k, \\ \varepsilon_v^k &= v(t_k) - V^k. \end{aligned} \tag{3.4.24}$$

If the inequality

$$(8C_1T^2 + 2T + 6)\tau < 1 \tag{3.4.25}$$

is satisfied, then there exists a constant $C > 0$, independent of h and τ, such that

$$\max_{0\leq k\leq N} \left(\|\varepsilon_u^k\|_2 + \|\varepsilon_v^k\|_2 \right) \leq C(\tau^2 + h^2). \tag{3.4.26}$$

Proof. Let $R_{i,j}^k$ and $S_{i,j}^k$ denote the local truncation errors at grid point (x_i, y_j, t_k). From Theorem 3.10, there exists $C_{RS} > 0$, such that

$$\|R^k\|_2 + \|S^k\|_2 \leq C_{RS}(\tau^2 + h^2), \quad 0 \leq k \leq N. \tag{3.4.27}$$

Notice that the approximation errors satisfy

$$\delta_t \varepsilon_u^{k+\frac{1}{2}} = \mu_t \varepsilon_v^{k+\frac{1}{2}} + R^{k+\frac{1}{2}}, \tag{3.4.28}$$

$$\delta_t \varepsilon_v^{k+\frac{1}{2}} = -\gamma \delta_t \varepsilon_u^{k+\frac{1}{2}} + \lambda \delta_{x,y}^{\alpha,\beta} \mu_t \varepsilon_u^{k+\frac{1}{2}} + \phi \widetilde{\cos}^k + \widetilde{G}^k + S^{k+\frac{1}{2}}. \tag{3.4.29}$$

Following arguments similar to those used in the proof of Theorem 3.13, we establish the following:

$$\|\varepsilon_v^n\|_2^2 + \|\varepsilon_u^n\|_2^2 \leq C_2\tau \sum_{k=0}^{n} \left(\|\varepsilon_v^k\|_2^2 + \|\varepsilon_u^k\|_2^2 \right) + C_3(\tau^4 + h^4), \tag{3.4.30}$$

where $C_2 = 8C_1T^2 + 2T + 6$ and $C_3 = 5TC_{RS}^2$. Applying Lemma 3.12 with $\omega^n = \|\varepsilon_v^n\|_2^2 + \|\varepsilon_u^n\|_2^2$ and $\rho^n = C_2(\tau^4 + h^4)$, we can readily obtain that

$$\max_{0\leq k\leq N} \left(\|\varepsilon_u^k\|_2^2 + \|\varepsilon_v^k\|_2^2 \right) \leq C_4 e^{C_5T}(\tau^4 + h^4), \tag{3.4.31}$$

with suitable positive constants C_4 and C_5. By taking square roots and letting $C = \sqrt{C_4 e^{C_5T}}$, we readily obtain the inequality (3.4.26). ■

TESIS TESIS TESIS TESIS TESIS

TESIS TESIS TESIS TESIS TESIS

3.5 Simulations

The purpose of the present section is to provide some computer simulations that illustrate the capability of the scheme to preserve the total energy and explore how solutions to (3.2.15) behave under different fractional orders, α and β. Our simulations were obtained using the MATLAB code of our finite-difference scheme based on a fixed-point approach. All simulations were conducted on a Lenovo LOQ 15ARP9 laptop equipped with an AMD Ryzen 7 7435HS 8-core/16-thread processor, paired with an NVIDIA Laptop GPU, featuring 3072 CUDA cores and 8 GB GDDR6 VRAM (128-bit interface). The system had 24 GB DDR5-4800 RAM and a 512 GB NVMe SSD.

To verify our numerical method's accuracy, we considered the following analytical solution:

$$u(x,y,t) = \cos(\pi x)\cos(\pi y)\cos(t), \tag{3.5.1}$$

$$v(x,y,t) = -\cos(\pi x)\cos(\pi y)\sin(t), \tag{3.5.2}$$

on $\overline{\Omega} = \left[-\frac{1}{2},\frac{1}{2}\right] \times \left[-\frac{1}{2},\frac{1}{2}\right] \times [0,5]$ with $\phi(x,y) = 1$, $\alpha = \beta = 2$, $\gamma = 0$, $\lambda = \frac{1}{2\pi^2}$, $F(x,y,t) = \sin\left(\cos(\pi x)\cos(\pi y)\cos(t)\right)$, and $G \equiv 0$. Initial conditions correspond to (3.5.1) and (3.5.2).

Figures 3.1 and 3.2 compare analytical and numerical solutions at $t = 0.8$ and $t = 3$ using the spatial step $h = 0.025$ and the time step $\tau = 0.1$. Both solutions show strong visual agreement at these times. Figure 3.3 confirms this by plotting the L^2-error over time, which remains below 1.6×10^{-2} and peaks near the simulation's end.

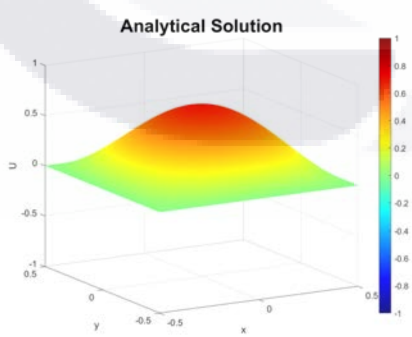

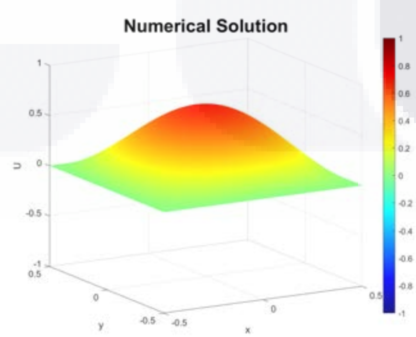

(**a**) (**b**)

Figure 3.1: (**a**) Analytical solution (3.5.1) at $t = 0.8$. (**b**) Numerical approximation ($h = 0.025$ and $\tau = 0.1$).

TESIS TESIS TESIS TESIS TESIS

TESIS TESIS TESIS TESIS TESIS

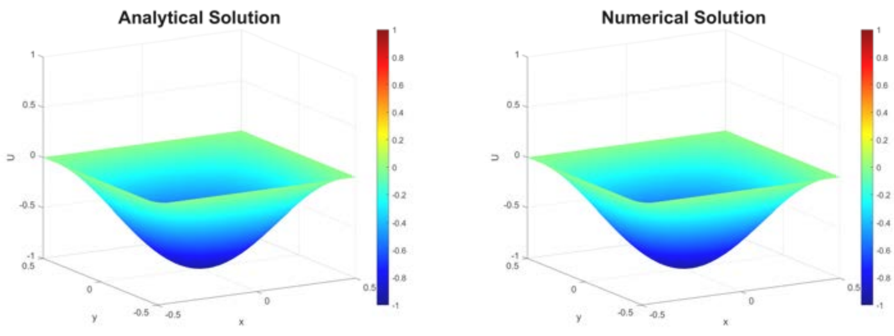

(**a**) (**b**)

Figure 3.2: (**a**) Analytical solution (3.5.1) at $t = 3$. (**b**) Numerical approximation ($h = 0.025$ and $\tau = 0.1$).

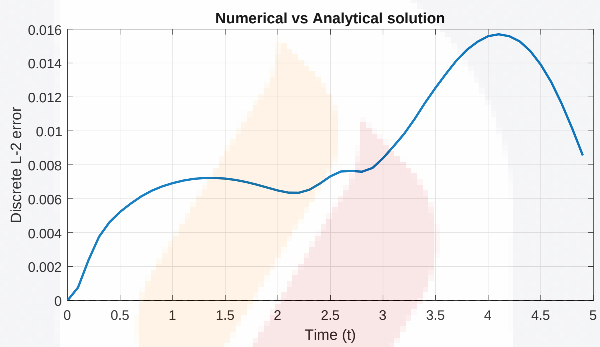

Figure 3.3: L^2-error between the analytical solution (3.5.1) and numerical approximation ($h = 0.025$, $\tau = 0.1$).

3.5.1 Impact of Fractional Orders α and β

Figures 3.4–3.6 demonstrate how changing the fractional orders α and β affects solution behavior. The most noticeable difference from the integer-order case is the wave amplitude: for $\alpha = \beta = 1.1$ and 1.5 (Figures 3.4 and 3.5), amplitudes exceed 8, but decrease toward the non-fractional amplitude of 1 as α, β tend to 2 (Figure 3.6). We also observe waveform deformations near the wave center when α and β deviate from 2 (e.g., panels (d) in Figures 3.4 and 3.5). These resemble deformations in vibrating membrane problems, contrasting with the integer-order solutions in Figures 3.1 and 3.2. As expected, deformations diminish as orders approach integer values.

TESIS TESIS TESIS TESIS TESIS

TESIS TESIS TESIS TESIS TESIS

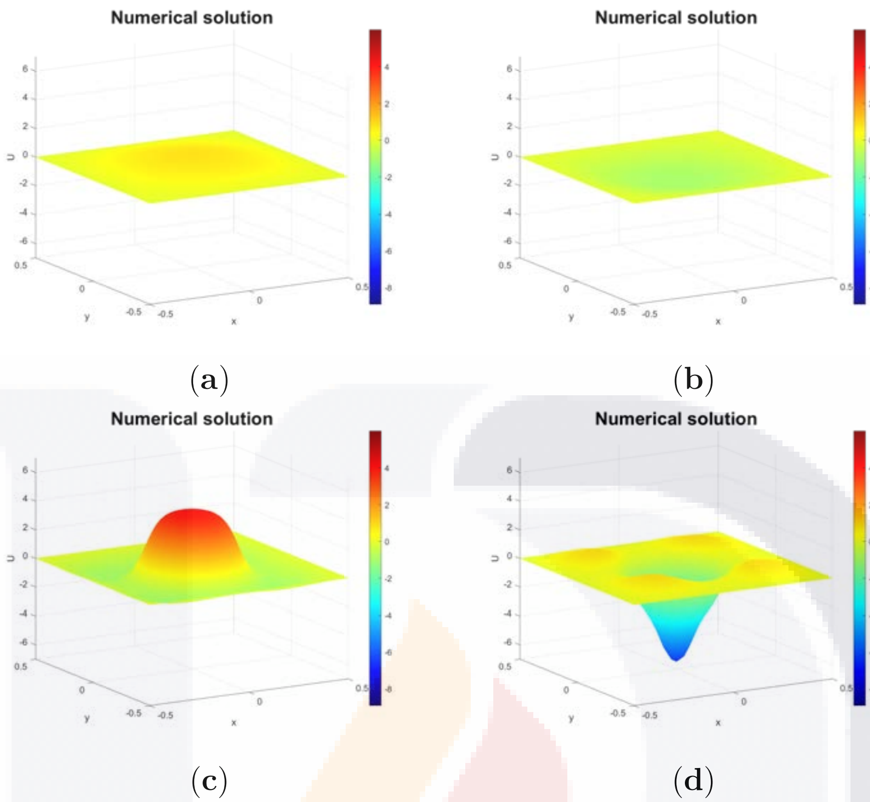

Figure 3.4: Solution profiles for $\alpha = \beta = 1.1$ at (**a**) $t = 1$, (**b**) $t = 3$, (**c**) $t = 10$, and (**d**) $t = 14$ ($h = 0.025$ and $\tau = 0.1$).

TESIS TESIS TESIS TESIS TESIS

TESIS TESIS TESIS TESIS TESIS

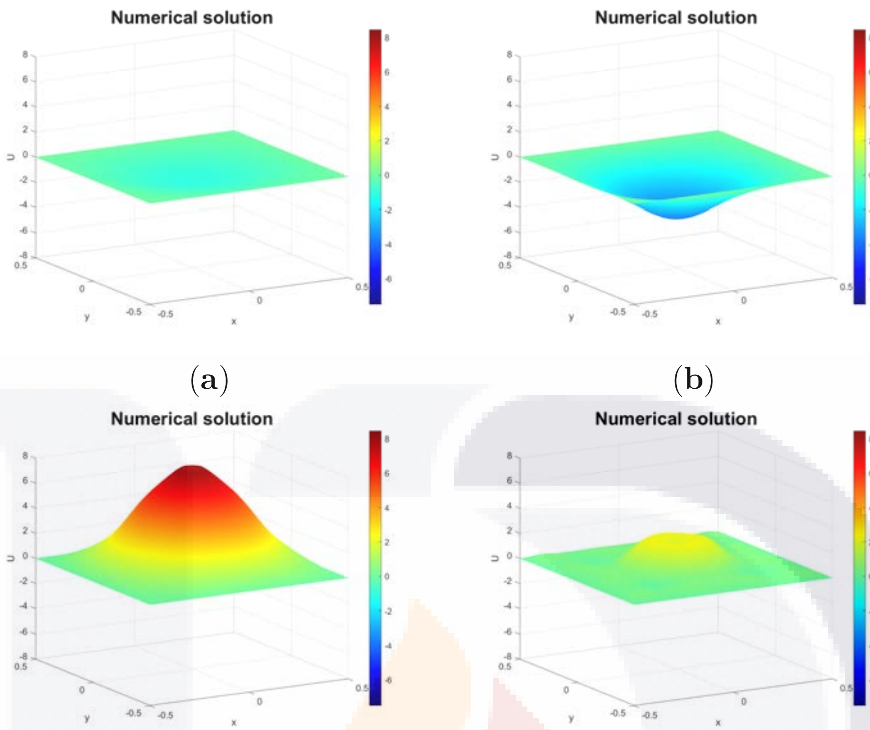

(**a**) (**b**)

(**c**) (**d**)

Figure 3.5: Solution profiles for $\alpha = \beta = 1.5$ at (**a**) $t = 3$, (**b**) $t = 10$, (**c**) $t = 15$, and (**d**) $t = 25$ ($h = 0.025$ and $\tau = 0.1$).

TESIS TESIS TESIS TESIS TESIS

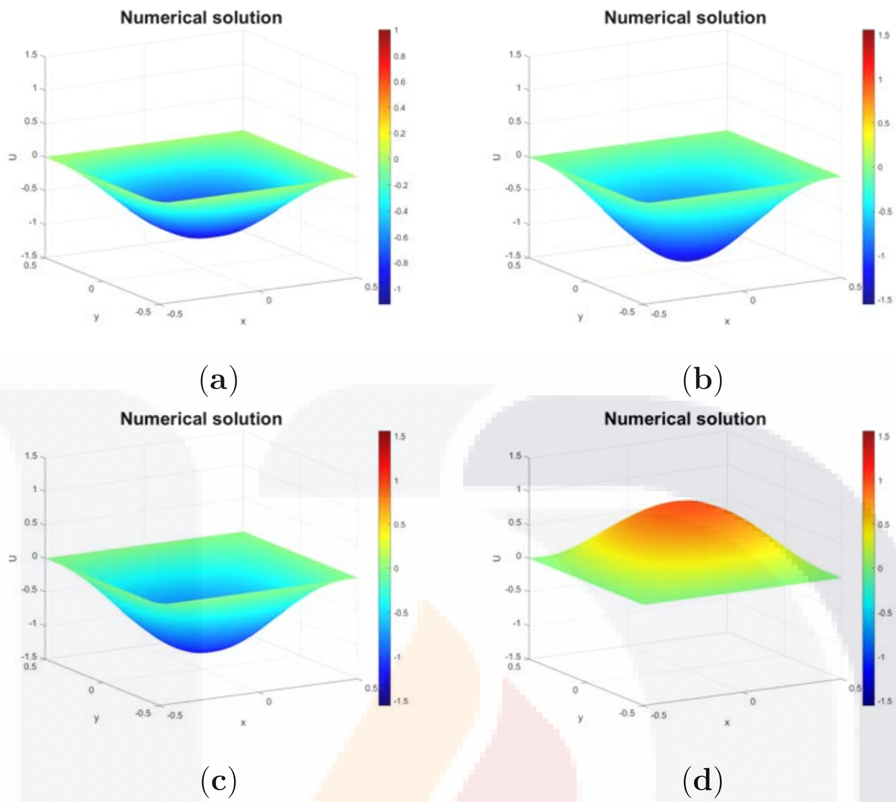

Figure 3.6: Solution profiles for $\alpha = \beta = 1.9$ at (**a**) $t = 3$, (**b**) $t = 10$, (**c**) $t = 15$, and (**d**) $t = 25$ ($h = 0.025$ and $\tau = 0.1$).

3.5.2 Evolution of a Circular Ring Soliton

In the second scenario, we examine a localized, radially symmetric wave ("pulson") on the spatial domain $D = [-4, 4]$ with parameters $\gamma = 0$ (conservative case), $\gamma = 0.5$ (dissipative case), and $\lambda = 1$, and no external forcing ($F \equiv 0$, $G \equiv 0$). The initial conditions are as follows:

$$\psi_1(x, y) = 2\arctan\left(e^{3-5\sqrt{x^2+y^2}}\right), \tag{3.5.3}$$

$$\psi_2(x, y) = 0, \tag{3.5.4}$$

as in [63]. We compare three different grid choices:

6. Long-time wave evolution: $h = \tau = 0.1$ over $0 \leq t \leq 30$,

7. Conservation of energy: $h = 0.1$, $\tau = 0.005$ over $0 \leq t \leq 1.5$,

8. Dissipation of energy: $h = 0.1$, $\tau = 0.01$ over $0 \leq t \leq 5$.

TESIS TESIS TESIS TESIS TESIS

In the first two experiments, we compare solutions with fractional orders $\alpha = \beta = 1.5$ against the integer case $\alpha = \beta = 2$, while the third experiment examines both fractional orders (1.1, 1.4, and 1.7) and the integer order 2. Figure 3.7 shows that at $t = 0$, the ring soliton shrinks similarly for both fractional and integer solutions. However, different derivative orders produce distinct oscillation patterns by $t = 5$ and $t = 10$ (panels c–f). These differences diminish by $t = 20$, where both solutions develop nearly identical structures (panels g–h). Despite variations in oscillation formation and radiation patterns, the overall evolution aligns with observations in [64, 65]. Physically, the intermediate divergence reflects the stronger non-local restoring force produced by lower fractional orders, which modifies the effective wave speed and alters the radiation emitted as the soliton contracts; at long times the system relaxes toward a common attractor determined by the potential well rather than by the fractional geometry of the operator, consistent with the energy-preserving character established in Theorem 3.9.

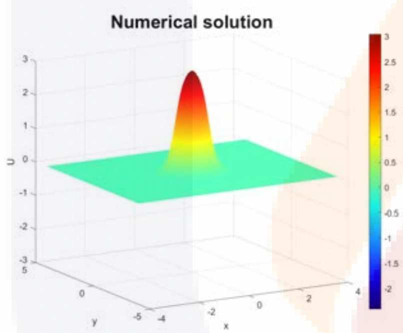

(**a**) $\alpha = \beta = 1.5$ at $t = 0$

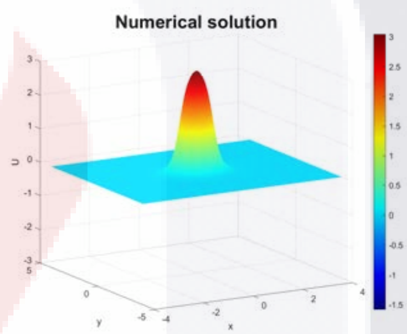

(**b**) $\alpha = \beta = 2.0$ at $t = 0$

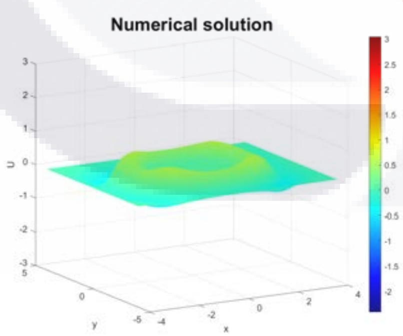

(**c**) $\alpha = \beta = 1.5$ at $t = 5$

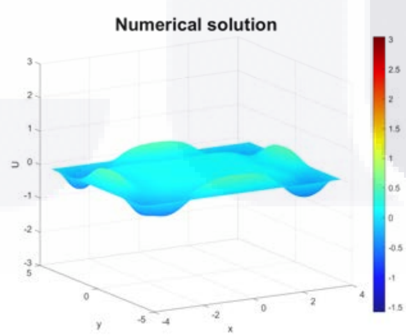

(**d**) $\alpha = \beta = 2.0$ at $t = 5$

TESIS TESIS TESIS TESIS TESIS

TESIS TESIS TESIS TESIS TESIS

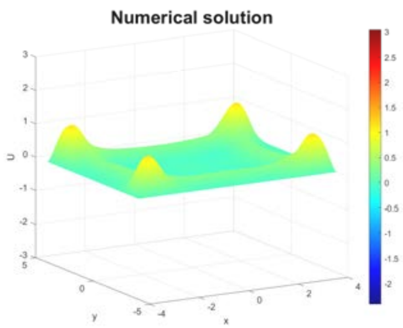

(**e**) $\alpha = \beta = 1.5$ at $t = 10$

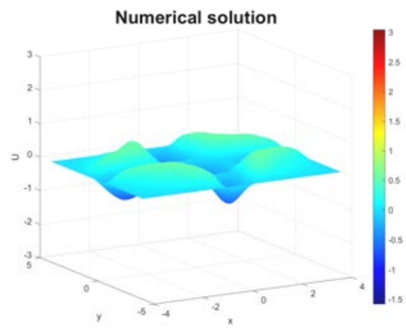

(**f**) $\alpha = \beta = 2.0$ at $t = 10$

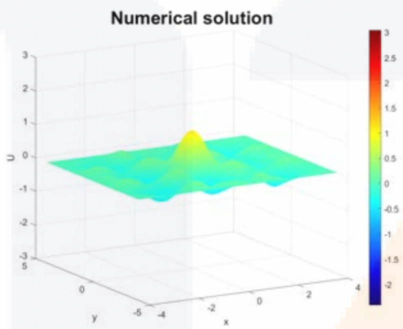

(**g**) $\alpha = \beta = 1.5$ at $t = 20$

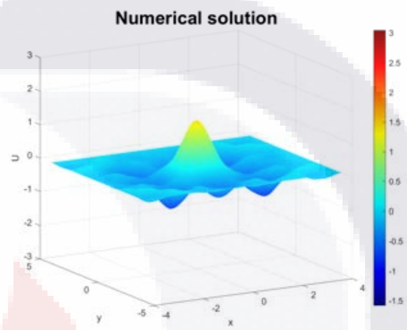

(**h**) $\alpha = \beta = 2.0$ at $t = 20$

Figure 3.7: Numerical profiles at $t = 0, 5, 10, 20$ for (**left**) the fractional order $\alpha = \beta = 1.5$ and (**right**) integer order $\alpha = \beta = 2.0$. All runs use $h = \tau = 0.1$.

Figure 3.8 confirms energy conservation in both cases. For $\alpha = \beta = 1.5$ (panel a), the maximum deviation is approximately 6.1×10^{-3}, while for $\alpha = \beta = 2$ (panel b), it reaches 2.9×10^{-3}. Figure 3.9 shows the dissipative case with $\gamma = 0.5$. Together, Figures 3.8 and 3.9 demonstrate that α and β do not affect energy behavior, they only γ control energy conservation/dissipation, confirming Theorem 3.9.

TESIS TESIS TESIS TESIS TESIS

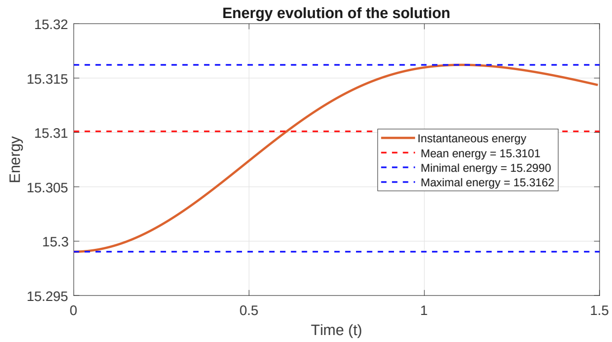

(**a**) $\alpha = \beta = 1.5$

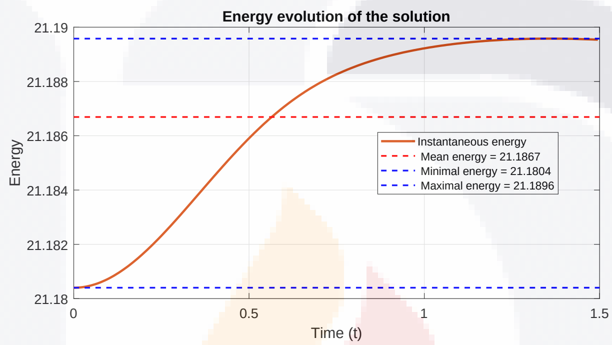

(**b**) $\alpha = \beta = 2.0$

Figure 3.8: Energy versus time for the same runs shown in Figure 3.7, with $\tau = 0.005$ and $h = 0.1$ over $0 \leq t \leq 1.5$.

TESIS TESIS TESIS TESIS TESIS

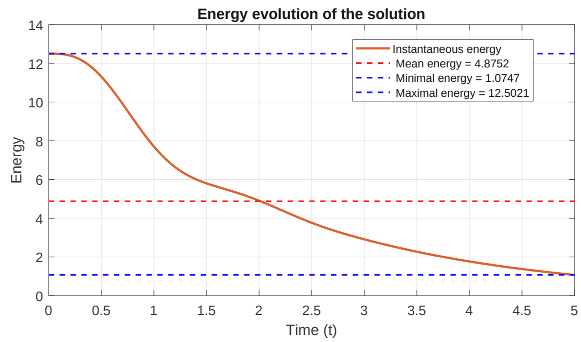

(a) $\alpha = \beta = 1.1$

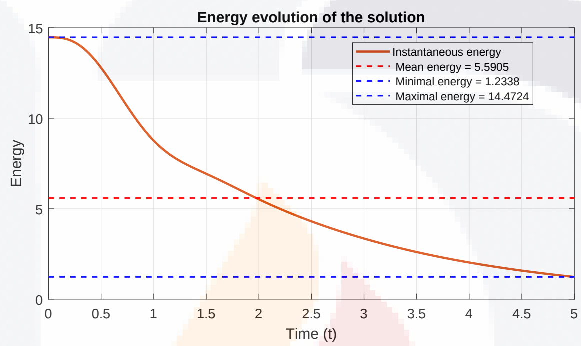

(b) $\alpha = \beta = 1.4$

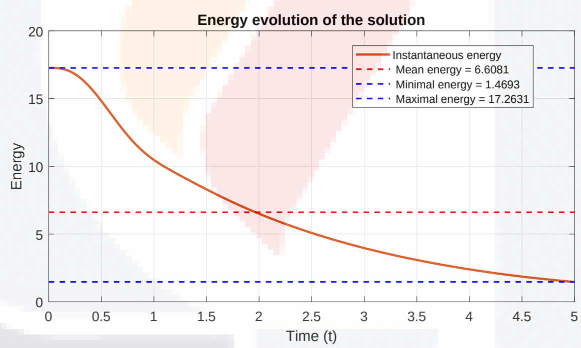

(c) $\alpha = \beta = 1.7$

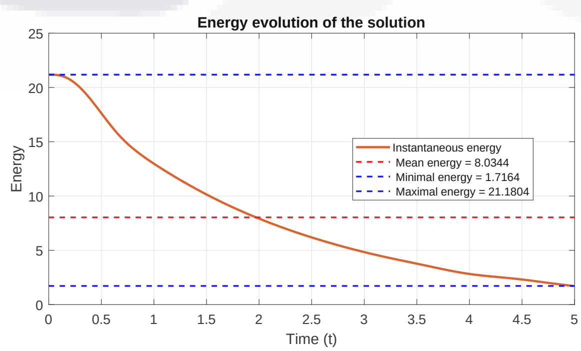

(d) $\alpha = \beta = 2$

Figure 3.9: Energy dissipation for different derivative orders α and β with fixed $\gamma = 0.5$, $\tau = 0.01$, $h = 0.1$, and $0 \leq t \leq 5$.

TESIS TESIS TESIS TESIS TESIS

TESIS TESIS TESIS TESIS TESIS

3.5.3 Numerical Study of Convergence

Before closing this section, we provide a brief numerical experiment to confirm the order of convergence of the scheme. To that end, we consider the setting used in Section 3.5.1 and fix $\alpha = \beta = 1.5$. As an approximate to the exact solution, we employ values of $\tau = 0.0001$ and $h = 0.001$. Under these circumstances, Tables 3.1 and 3.2 provide numerical studies of the convergence of the scheme with respect to space and time, respectively. Notice that the standard convergence rates are, at most, of the second order in space and time in the L^2-norm. These results confirm the conclusion of the theorem on the convergence of the scheme, which states that the finite-difference method proposed in this work has second-order convergence in the L^2-norm.

Table 3.1: Numerical study of the temporal convergence of the finite-difference scheme (3.3.13). Various values for parameters τ and h were employed to that end. We provide the errors in the L^2-norm and the standard convergence rate in time.

	$h = 0.05$		$h = 0.025$	
τ	**Error**	**Rate**	**Error**	**Rate**
$0.1/2^0$	2.8589×10^{-2}	–	1.0034×10^{-2}	–
$0.1/2^1$	8.6063×10^{-3}	1.7320	3.3118×10^{-3}	1.5992
$0.1/2^2$	2.6621×10^{-3}	1.6928	9.9304×10^{-4}	1.7377
$0.1/2^3$	7.5022×10^{-4}	1.8272	2.7521×10^{-4}	1.8513

Table 3.2: Numerical study of the spatial convergence of the finite-difference scheme (3.3.13). Various values for parameters τ and h were employed to that end. We provide the errors in the L^2-norm and the standard convergence rate in space.

	$\tau = 0.05$		$\tau = 0.025$	
h	**Error**	**Rate**	**Error**	**Rate**
$0.05/2^0$	8.6063×10^{-3}	–	2.6621×10^{-3}	–
$0.05/2^1$	3.3118×10^{-3}	1.3777	9.9304×10^{-4}	1.4213
$0.05/2^2$	1.0198×10^{-3}	1.6992	3.7077×10^{-4}	1.7828
$0.05/2^3$	3.3695×10^{-4}	1.5978	1.1811×10^{-4}	1.6503

TESIS TESIS TESIS TESIS TESIS

TESIS TESIS TESIS TESIS TESIS

3.6 Conclusions

In this manuscript, a double space-fractional generalization of the sine-Gordon equation in two spatial dimensions was investigated. The generalization considered in this work uses space-fractional derivatives of the Riesz type in both spatial dimensions, with not necessarily equal orders of differentiation in the interval $(1, 2]$. In our model, a generalized potential was employed, and the sine-Gordon potential function is one of the summands. Suitable initial conditions were considered, and homogeneous Neumann data were imposed as boundary conditions on the spatial domain. Using the properties of Riesz fractional derivatives, we rigorously established that the system is dissipative in the most general case. Moreover, under suitable conditions, the energy of the system is conserved over time. Some corollaries on the regularity of the solutions of the system were obtained as a consequence of the property of the dissipativity of the energy.

Motivated by these analytical results, we proposed a numerical scheme to approximate the solution. The discrete model was obtained using finite differences. To approximate the Riesz fractional operators, we used fractional-order centered differences in space. The methodology is a nonlinear two-step Crank–Nicolson-type scheme that yields second-order approximations in both space and time. Together with the numerical integrator for the mathematical model, we also proposed a discrete form of the energy functional. As in the continuous counterpart, we showed that the discrete energy is dissipative in general, and it is conserved over the discrete time interval under the same assumptions imposed on the mathematical model. Moreover, by using a fixed-point theorem, we proved that the discrete model is always solvable.

From a theoretical point of view, we established the second-order consistency of the scheme in both space and time. The properties of convergence and stability were also proved theoretically using a suitable discrete form of Gronwall's inequality. The uniqueness of the numerical solutions was a consequence of the conditional stability of the scheme. Computationally, the numerical model was implemented using a form of the fixed-point method. Various numerical simulations were carried out in order to assess the validity of some of our theoretical results. For example, we confirmed that the numerical model was dissipative in general and conservative under the theoretical assumptions made in this work. Other simulations considered the integer-order case, and the solutions obtained in this work qualitatively agree with the known solutions for the sine-Gordon equation. For the sake of convenience, the MATLAB code used to produce the simulations of this work is provided in Appendix A at the end of the manuscript.

TESIS TESIS TESIS TESIS TESIS

TESIS TESIS TESIS TESIS TESIS

Before closing this work, we would like to address some interesting comments and limitations of the present work that were noted by some of our reviewers:

- To start with, the case with different fractional orders α and β is mainly mentioned but not deeply explored numerically in the present work. We do not consider this case in light of the fact that the outcomes are qualitatively similar to the case when $\alpha = \beta$. However, it is important to discuss the physical significance and additional challenges of this anisotropy. The classical sine-Gordon equation is usually referred to as certain mechanical systems in quantum mechanics. In that context, the different orders of the fractional derivatives could represent different degrees of elasticity or damping in different directions, affecting the response of the material to external forces. Evidently, this can result in complex dynamics that merit attention in future works.

- Theorem 3.4 is satisfied for sufficiently regular solutions of (3.2.5). In this case, the meaning of 'sufficiently regular' is evidently ambiguous, since various hypotheses on the smoothness of the solutions of (3.2.5) may lead to the same conclusion of the theorem. For example, since the spatial domain has a finite area, we may require solutions of the continuous system to possess continuous derivatives up to order 2, in addition to requiring that homogeneous Dirichlet conditions be satisfied at the boundary. Also, functions ϕ and F must be continuous, while G needs to be continuously differentiable and non-negative. Evidently, more general conditions could be imposed in order to reach the same conclusion of the theorem.

- As one of the reviewers pointed out, the fractional centered difference scheme approximates Riesz fractional derivatives with second-order accuracy, but no stability analysis specific to this discretization is provided. Unfortunately, this is one of the various limitations that are inherent to the current approach. However, on the other hand, the use of fractional centered differences has the advantage that its computational implementation is relatively straightforward, especially when it is compared to other approaches available in the literature [66].

- The theorem on the convergence property of the finite-difference scheme imposes very restrictive assumptions on the regularity of the solutions. Those assumptions were established in the article [10], and the proof of the consistency property of those discrete operators relies on Taylor's theorem and the mean-value theorem. In light of those facts, the regularity assumptions are indispensable, indeed. Obviously, these conditions are an important limitation in our approach. Evidently, they

TESIS TESIS TESIS TESIS TESIS

TESIS TESIS TESIS TESIS TESIS

can be fixed by using a different approach, such as the use of weighted-shifted Grünwald differences [66]. Unfortunately, this last methodology requires a more complicated computational implementation, which leads to longer computational time.

TESIS TESIS TESIS TESIS TESIS

TESIS TESIS TESIS TESIS TESIS

Chapter 4. A Scheme to Solve a Generalized Space-Bifractional 2D Sine–Gordon Equation: Conservation and Efficiency Analysis

4.1 Introduction

In recent years, fractional calculus-generalizing differentiation and integration to non-integer orders-has garnered significant interest as a modeling tool for complex physical and engineering systems. Because fractional derivatives inherently capture long-range interactions and memory effects, they provide a more flexible description of anomalous diffusion, viscoelastic behavior, and other non-classical processes [67, 9, 68, 69]. Indeed, fractional models of dynamic systems often yield simpler equations that match empirical data more closely than classical models. Applications of fractional PDEs span many areas: for example, they have been used in fluid dynamics and electromagnetics to describe anomalous transport, and in biological models of population dynamics and epidemiology where memory effects are pronounced [70, 71, 24]. Recent reviews highlight the increasing relevance of fractional methods even in cutting-edge fields such as machine learning, network dynamics, and signal processing [72, 73, 74]. Because fractional derivatives introduce nonlocal couplings, traditional numerical solvers require adaptation. This challenge has spurred the development of specialized algorithms for fractional PDEs, as we discuss below.

Since fractional PDEs have come to the forefront of modeling real-world phenomena, many numerical methods have been created to solve them. For example, traditional equations like the Schrodinger equation, the Klein–Gordon equation, and reaction–diffusion models have been generalized to fractional form [75, 76, 77]. In practice, finite-difference techniques (explicit, implicit, or Crank–Nicolson schemes) are common, but they tend to yield large dense linear systems since the Riesz Laplacian couples all the grid points [21, 12]. Spectral schemes (e.g., Chebyshev or Fourier spectral methods) project the problem onto global bases, reducing the fractional PDE to a system of algebraic equations for modal coefficients [78]. Pseudospectral versions accomplish similar objectives via discrete transforms, although they need homogeneous or periodic boundary conditions in order to be simple [79]. Finite-element formulations have also been constructed, using appropriate basis functions to deal with irregular geometries using fractional operators [80]. Alternatively, mesh-free collocation schemes—e.g., radial-basis function

TESIS TESIS TESIS TESIS TESIS

TESIS TESIS TESIS TESIS TESIS

or reproducing-kernel methods—approximate the solution without a mesh [81, 82]. Aside from these, boundary-element techniques reformulate the PDE on the domain boundary, with benefits for infinite or irregular domains. Differential quadrature methods have also been employed, approximating spatial derivatives with weighted sums of nodal values [83]. Each has trade-offs: spectral methods yield very high accuracy for smooth solutions, while finite-element and meshfree schemes are good on complex geometries. Crucially, since the undamped sine-Gordon equation is conservative, numerical schemes preserving a discrete energy or other invariants will perform better on long-time simulations. Collectively, this set of algorithms provides a rich framework for approximating multidimensional fractional wave equations.

The two-dimensional sine-Gordon equation is an important nonlinear wave equation, initially derived from differential geometry principles [1]. It is an integrable model with stable soliton (kink) solutions, which preserve their shape and speed in interactions [84]. The soliton-supporting property makes the sine-Gordon equation a cornerstone of nonlinear science. The sine-Gordon equation has deep implications in physics; for example, it governs the quantized magnetic flux (fluxon) dynamics in large Josephson junctions and the propagation of certain optical pulse structures in nonlinear photonic media [85, 86, 87]. More generally, it is a successful field theory for a wide range of two-dimensional systems in condensed matter physics and field theory [88, 89]. A broad range of analytical techniques (such as inverse scattering and Backlund transformations) has been developed for the integrable sine-Gordon model [90]. In more recent studies, dynamics similar to those governed by the sine-Gordon equation have been realized in engineered materials. As an example, experiments on active mechanical metamaterials exhibited unidirectional soliton propagation that maps well onto a modified, non-reciprocal sine-Gordon equation [91]. These examples demonstrate the continued relevance of the sine-Gordon framework to both classical and applied contexts. In that the undamped sine-Gordon system conserves energy, numerical methods that do likewise are especially beneficial. These considerations provide motivation for the development of conservative discretizations to generalized (e.g., fractional) sine-Gordon equations.

A more general form of the classical two-dimensional sine-Gordon equation (SGE) takes the following form:

$$\frac{\partial^2 v}{\partial t^2} + \eta \frac{\partial v}{\partial t} - \lambda_1 \frac{\partial^2 v}{\partial x^2} - \lambda_2 \frac{\partial^2 v}{\partial y^2} = -\varphi(x, y) \sin v + F(x, y, t) - G'(v). \qquad (4.1.1)$$

TESIS TESIS TESIS TESIS TESIS

TESIS TESIS TESIS TESIS TESIS

A possible fractional extension of this equation is defined by replacing the classical Laplacian with Riesz fractional derivatives of order α and β along the x and y axes, respectively. This extension combines anomalous space dispersion with standard integer-order time evolution. Previous work on space-fractional sine-Gordon models has shown that changes in the orders of the spatial derivatives may have considerable effects on soliton interactions; for example, when one Riesz order is less than a critical value, kinks display monotonically attractive behavior, while above this value, they oscillate or even repel each other [20]. These findings mean that a numerical method must effectively incorporate the action of the fractional operators.

A wide range of numerical methods has been developed for the 2D sine-Gordon equation. Each class of method has its own trade-offs in terms of accuracy, complexity, and implementation effort. Importantly, the undamped sine-Gordon equation conserves a continuous energy, so there is strong interest in discrete schemes that preserve analogous invariants [13]. For the space-fractional sine-Gordon, recent research has begun to explore energy-preserving schemes. For example, Xing *et al.* ([14]) proposed an explicit fourth-order finite-difference scheme for the 2D space-fractional SGE that provably preserves a discrete energy. Other works have introduced fast implicit or exponential integrator methods for related fractional wave systems, but often only in one dimension [16]. Thus a comprehensive conservative scheme for the 2D space bifractional Sine-Gordon equation remains an active area of research. These schemes have demonstrated high accuracy for smooth solutions, but formal analysis of their convergence and stability in two dimensions is generally lacking. In summary, while many numerical approaches exist for the classical 2D Sine-Gordon equation, and even some high-order, energy-preserving methods have been developed for fractional versions, there remains a need for a fully discrete, provably convergent conservative scheme for the general 2D bifractional problem.

This paper makes two main contributions. First, we develop a structure-preserving finite-difference formulation: by discretizing spatial derivatives with centered differences, we derive a fully discrete scheme that satisfies a discrete energy balance. In the absence of damping, the scheme exactly conserves the discrete energy, mirroring the continuum model. Second, we provide a complete convergence analysis of the method: under suitable regularity assumptions, we prove that it is second-order consistent, (conditionally) stable, and converges to the exact solution of the bifractional sine-Gordon system. These results extend earlier analyses of 1D or non-fractional cases.

TESIS TESIS TESIS TESIS TESIS

TESIS TESIS TESIS TESIS TESIS

The the paper is organized as follows: Section 4.2 introduces notation and fractional derivative preliminaries. Section 4.3 details the fully discrete scheme and defines the discrete energy; Section 4.4 contains the proofs of consistency, stability, and convergence; Section 4.5 provides the numerical examples; and Section 4.6 concludes with a summary and discussion of future work. Overall, the new scheme provides a reliable tool for simulating 2D fractional sine-Gordon dynamics with provable structure-preserving properties.

4.2 Preliminaries

Let $T > 0$ and $I = (a, b)$ with $a < b$. We set $I^2 = I \times I$ and $\Omega = I^2 \times (0, T) \subset \mathbb{R}^3$. Throughout we assume the solution $v : \Omega \to \mathbb{R}$ is sufficiently smooth so that the identities below are valid. Let $\varphi : I^2 \to \mathbb{R}$ and $F : \Omega \to \mathbb{R}$ be continuous, and let $G : \mathbb{R} \to \mathbb{R}$ be a continuously differentiable function. We will also assume φ and G are non-negative. Denote $\Lambda = (\lambda_1, \lambda_2)$ with $\lambda_1, \lambda_2, \eta \geq 0$ and let fractional orders satisfy $\alpha, \beta \in (1, 2]$.

Definition 4.1 (Podlubny [7])**.** For $n \in \mathbb{N}$ with $n - 1 < \alpha < n$, the Riesz fractional derivative of order α with respect to x is given at $(x, y, t) \in \Omega$ by

$$\frac{\partial^\alpha v(x,y,t)}{\partial |x|^\alpha} = -\frac{1}{2\cos(\pi\alpha/2)\Gamma(n-\alpha)} \frac{\partial^n}{\partial x^n} \int_{-\infty}^{\infty} \frac{v(\xi, y, t)}{|x-\xi|^{\alpha-n+1}} \, \mathrm{d}\xi, \tag{4.2.1}$$

with the analogous formula in y for order β. When α (or β) is an integer n the Riesz derivative coincides with the usual n-th derivative. Here $\Gamma(\cdot)$ denotes the Gamma function.

We define the fractional Laplacian and gradient by

$$\Delta_{\alpha,\beta} v = \frac{\partial^\alpha v}{\partial |x|^\alpha} + \frac{\partial^\beta v}{\partial |y|^\beta}, \qquad \nabla_{\alpha,\beta} v = \left(\frac{\partial^\alpha v}{\partial |x|^\alpha}, \ \frac{\partial^\beta v}{\partial |y|^\beta} \right), \tag{4.2.2}$$

which reduce to the classical Laplacian and gradient when $\alpha = \beta = 2$. We will also assume that

$$\Lambda \cdot \Delta_{\alpha,\beta} v = \lambda_1 \frac{\partial^\alpha v}{\partial |x|^\alpha} + \lambda_2 \frac{\partial^\beta v}{\partial |y|^\beta}$$

We consider the following two-dimensional fractional sine–Gordon equation:

$$\frac{\partial^2 v}{\partial t^2} + \eta \frac{\partial v}{\partial t} - \lambda_1 \frac{\partial^\alpha v}{\partial |x|^\alpha} - \lambda_2 \frac{\partial^\beta v}{\partial |y|^\beta} = -\varphi(x,y) \sin v + F(x,y,t) - G'(v). \tag{4.2.3}$$

TESIS TESIS TESIS TESIS TESIS

TESIS TESIS TESIS TESIS TESIS

Note that (4.2.3) recovers the classical sine–Gordon equation when $\alpha = \beta = 2$.

We prescribe homogeneous Dirichlet boundary conditions and initial data:

$$\begin{aligned} v(x,y,0) &= \psi_1(x,y), && (x,y) \in I^2, \\ \partial_t v(x,y,0) &= \psi_2(x,y), && (x,y) \in I^2, \\ v(x,y,t) &= 0, && (x,y,t) \in \partial I^2 \times (0,T). \end{aligned} \tag{4.2.4}$$

It will be convenient to set

$$H(v) = \varphi(x,y)\cos v - G(v), \qquad H'(v) = -\varphi(x,y)\sin v - G'(v),$$

so that (4.2.3) can be compactly written as

$$\partial_{tt} v + \eta \partial_t v - \Lambda \cdot \Delta_{\alpha,\beta} v = H'(v) + F. \tag{4.2.5}$$

We use the usual Lebesgue spaces $L^p(I^2)$ and, for each fixed $t \in [0,T]$, the L^2-inner product

$$\langle v, w \rangle_{L^2(I^2)} = \int_{I^2} v(x,y,t)\, w(x,y,t)\, \mathrm{d}x\mathrm{d}y, \qquad \|v\|^2_{L^2(I^2)} = \langle v, v \rangle_{L^2(I^2)}.$$

We also write

$$\Lambda \|\nabla_{\alpha/2,\beta/2} v\|^2_{L^2(I^2)} = \lambda_1 \left\| \tfrac{\partial^{\alpha/2} v}{\partial |x|^{\alpha/2}} \right\|^2_{L^2(I^2)} + \lambda_2 \left\| \tfrac{\partial^{\beta/2} v}{\partial |y|^{\beta/2}} \right\|^2_{L^2(I^2)}.$$

Definition 4.2. Assume v solves (4.2.3) with conditions (4.2.4). The total energy at time t is defined by

$$E(t) = \frac{1}{2}\left\|\partial_t v\right\|^2_{L^2(I^2)} + \frac{1}{2}\Lambda\left\|\nabla_{\alpha/2,\beta/2} v\right\|^2_{L^2(I^2)} + \left\|\varphi(1-\cos v)\right\|_{L^1(I^2)} + \|G(v)\|_{L^1(I^2)}. \tag{4.2.6}$$

A standard property of Riesz derivatives is the fractional integration-by-parts identity [92]. For $\alpha, \beta \in (1,2)$ and all $v, w \in L^2(I^2)$ we have

$$\left\langle -\partial^{\alpha}_{|x|} v, w \right\rangle_{L^2} = \left\langle v, -\partial^{\alpha}_{|x|} w \right\rangle_{L^2} = \left\langle \partial^{\alpha/2}_{|x|} v,\ \partial^{\alpha/2}_{|x|} w \right\rangle_{L^2}, \tag{4.2.7}$$

and an analogous identity for the y-direction with order β. These identities are central

TESIS TESIS TESIS TESIS TESIS

TESIS TESIS TESIS TESIS TESIS

when deriving energy balances and for the construction of structure-preserving numerical methods.

Theorem 4.3. *Let v be a smooth solution of* (4.2.3) *with* (4.2.4). *Then*

$$E'(t) = -\eta\|\partial_t v\|^2_{L^2(I^2)} + \langle F, \partial_t v\rangle_{L^2(I^2)}, \qquad t \in [0,T], \tag{4.2.8}$$

so the system is conservative when $\eta = 0$ and $F \equiv 0$.

Proof. Differentiate $E(t)$ in (4.2.6), exchange differentiation and integration, applying the chain rule and using the fractional integration-by-parts identities (4.2.7) yields to:

$$\begin{aligned}
\frac{\mathrm{d}E}{\mathrm{d}t} &= \langle \partial_{tt} v - H'(v), \partial_t v\rangle^2_L (I^2) + \lambda_1 \left\langle \partial^{\alpha/2}_{|x|}\partial_t v, \partial^{\alpha/2}_{|x|} v\right\rangle^2_L (I^2) + \lambda_2 \left\langle \partial^{\beta/2}_{|y|}\partial_t v, \partial^{\beta/2}_{|y|} v\right\rangle^2_L (I^2)\\
&= \langle \partial_{tt} v - \Lambda \cdot \Delta_{\alpha,\beta} v - H'(v), \partial_t v\rangle^2_L (I^2)\\
&= \langle -\eta\partial_t v + F, \partial_t v\rangle^2_L (I^2)\\
&= -\eta \left\|\partial_t v\right\|^2_{L^2(I^2)} + \langle F, \partial_t v\rangle_{L^2(I^2)}
\end{aligned}$$

■

4.3 Numerical model

We now present a fully discrete finite-difference scheme for (4.2.3). Partition $I = [a, b]$ uniformly with spatial step h (take $\Delta x = \Delta y = h$) and the time interval $[0, T]$ with step $\tau > 0$. Set

$$M = \frac{b-a}{h}, \qquad N = \frac{T}{\tau},$$

and grid points $x_i = a + ih,\ y_j = a + jh,\ t_n = n\tau$ for $0 \le i, j \le M$ and $0 \le n \le N$. Denote exact nodal values $v^n_{i,j} = v(x_i, y_j, t_n)$ and numerical approximations $V^n_{i,j}$.

Let $R_h = \{(x_i, y_j) : 0 \le i, j \le M\}$ and define the discrete space $\mathcal{V}_h$ of real arrays indexed by interior nodes vanishing on the grid boundary. For $F, G \in \mathcal{V}_h$ introduce the discrete inner product and norms

$$\langle F, G\rangle_h = h^2 \sum_{i,j=1}^{M-1} F_{i,j} G_{i,j}, \qquad \|F\|_{1,h} = h^2 \sum_{i,j=1}^{M-1} |F_{i,j}|, \qquad \|F\|^2_{2,h} = \langle F, F\rangle_h.$$

TESIS TESIS TESIS TESIS TESIS

TESIS TESIS TESIS TESIS TESIS

For a sequence $\{W^n\}_{n=0}^{N} \subset \mathcal{V}_h$ define time finite differences and averages:

$$\delta_t W_{i,j}^n = \frac{W_{i,j}^{n+1} - W_{i,j}^n}{\tau}, \qquad \mu_t W_{i,j}^n = \frac{W_{i,j}^{n+1} + W_{i,j}^n}{2},$$

and the centered first/second temporal differences

$$\delta_t^{(1)} W_{i,j}^n = \frac{W_{i,j}^{n+1} - W_{i,j}^{n-1}}{2\tau}, \qquad \delta_t^{(2)} W_{i,j}^n = \frac{W_{i,j}^{n+1} - 2W_{i,j}^n + W_{i,j}^{n-1}}{\tau^2}.$$

For nonlinear terms we employ the consistent discrete derivative

$$\delta_{v,t} G\Big(V_{i,j}^n\Big) := \begin{cases} \dfrac{G(V_{i,j}^{n+1}) - G(V_{i,j}^{n-1})}{V_{i,j}^{n+1} - V_{i,j}^{n-1}}, & V_{i,j}^{n+1} \neq V_{i,j}^{n-1}, \\ G'\Big(\frac{V_{i,j}^{n+1} + V_{i,j}^{n-1}}{2}\Big), & \text{otherwise}, \end{cases}$$

which is second-order consistent.

For spatial fractional differentiation we use centered fractional differences. Given $\alpha > -1$ and a sufficiently smooth scalar ϕ, the fractional centered difference is

$$\Delta_h^\alpha \phi(x) = \sum_{\ell=-\infty}^{\infty} g_\ell^{(\alpha)} \, \phi(x - \ell h), \qquad g_\ell^{(\alpha)} = \frac{(-1)^\ell \Gamma(\alpha+1)}{\Gamma(\frac{\alpha}{2} + \ell + 1)\Gamma(\frac{\alpha}{2} - \ell + 1)}.$$

On the grid, and with the usual zero extension outside I, one obtains the discrete Riesz operators

$$\delta_x^{(\alpha)} W_{i,j} = -\frac{1}{h^\alpha} \sum_{\ell=0}^{M} g_{i-\ell}^{(\alpha)} W_{\ell,j}, \qquad \delta_y^{(\beta)} W_{i,j} = -\frac{1}{h^\beta} \sum_{\ell=0}^{M} g_{j-\ell}^{(\beta)} W_{i,\ell},$$

and the discrete fractional Laplacian $\Delta_h^{\alpha,\beta} W_{i,j} = \delta_x^{(\alpha)} W_{i,j} + \delta_y^{(\beta)} W_{i,j}$. These approximations are $O(h^2)$ for smooth solutions [10].

We propose the following discrete scheme for the bifractional sine–Gordon equation. Let V^n approximate $v(\cdot, \cdot, t_n)$. For each interior node (i, j) and time index $n = 0, \ldots, N-1$ solve

$$\delta_t^{(2)} V^n + \eta \delta_t^{(1)} V_{i,j}^n - \Lambda \cdot \Delta_h^{\alpha,\beta} V_{i,j}^n - \delta_{v,t}^{(1)} H(V_{i,j}^n) - F_{i,j}^n = 0, \tag{4.3.1}$$

TESIS TESIS TESIS TESIS TESIS

TESIS TESIS TESIS TESIS TESIS

with discrete initial and boundary conditions

$$V_{i,j}^{0} = \psi_1(x_i, y_j), \quad \forall i,j \in \{1,\dots,M-1\}, \tag{4.3.2}$$

$$\delta_t V_{i,j}^{0} = \psi_2(x_i, y_j), \quad \forall i,j \in \{1,\dots,M-1\}, \tag{4.3.3}$$

$$V_{i,j}^{n} = 0, \quad \forall n \in \{0,1,\dots,N\}, \ \forall (i,j) \in \partial I^2. \tag{4.3.4}$$

The scheme is implicit in the nonlinear terms; in practice we solve the nonlinear system at each time level via a fixed-point iteration. A convenient fixed-point mapping S is constructed from a rearrangement of (4.3.1).

Theorem 4.4. *Let $\rho_\pm = 1 \pm \frac{\eta\tau}{2}$ and $H_0 = \|\varphi\|_\infty + \|G''\|_\infty$. Assume $\eta \geq 0$ and consider the mapping*

$$S(v)_{i,j}^{n} = \frac{1}{\rho_+}\left(2v_{i,j}^{n} + \tau^2\Lambda \cdot \Delta_h^{\alpha,\beta} v_{i,j}^{n} - \rho_- v_{i,j}^{n-1} + \tau^2 \frac{H(v) - H(v_{i,j}^{n-1})}{v - v_{i,j}^{n-1}} + \tau^2 F_{i,j}^{n}\right). \tag{4.3.5}$$

If the time step $\tau > 0$ satisfies

$$\tau < \frac{\eta + \sqrt{\eta^2 + 16H_0}}{4H_0},$$

then S is a contraction, therefore has a unique fixed point.

Proof. Fix an index (i,j) and two admissible grid functions v, w. Observe that all terms in (4.3.5) except the nonlinear divided–difference cancel when taking the difference $S(v) - S(w)$. Hence

$$\left|S(v)_{i,j}^{n} - S(w)_{i,j}^{n}\right| = \frac{\tau^2}{\rho_+}\left|\frac{H(v) - H(a)}{v - a} - \frac{H(w) - H(a)}{w - a}\right|,$$

where for brevity we set $a = v_{i,j}^{n-1}$.

Define the auxiliary function

$$\Phi(s) = \frac{H(s) - H(a)}{s - a} \qquad (s \neq a), \qquad \Phi(a) := H'(a).$$

Since $H \in C^2(\mathbb{R})$ and H'' is bounded by H_0, the function Φ is C^1 on any interval of

TESIS TESIS TESIS TESIS TESIS

TESIS TESIS TESIS TESIS TESIS

interest and satisfies

$$|\Phi'(s)| \leq \sup_r |H''(r)| \leq H_0 \qquad \text{for all } s.$$

By the mean value theorem applied to Φ we obtain

$$\left|\Phi(v_{i,j}^n) - \Phi(w_{i,j}^n)\right| \leq H_0 \, |v_{i,j}^n - w_{i,j}^n|.$$

Combining the two previous displays yields, for each node (i, j),

$$\left|S(v)_{i,j}^n - S(w)_{i,j}^n\right| \leq \frac{\tau^2}{\rho_+} H_0 \, |v_{i,j}^n - w_{i,j}^n|.$$

Taking the supremum over all grid nodes gives

$$\|S(v) - S(w)\|_\infty \leq L \, \|v - w\|_\infty, \qquad L = \frac{\tau^2 H_0}{\rho_+}.$$

Thus S is a contraction provided $L < 1$, i.e.

$$\tau^2 H_0 < 1 + \frac{\eta\tau}{2}.$$

Rearranging yields the quadratic inequality

$$H_0\tau^2 - \frac{\eta}{2}\tau - 1 < 0,$$

whose positive root equals

$$\tau_* = \frac{\eta + \sqrt{\eta^2 + 16H_0}}{4H_0}.$$

The inequality holds for $0 < \tau < \tau_*$, which is exactly the stated time constraint. Under this condition and Banach's fixed point theorem gives existence and uniqueness of a fixed point of S. ■

Definition 4.5. For a discrete solution $\{V^n\}_{n=0}^N$ we define the discrete energy at time level n by

$$\begin{aligned} E^n = \frac{1}{2}\|\delta_t V^n\|_{2,h}^2 + \frac{\lambda_1}{2}\left\langle \delta_x^{(\alpha/2)} V^{n+1}, \delta_x^{(\alpha/2)} V^n \right\rangle_h + \frac{\lambda_2}{2}\left\langle \delta_y^{(\beta/2)} V^{n+1}, \delta_y^{(\beta/2)} V^n \right\rangle_h \\ + \mu_t \|\varphi(1 - \cos V^n)\|_{1,h} + \mu_t \|G(V^n)\|_{1,h}. \end{aligned} \tag{4.3.6}$$

TESIS TESIS TESIS TESIS TESIS

TESIS TESIS TESIS TESIS TESIS

We recall a discrete analogue of the integration-by-parts identity for the fractional finite differences. This identity is essential to show energy conservation at the discrete level.

Lemma 4.6 (Macías-Díaz [12]). *Let $\alpha, \beta \in (1,2]$ and $V, W \in \mathcal{V}_h$. Then*

$$\langle -\delta_x^{(\alpha)} V, W \rangle_h = \left\langle \delta_x^{(\alpha/2)} V, \delta_x^{(\alpha/2)} W \right\rangle_h = \langle V, -\delta_x^{(\alpha)} W \rangle_h,$$

and an analogous identity holds in the y-direction with order β.

Theorem 4.7. *Let $V = \{V^n\}_{n=0}^N$ be a solution of* (4.3.6) *satisfying conditions* (4.3.2). *Then the discrete energy E^n defined in* (4.3.6) *satisfies*

$$\delta_t E^{n-1} = -\eta \left\| \delta_t^{(1)} V^n \right\|_{2,h}^2 + \left\langle F^n,\ \delta_t^{(1)} V^n \right\rangle_h, \qquad n = 1, \ldots, N, \tag{4.3.7}$$

and, in particular, the scheme is energy-preserving when $\eta = 0$ and $F \equiv 0$.

Proof. Taking the discrete inner product of the equation (4.3.6) with $\delta_t^{(1)} V^n$ yields the identity

$$\begin{aligned}\left\langle \delta_t^{(2)} V^n,\ \delta_t^{(1)} V^n \right\rangle_h + \eta \left\| \delta_t^{(1)} V^n \right\|_{2,h}^2 - \left\langle \Lambda \cdot \Delta_h^{\alpha,\beta} V^n,\ \delta_t^{(1)} V^n \right\rangle_h \\ - \left\langle \delta_{v,t}^{(1)} H(V^n),\ \delta_t^{(1)} V^n \right\rangle_h - \left\langle F^n,\ \delta_t^{(1)} V^n \right\rangle_h = 0.\end{aligned} \tag{4.3.8}$$

Using the discrete time identities and straightforward algebra one checks

$$\left\langle \delta_t^{(2)} V^n,\ \delta_t^{(1)} V^n \right\rangle_h = \frac{1}{2}\, \delta_t \left\| \delta_t V^{n-1} \right\|_{2,h}^2, \tag{4.3.9}$$

Applying the discrete summation-by-parts identities of Lemma 4.6 to the fractional difference operators, we obtain

$$\left\langle \delta_x^{(\alpha)} V^n,\ \delta_t^{(1)} V^n \right\rangle_h = -\frac{1}{2}\, \delta_t \left\langle \delta_x^{(\alpha/2)} V^n,\ \delta_x^{(\alpha/2)} V^{n-1} \right\rangle_h, \tag{4.3.10}$$

$$\left\langle \delta_y^{(\beta)} V^n,\ \delta_t^{(1)} V^n \right\rangle_h = -\frac{1}{2}\, \delta_t \left\langle \delta_y^{(\beta/2)} V^n,\ \delta_y^{(\beta/2)} V^{n-1} \right\rangle_h. \tag{4.3.11}$$

TESIS TESIS TESIS TESIS TESIS

TESIS TESIS TESIS TESIS TESIS

For the non-linear terms we have that

$$\left\langle \delta_{v,t}^{(1)} G(V^n),\ \delta_t^{(1)} V^n \right\rangle_h = \delta_t\Big(\mu_t \big\| G(V^{\,n-1}) \big\|_{1,h}\Big), \tag{4.3.12}$$

$$\left\langle \delta_{v,t}^{(1)} \Big(\varphi(1-\cos V^n)\Big),\ \delta_t^{(1)} V^n \right\rangle_h = \delta_t\Big(\mu_t \big\| \varphi(1-\cos V^{\,n}) \big\|_{1,h}\Big). \tag{4.3.13}$$

Substituting (4.3.9)–(4.3.13) into (4.3.8) yields

$$\begin{aligned}
&\frac{1}{2}\,\delta_t \big\|\delta_t V^{\,n-1}\big\|_{2,h}^2 + \frac{\lambda_1}{2}\,\delta_t \Big\langle \delta_x^{(\alpha/2)} V^n, \delta_x^{(\alpha/2)} V^{\,n-1} \Big\rangle_h + \frac{\lambda_2}{2}\,\delta_t \Big\langle \delta_y^{(\beta/2)} V^n, \delta_y^{(\beta/2)} V^{\,n-1} \Big\rangle_h \\
&+ \delta_t\Big(\mu_t \|G(V^{\,n-1})\|_{1,h} + \mu_t \|\varphi(1-\cos V^{\,n})\|_{1,h} \Big) = -\eta \big\|\delta_t^{(1)} V^n\big\|_{2,h}^2 + \Big\langle F^n, \delta_t^{(1)} V^n \Big\rangle_h.
\end{aligned}$$

Recognizing the left-hand side as $\delta_t E^{\,n-1}$ by the definition (4.3.6) of the discrete energy completes the proof. ■

Corollary 4.8. *Let V satisfy* (4.3.1) *with* (4.3.2)*. Then, for every $n = 1, \ldots, N-1$,*

$$E^n = E^0 + \tau \sum_{k=1}^{n} \Big(-\eta \big\|\delta_t^{(1)} V^k\big\|_{2,h}^2 + \Big\langle F^k, \delta_t^{(1)} V^k \Big\rangle_h \Big). \tag{4.3.14}$$

In particular, if $\eta = 0$ and $F \equiv 0$ then $E^n = E^0$ for all n.

Proof. Sum the identity (4.3.7) for $k = 1, 2, \ldots, n$ and multiply by τ. The telescoping sum on the left gives $E^n - E^0$, while the right-hand side accumulates into the discrete sum in (4.3.14). ■

This discrete framework provides a structure-preserving approximation of the bifractional sine–Gordon equation. In the next sections we analyze consistency, stability, and prove convergence under suitable regularity assumptions. Numerical experiments illustrating energy conservation and accuracy are presented thereafter.

4.4 Numerical properties

To establish the consistency, stability, and convergence of the proposed finite-difference scheme, it is convenient to introduce the continuous residual operator $\mathcal{L}$, defined for sufficiently smooth functions v by

$$\mathcal{L}(v) = \partial_{tt} v + \eta\, \partial_t v - \Lambda \cdot \Delta_{\alpha,\beta} v - H'(v) - F. \tag{4.4.1}$$

TESIS TESIS TESIS TESIS TESIS

TESIS TESIS TESIS TESIS TESIS

This operator coincides with the residual of the fractional sine–Gordon equation (4.2.5).

In the discrete setting, for the numerical approximation $V_{i,j}^n$ at the grid point (x_i, y_j, t_n), we define the discrete residual operator L by

$$L(V_{i,j}^n) = \delta_t^{(2)} V_{i,j}^n + \eta\, \delta_t^{(1)} V_{i,j}^n - \Lambda \cdot \Delta_h^{\alpha,\beta} V_{i,j}^n - \delta_{v,t}^{(1)} H(V_{i,j}^n) - F_{i,j}^n. \tag{4.4.2}$$

By construction, the operator L mirrors the structure of $\mathcal{L}$, so that $L(V^n)$ measures the residual of the discretized equation (4.3.1) at each grid node.

The next result states the basic consistency property of the finite-difference approximation (4.3.1) under suitable smoothness assumptions on the exact solution of the fractional sine–Gordon equation.

Theorem 4.9 (Consistency)**.** *Let v be a sufficiently smooth solution, with $v \in \mathcal{C}_{x,y,t}^{5,5,4}(\overline{\Omega})$. Then there exists a constant $C > 0$, independent of h and τ, such that for every grid point (x_i, y_j, t_n),*

$$\Big|\mathcal{L}(v) - L(V_{i,j}^n)\Big| \leq C\Big(h^2 + \tau^2\Big). \tag{4.4.3}$$

Proof. The proof relies on standard Taylor expansions of v about the grid node (x_i, y_j, t_n). Under the assumed regularity, the following truncation error bounds hold for the discrete operators, where $C_1, \ldots, C_4$ are constants depending on the sup-norms of the corresponding fifth-order spatial and fourth-order temporal derivatives of v:

$$\begin{aligned}
\Big|\partial_{tt} v(x_i, y_j, t_n) - \delta_t^{(2)} V_{i,j}^n\Big| &\leq C_1 \tau^2, \\
\Big|\partial_t v(x_i, y_j, t_n) - \delta_t^{(1)} V_{i,j}^n\Big| &\leq C_2 \tau^2, \\
\Big|H'(v(x_i, y_j, t_n)) - \delta_{v,t}^{(1)} H(V_{i,j}^n)\Big| &\leq C_3 \tau^2, \\
\Big|\Delta_{\alpha,\beta} v(x_i, y_j, t_n) - \Delta_h^{\alpha,\beta} V_{i,j}^n\Big| &\leq C_4 h^2.
\end{aligned} \tag{4.4.4}$$

Adding these estimates and applying the triangle inequality gives

$$\Big|\mathcal{L}(v) - L(V_{i,j}^n)\Big| \leq C_1 \tau^2 + \eta C_2 \tau^2 + C_3 \tau^2 + (\lambda_1 + \lambda_2) C_4 h^2.$$

Finally, setting

$$C = \max\{C_1,\ \eta C_2,\ C_3,\ (\lambda_1 + \lambda_2) C_4\},$$

we obtain the desired estimate (4.4.3). ■

TESIS TESIS TESIS TESIS TESIS

TESIS TESIS TESIS TESIS TESIS

We start with two standard auxiliary results used in the stability and convergence analysis.

Lemma 4.10 (Pen–Yu [93]). *Let $\{\omega^n\}_{n=0}^N$ and $\{\rho^n\}_{n=0}^N$ be nonnegative sequences and let $C \geq 0$ be a constant. If for every $n = 0, \ldots, N$*

$$\omega^n \leq \rho^n + C\tau \sum_{k=0}^{n-1} \omega^k,$$

then for all n

$$\omega^n \leq \rho^n \, e^{Cn\tau}.$$

Lemma 4.11 (Mares-Rincón [21]). *Let $H \in C^2(\mathbb{R})$ and let $V_a^n, V_b^n \in \mathbb{R}^{(M-1)\times(M-1)}$ be two discrete sequences. Define $\varepsilon^n = V_a^n - V_b^n$ and $\widetilde{H}^n = \delta_{v_a,t}^{(1)} H(V_a^n) - \delta_{v_b,t}^{(1)} H(V_b^n)$. Then there exist positive constants C_1, C_2, C_3 (depending only on $\|H''\|_\infty$ and T) such that for each n:*

$$\Big|\langle \widetilde{H}^n,\ \delta_t^{(1)} \varepsilon^n \rangle_h\Big| \leq C_1\Big(\|\varepsilon^{n+1}\|_{2,h}^2 + \|\varepsilon^{n-1}\|_{2,h}^2 + \|\delta_t \varepsilon^n\|_{2,h}^2 + \|\delta_t \varepsilon^{n-1}\|_{2,h}^2 \Big), \quad (4.4.5)$$

$$2\tau \Big| \sum_{k=1}^{n} \langle \widetilde{H}^k,\ \delta_t^{(1)} \varepsilon^k \rangle_h \Big| \leq C_2 \|\varepsilon^0\|_{2,h}^2 + C_3 \tau \sum_{k=0}^{n} \|\delta_t \varepsilon^k\|_{2,h}^2. \quad (4.4.6)$$

Sketch of proof. The pointwise bound $|\widetilde{H}_{i,j}^k| \lesssim H_0(|\varepsilon_{i,j}^{k+1}| + |\varepsilon_{i,j}^{k-1}|)$ with $H_0 = \|H''\|_\infty$ follows from the mean value theorem applied to the divided differences. The estimate (4.4.5) is then obtained by Cauchy–Schwarz and Young inequalities. To obtain the cumulative bound (4.4.6) one uses the elementary identity $\varepsilon^n = \varepsilon^0 + \tau \sum_{k=0}^{n-1} \delta_t \varepsilon^k$ together with the inequality $(a+b)^2 \leq 2a^2 + 2b^2$, sums the pointwise estimates, and collects terms; the constants C_2, C_3 depend only on H_0 and T. The details are routine and mirror the calculations in the original manuscript. ■

We denote $\varepsilon^n = V_a^n - V_b^n$ the difference between two solutions corresponding to two distinct initial data sets ψ_a, ψ_b.

Theorem 4.12 (Numerical stability). *Let $H \in C^2(\mathbb{R})$ with $H'' \in L^\infty(\mathbb{R})$. Assume the time step $\tau > 0$ is small enough so that $C_3\tau < 1$ (with C_3 from Lemma 4.11). Then there are positive constants C_4, C_5 such that for every $n = 1, \ldots, N$*

$$\|\delta_t \varepsilon^n\|_{2,h}^2 \leq C_4 \Big(C_2 \|\varepsilon^0\|_{2,h}^2 + \|\delta_t \varepsilon^0\|_{2,h}^2 + \lambda_1 \langle \delta_x^{(\alpha/2)} \varepsilon^1, \delta_x^{(\alpha/2)} \varepsilon^0 \rangle_h + \lambda_2 \langle \delta_y^{(\beta/2)} \varepsilon^1, \delta_y^{(\beta/2)} \varepsilon^0 \rangle_h \Big) e^{C_5 n\tau}, \quad (4.4.7)$$

TESIS TESIS TESIS TESIS TESIS

TESIS TESIS TESIS TESIS TESIS

where C_2 is the constant appearing in Lemma 4.11.

Proof. The error satisfies:

$$\delta_t^{(2)}\varepsilon^n = -\gamma\,\delta_t^{(1)}\varepsilon^n + \Lambda\cdot\Delta_h^{\alpha,\beta}\varepsilon^n + \widetilde{H}^n, \tag{4.4.8}$$

where $\widetilde{H}^n$ is defined as in Lemma 4.11. Take the discrete inner product of (4.4.8) with $\delta_t^{(1)}\varepsilon^n$ and sum in time from $k=0$ to n. This yields, after algebraic rearrangement and use of the discrete summation-by-parts identities,

$$\begin{aligned}\|\delta_t\varepsilon^n\|_{2,h}^2 \le C_2\|\varepsilon^0\|_{2,h}^2 + \|\delta_t\varepsilon^0\|_{2,h}^2 + \lambda_1\Big\langle \delta_x^{(\alpha/2)}\varepsilon^1, \delta_x^{(\alpha/2)}\varepsilon^0\Big\rangle_h \\ + \lambda_2\Big\langle \delta_y^{(\beta/2)}\varepsilon^1, \delta_y^{(\beta/2)}\varepsilon^0\Big\rangle_h + C_3\tau\sum_{k=0}^{n}\|\delta_t\varepsilon^k\|_{2,h}^2,\end{aligned} \tag{4.4.9}$$

where the last term originates from the cumulative nonlinear bound (4.4.6). Set

$$\omega^n = \|\delta_t\varepsilon^n\|_{2,h}^2, \qquad \rho^n = C_2\|\varepsilon^0\|_{2,h}^2 + \|\delta_t\varepsilon^0\|_{2,h}^2 + \lambda_1\langle \delta_x^{(\alpha/2)}\varepsilon^1, \delta_x^{(\alpha/2)}\varepsilon^0\rangle_h + \lambda_2\langle \delta_y^{(\beta/2)}\varepsilon^1, \delta_y^{(\beta/2)}\varepsilon^0\rangle_h.$$

Then (4.4.9) has the form $\omega^n \le \rho^n + C_3\tau\sum_{k=0}^{n}\omega^k$. Applying Lemma 4.10 (noting $C_3\tau < 1$) we obtain $\omega^n \le \rho^n e^{C_3 n\tau}$. The constants C_4 and C_5 in (4.4.7) are chosen so that the factor and the exponential match this bound, completing the proof. ∎

We denote the pointwise truncation residual by $R^n_{i,j}$ (so R^n is the vector of local truncation errors at time t_n). By Theorem 4.9 there exists $C_R > 0$ such that $\|R^n\|_{2,h} \le C_R(\tau^2 + h^2)$ for all n.

Theorem 4.13 (Convergence)**.** *Let $v \in \mathcal{C}^{4,4,3}(\overline{\Omega})$ be the exact solution of* (4.2.5) *and assume $H \in C^2(\mathbb{R})$ with $H'' \in L^\infty$. Let $\{V^n\}_{n=0}^N$ be the numerical approximations produced by* (4.3.1) *with compatible initial data. If the time step τ is small enough to satisfy $(8C_1T^2 + 2T + 6)\tau < 1$ (with C_1 from Lemma 4.11), then there exists a constant $C > 0$ such that*

$$\max_{0\le n\le N}\|\varepsilon^n\|_{2,h} \le C\Big(\tau^2 + h^2\Big).$$

Proof. Subtracting the discrete scheme from the continuous operator evaluated at the grid and collecting truncation terms leads to the discrete error equation

$$\delta_t^{(2)}\varepsilon^n = -\gamma\,\delta_t^{(1)}\varepsilon^n + \Lambda\cdot\Delta_h^{\alpha,\beta}\varepsilon^n + \widetilde{H}^n + R^n. \tag{4.4.10}$$

TESIS TESIS TESIS TESIS TESIS

TESIS TESIS TESIS TESIS TESIS

Proceeding as in the stability proof (take inner product with $\delta_t^{(1)}\varepsilon^n$ and sum in time), and using Lemma 4.11 together with the bound on $\|R^n\|_{2,h}$, one obtains an inequality of the form

$$\|\delta_t\varepsilon^n\|_{2,h}^2 \leq C_R^2 N(\tau^4 + h^4) + \widetilde{C}\tau \sum_{k=0}^{n} \|\delta_t\varepsilon^k\|_{2,h}^2, \tag{4.4.11}$$

for some constant $\widetilde{C}$ depending only on the problem data and T. Under the smallness hypothesis on τ we have $\widetilde{C}\tau < 1$ and we may apply Lemma 4.10 to deduce

$$\max_{0\leq n\leq N} \|\delta_t\varepsilon^n\|_{2,h}^2 \leq C_4' e^{C_5' T}(\tau^4 + h^4)$$

for suitable constants C_4', C_5'. Taking square roots and integrating the discrete time derivative yields

$$\max_{0\leq n\leq N} \|\varepsilon^n\|_{2,h} \leq C(\tau^2 + h^2),$$

which completes the proof. ■

4.5 Simulations

This section presents representative numerical experiments that (i) validate the order of accuracy of the proposed finite-difference scheme, (ii) illustrate the scheme's ability to preserve (or dissipate) the discrete energy under the appropriate hypotheses, and (iii) explore how the solution morphology depends on the fractional orders α and β. All tests were implemented in MATLAB using our fixed-point solver for the nonlinear time step. The runs shown below were performed on a Lenovo LOQ 15ARP9 laptop with an AMD Ryzen 7 7435HS (8 cores/16 threads), an NVIDIA laptop GPU (3072 CUDA cores, 8 GB GDDR6), 24 GB DDR5 RAM and a 512 GB NVMe drive.

4.5.1 Analytical benchmark

We first test the scheme against a manufactured solution to verify the convergence rates. Consider the exact solution

$$v(x, y, t) = \cos(\pi x)\cos(\pi y)\cos(t), \tag{4.5.1}$$

on $\overline{\Omega} = [-1/2, 1/2]^2 \times [0, 5]$ with $\varphi \equiv 1$, $\alpha = \beta = 2$, $\eta = 0$, $\lambda_1 = \lambda_2 = (2\pi^2)^{-1}$, $G \equiv 0$, and a forcing term chosen so that (4.5.1) is an exact solution: $F(x, y, t) = \sin(\cos\pi x \cos\pi y \cos t)$. Initial data are taken from (4.5.1) (with $\partial_t v(\cdot, 0) \equiv 0$).

Figure 4.1 displays numerical snapshots at representative times (using $h = 0.025$ and $\tau = 0.010$). Table 4.1 reports the discrete L^2-errors $\|\epsilon\|_{2,h}$ for a sequence of refinements

TESIS TESIS TESIS TESIS TESIS

TESIS TESIS TESIS TESIS TESIS

in space and time.

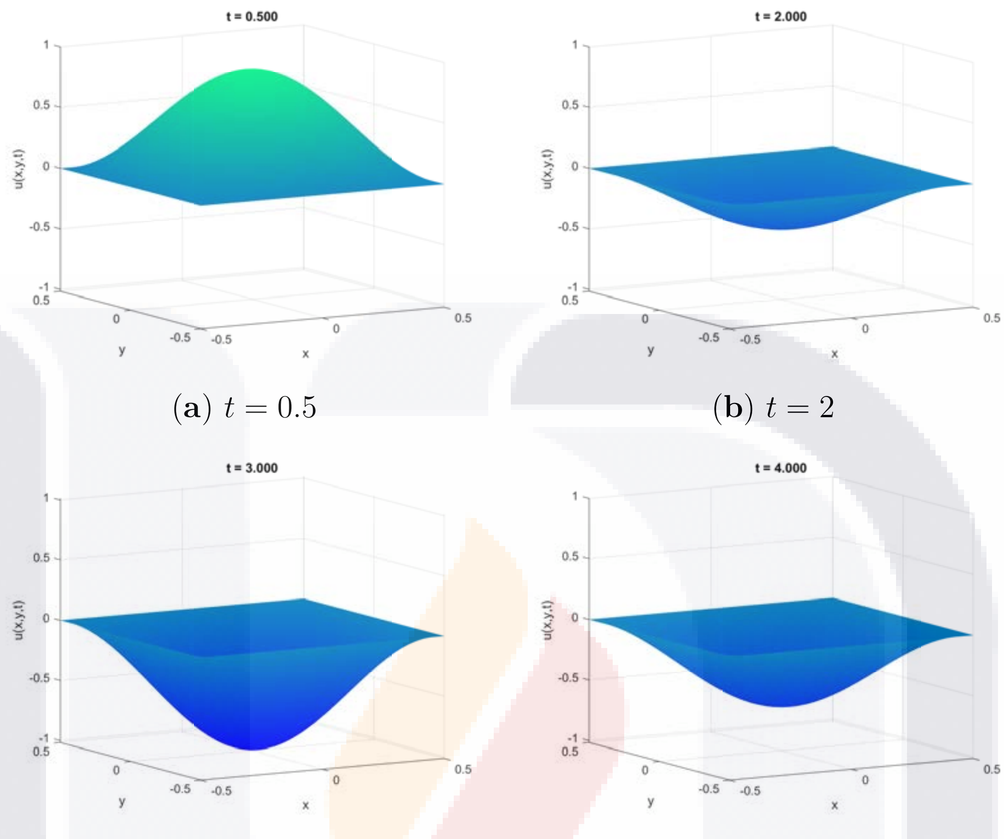

(**a**) $t = 0.5$ (**b**) $t = 2$

(**c**) $t = 3$ (**d**) $t = 4$

Figure 4.1: Numerical solution for the manufactured test (4.5.1) at four times. Spatial step $h = 0.025$, time step $\tau = 0.010$.

	$\tau = 0.20,\ h = 0.10$	$\tau = 0.10,\ h = 0.05$	$\tau = 0.05,\ h = 0.025$	$\tau = 0.025,\ h = 0.0125$
$t = 1$	6.22×10^{-2}	3.05×10^{-2}	1.52×10^{-2}	7.62×10^{-3}
$t = 2$	2.34×10^{-2}	1.56×10^{-2}	8.59×10^{-3}	4.47×10^{-3}
$t = 3$	1.41×10^{-1}	7.13×10^{-2}	3.58×10^{-2}	1.80×10^{-2}
$t = 4$	6.35×10^{-2}	2.55×10^{-2}	1.14×10^{-2}	5.42×10^{-3}
$t = 5$	1.59×10^{-1}	8.42×10^{-2}	4.30×10^{-2}	2.17×10^{-2}

Table 4.1: Discrete L^2-errors $\|\epsilon\|_{2,h}$ for the manufactured solution (4.5.1) at several refinement levels.

4.5.2 Impact of the fractional orders α and β

Next we examine how the spatial fractional orders affect solution morphology. Figures 4.2–4.5 compare the integer-order case $\alpha = \beta = 2$ with several fractional choices $\alpha = \beta \in$

TESIS TESIS TESIS TESIS TESIS

TESIS TESIS TESIS TESIS TESIS

$\{1.9, 1.5, 1.1\}$ at increasing times. All tests use $h = 0.025$, $\tau = 0.010$.

Two robust observations emerge from these experiments. First, departing from the integer Laplacian tends to amplify the wave amplitude in our setup; the effect is more pronounced as α and β move away from 2. Second, the temporal periodicity and phase of the solution are modified: the classical periodic pattern observed at $\alpha = \beta = 2$ is generally lost for fractional orders, and the waveform slowly deforms over long times. These deformations attenuate as the fractional orders approach the integer value, consistent with the fact that the model reduces to the standard wave operator when $\alpha = \beta = 2$.

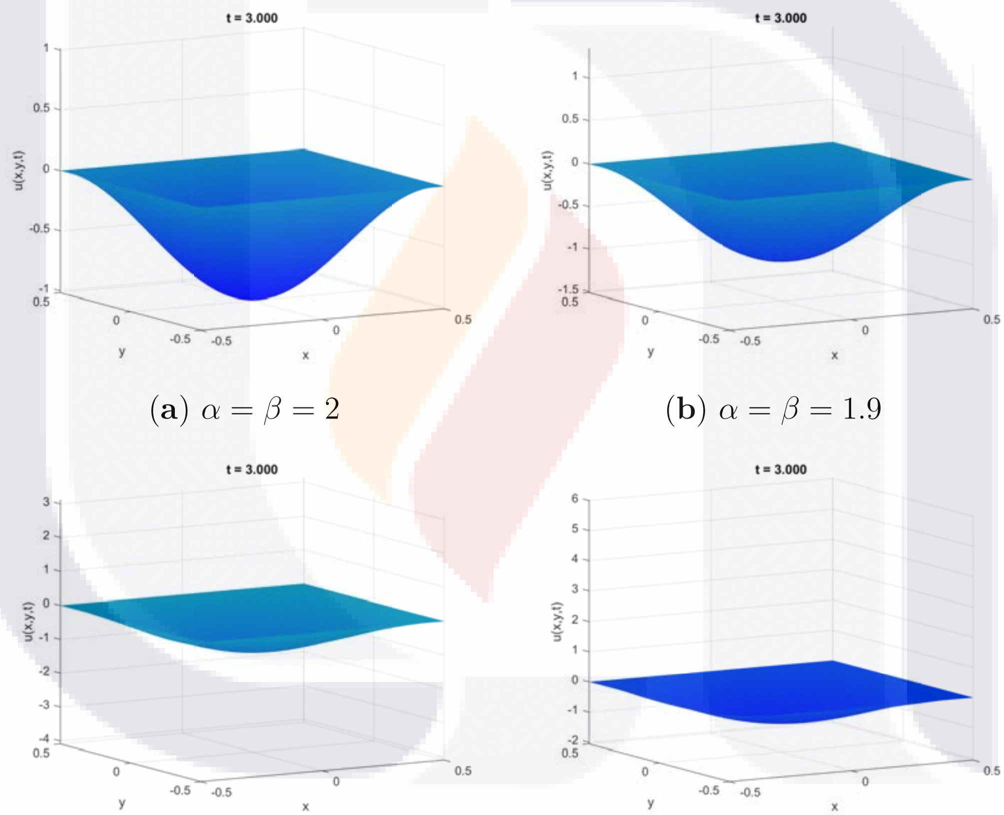

(**a**) $\alpha = \beta = 2$ (**b**) $\alpha = \beta = 1.9$

(**c**) $\alpha = \beta = 1.5$ (**d**) $\alpha = \beta = 1.1$

Figure 4.2: Snapshots at $t = 3$ comparing different fractional orders. Parameters: $h = 0.025$, $\tau = 0.010$.

Figures 4.3–4.5 present the same comparison at later times and further confirm the trends described above: fractional dispersion alters amplitude and long-time shape, while integer orders recover the familiar periodic pattern.

TESIS TESIS TESIS TESIS TESIS

TESIS TESIS TESIS TESIS TESIS

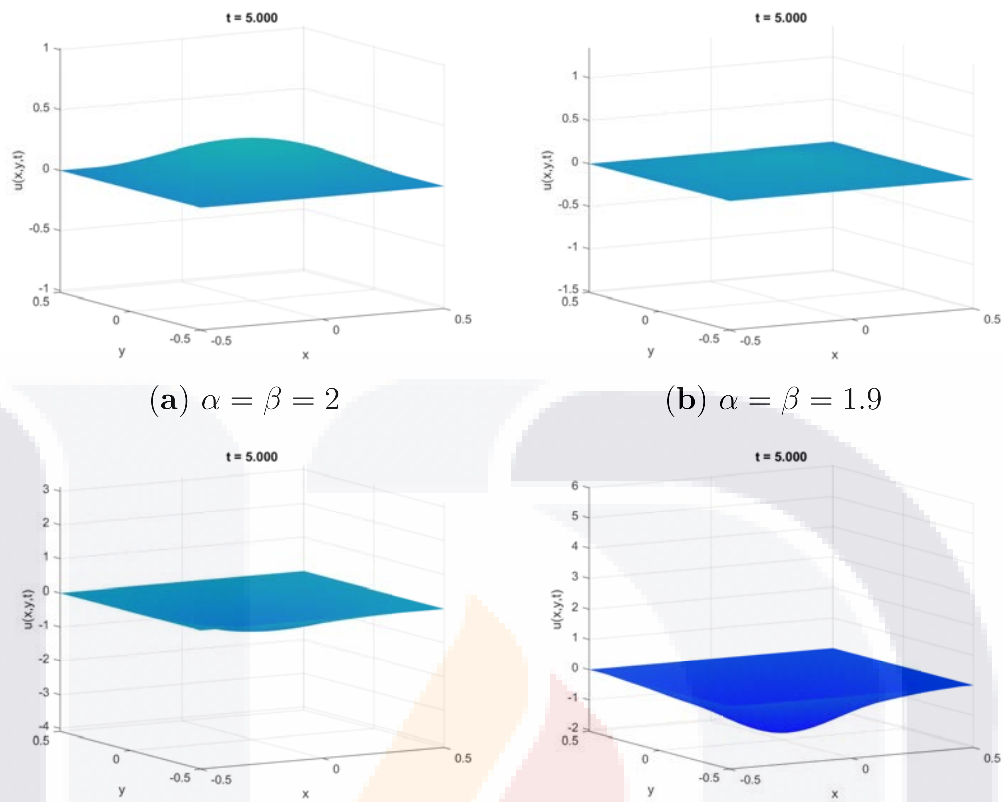

(**a**) $\alpha = \beta = 2$ (**b**) $\alpha = \beta = 1.9$

(**c**) $\alpha = \beta = 1.5$ (**d**) $\alpha = \beta = 1.1$

Figure 4.3: Snapshots at $t = 5$ comparing different fractional orders. Parameters: $h = 0.025$, $\tau = 0.010$.

4.5.3 Energy behavior for a ring soliton

Finally, we test the discrete energy behavior using a localized, radially symmetric initial condition (a ring soliton) on $D = [-4, 4]^2$. The initial data are

$$\psi_1(x, y) = 2 \arctan\left(e^{3-5\sqrt{x^2+y^2}}\right), \tag{4.5.2}$$

$$\psi_2(x, y) = 0, \tag{4.5.3}$$

as in Mares-Rincón *et al.* [21]. We ran two experiments:

1. **Conservative case:** $\eta = 0$, $h = 0.05$, $\tau = 0.005$, simulation interval $0 \leq t \leq 2$.

2. **Dissipative case:** $\eta = 2$, $h = 0.05$, $\tau = 0.01$, simulation interval $0 \leq t \leq 5$.

Both fractional ($\alpha = \beta = 1.4$) and integer ($\alpha = \beta = 2$) setups were considered in order to contrast conservation/dissipation behaviors.

TESIS TESIS TESIS TESIS TESIS

TESIS TESIS TESIS TESIS TESIS

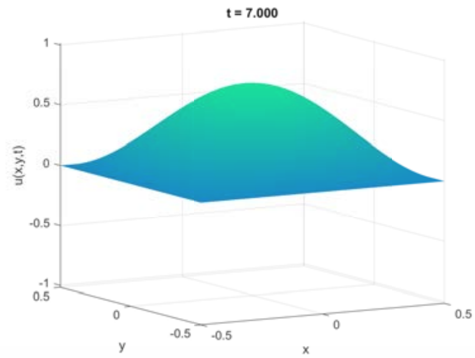

(**a**) $\alpha = \beta = 2$

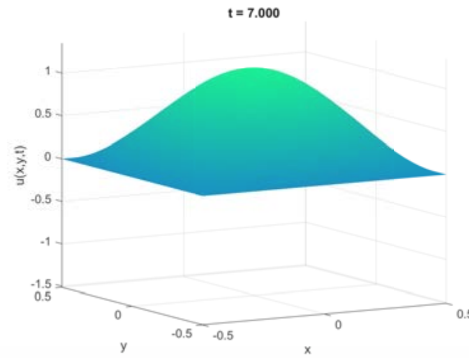

(**b**) $\alpha = \beta = 1.9$

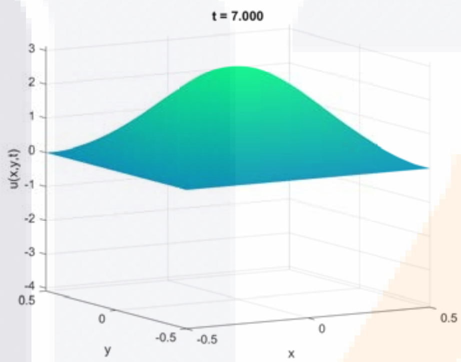

(**c**) $\alpha = \beta = 1.5$

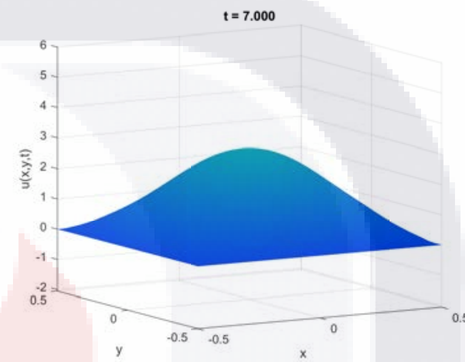

(**d**) $\alpha = \beta = 1.1$

Figure 4.4: Snapshots at $t = 7$ comparing different fractional orders. Parameters: $h = 0.025$, $\tau = 0.010$.

Figure 4.6 shows the discrete energy vs. time for these runs. In the conservative configuration the discrete energy remains essentially constant up to small oscillations caused by round-off and solver tolerances (the fluctuations are on the order of 10^{-2} relative to the mean in these tests). In the dissipative case the energy decays at a similar rate for both integer and fractional orders, vanishing near $t \approx 3$ under the chosen parameters. These results confirm that the discrete energy functional designed in Section 4.3 reproduces the expected preservation or dissipation behaviors.

4.6 Conclusions

We studied a bifractional extension of the two-dimensional sine–Gordon equation in which each spatial direction is governed by a Riesz fractional derivative of order $\alpha, \beta \in (1, 2]$. The model includes anisotropic diffusion coefficients and a generalized potential; the classical sine–Gordon equation is recovered when $\alpha = \beta = 2$. For the continuous problem we established an energy identity and showed that the system is dissipative in

TESIS TESIS TESIS TESIS TESIS

TESIS TESIS TESIS TESIS TESIS

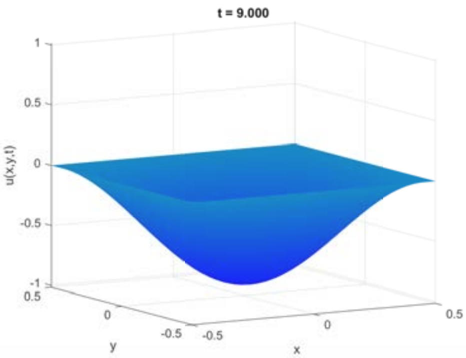

(**a**) $\alpha = \beta = 2$

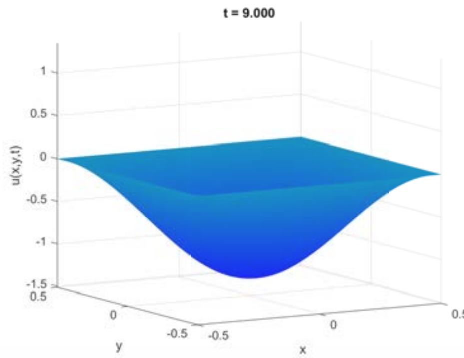

(**b**) $\alpha = \beta = 1.9$

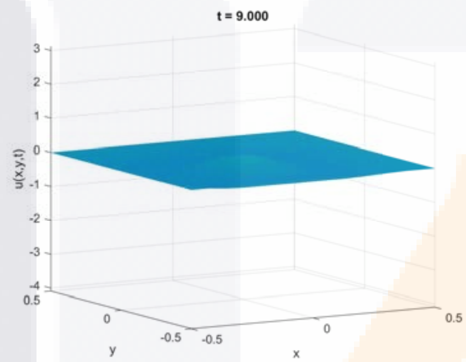

(**c**) $\alpha = \beta = 1.5$

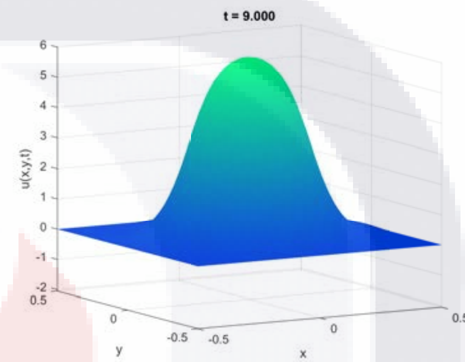

(**d**) $\alpha = \beta = 1.1$

Figure 4.5: Snapshots at $t = 9$ comparing different fractional orders. Parameters: $h = 0.025$, $\tau = 0.010$.

the presence of damping and conservative in the absence of damping and forcing. Some regularity corollaries follow from the energy estimates.

Motivated by these analytical properties, we proposed a centered finite-difference scheme that approximates the Riesz derivatives via fractional centered differences and uses a second-order, fixed-point time integrator. The scheme is nonlinear but, under a mild time-step restriction, a fixed-point argument guarantees solvability at each step. We defined a discrete energy functional that mirrors the continuous one and proved that the scheme preserves the expected dissipative or conservative behavior at the discrete level. In addition we proved second-order consistency in both time and space, and established stability and convergence results using discrete energy techniques and a discrete Grönwall inequality.

Numerical experiments corroborate the theoretical findings. The manufactured solution test confirms second-order accuracy; the parametric study of the fractional orders shows

TESIS TESIS TESIS TESIS TESIS

TESIS TESIS TESIS TESIS TESIS

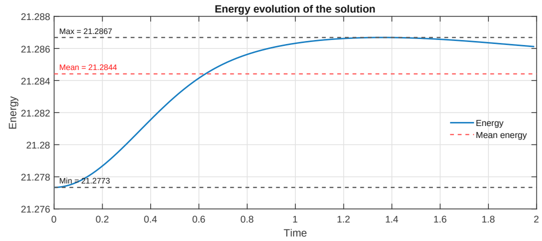

(a) $\alpha = \beta = 2,\ \eta = 0$

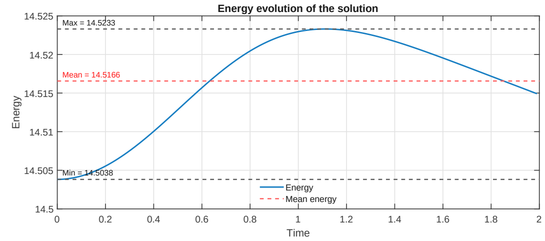

(b) $\alpha = \beta = 1.4,\ \eta = 0$

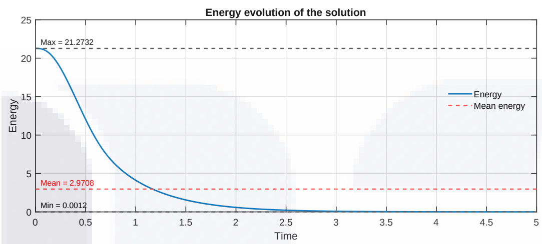

(c) $\alpha = \beta = 2,\ \eta = 2$

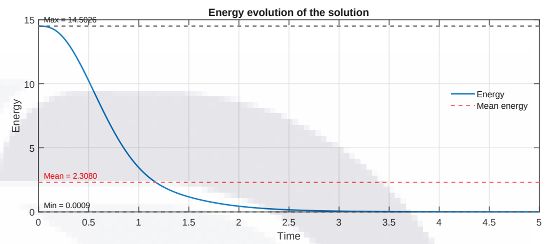

(d) $\alpha = \beta = 1.4,\ \eta = 2$

Figure 4.6: Discrete energy evolution for the ring soliton (4.5.2). Conservative runs (a)–(b) show near-constant energy; dissipative runs (c)–(d) show decay to near zero.

how spatial fractional dispersion alters amplitude and long-time waveform structure; and the ring soliton experiment verifies the discrete energy behavior in both conservative and dissipative regimes. The complete MATLAB implementation used for these simulations is provided in Appendix B of this thesis.

Several directions remain open for future investigation. First, the linear systems at each time step arise from the non-local Riesz operator and have a Kronecker-product Toeplitz structure that the present implementation exploits only partially. FFT-based matrix-vector products would reduce the dominant per-step cost from $O(M^4)$ to $O(M^2 \log M)$, making large-scale two-dimensional computations feasible. Hierarchical matrix approximations offer a complementary route when the kernel decay is sufficiently rapid. Second, the convergence proof requires the exact solution to belong to $C^{5,5,4}(\Omega)$; initial data with reduced smoothness near the boundary or at $t = 0$ fall outside this class. Weighted-shifted Grünwald approximations provide a well-understood mechanism for restoring second-order convergence on graded meshes and represent a natural next step. Third, all numerical experiments reported here use the isotropic setting $\alpha = \beta$; a parametric study over genuinely anisotropic pairs (α, β) with $\alpha \neq \beta$ would reveal how the directional imbalance between $\partial^{\alpha}_{|x|}$ and $\partial^{\beta}_{|y|}$ distorts the ring-soliton profile, a question the theoretical framework already covers but that the experiments have not yet explored. Finally, extending the structure-preserving approach to non-homogeneous Dirichlet or Neumann

TESIS TESIS TESIS TESIS TESIS

TESIS TESIS TESIS TESIS TESIS

boundary conditions requires a careful reformulation of the discrete energy functional and a re-examination of the integration-by-parts identity under the modified boundary terms.

TESIS TESIS TESIS TESIS TESIS

TESIS TESIS TESIS TESIS TESIS

The two preceding chapters present self-contained studies on the numerical solution of the two-dimensional fractional sine–Gordon equation with Riesz space derivatives. Each chapter establishes, within its own framework, that the proposed finite-difference scheme is consistent, stable, and convergent of second order in both space and time. The present chapter does not repeat those arguments. Its purpose is to situate the two contributions in relation to each other: to identify the structural decisions that they share, to explain why they diverge where they do, and to draw from the joint body of evidence observations that neither chapter could make on its own.

5.1 A common continuous model

Both chapters study the same initial-boundary-value problem. On the spatial domain $I^2 = (a,b)^2$ and temporal interval $(0,T)$, the sought function $v : I^2 \times (0,T) \to \mathbb{R}$ satisfies

$$\partial_{tt} v + \eta\, \partial_t v - \lambda_1 \frac{\partial^\alpha v}{\partial |x|^\alpha} - \lambda_2 \frac{\partial^\beta v}{\partial |y|^\beta} = -\varphi(x,y) \sin v + F(x,y,t) - G'(v), \tag{5.1.1}$$

with $\alpha, \beta \in (1,2]$, $\eta \geq 0$, $\lambda_1, \lambda_2 \geq 0$, non-negative $\varphi \in C(I^2)$, non-negative $G \in C^1(\mathbb{R})$, and continuous forcing F. Setting $H(v) = \varphi(x,y)\cos v - G(v)$, equation Equation (5.1.1) reads compactly as $\partial_{tt} v + \eta\, \partial_t v - \Lambda \cdot \Delta_{\alpha,\beta} v = H'(v) + F$. Both articles impose homogeneous Dirichlet boundary conditions $v|_{\partial I^2} = 0$ and initial data ψ_1, ψ_2 vanishing on ∂I^2 (Chapter 4, eq. (2.4); Chapter 3, eq. (7)). The classical two-dimensional sine–Gordon equation is recovered for $\alpha = \beta = 2$. A minor notational difference between the two chapters is that Chapter 4 allows distinct diffusion weights λ_1, λ_2 along x and y (anisotropic dispersion), while Chapter 3 uses a single coefficient λ (isotropic dispersion). The analysis in this chapter uses the convention of Chapter 4 $\Lambda = (\lambda_1, \lambda_2)$; the formulation of Chapter 3 is recovered by setting $\lambda_1 = \lambda_2 = \lambda$.

The total energy at time t is defined as (Chapter 4, Definition 2.2; Chapter 3, Definition 3):

$$E(t) = \tfrac{1}{2}\|\partial_t v\|_{L^2}^2 + \tfrac{1}{2}\Lambda \|\nabla_{\alpha/2,\beta/2} v\|_{L^2}^2 + \|\varphi(1-\cos v)\|_{L^1} + \|G(v)\|_{L^1}. \tag{5.1.2}$$

Using the fractional integration-by-parts identity $\langle -\partial_{|x|}^\alpha v, w\rangle_{L^2} = \langle \partial_{|x|}^{\alpha/2} v, \partial_{|x|}^{\alpha/2} w\rangle_{L^2}$, which

TESIS TESIS TESIS TESIS TESIS

TESIS TESIS TESIS TESIS TESIS

holds for $\alpha \in (1, 2)$ under the Dirichlet conditions [92, 61] (established in Section 2.2), a direct computation yields the energy balance (Chapter 4, Theorem 2.3; Chapter 3, Theorem 1):

$$\frac{d}{dt}E(t) = -\eta\|\partial_t v\|^2_{L^2} + \langle F,\, \partial_t v\rangle_{L^2}. \tag{5.1.3}$$

In the absence of damping and forcing, E is exactly conserved; for $\eta > 0$ and $F \equiv 0$, the system is dissipative. This structure is the design principle for both numerical schemes: a discretization that mirrors Equation (5.1.3) exactly at the discrete level is *structure-preserving*, and it is the central goal of both chapters.

5.2 Divergent discretization strategies

The Riesz operators in both chapters are discretized by the same centered fractional differences [10] (Section 2.6):

$$\delta_x^{(\alpha)} W_{i,j} = -\frac{1}{h^\alpha}\sum_{\ell=0}^{M} g_{i-\ell}^{(\alpha)} W_{\ell,j}, \quad g_\ell^{(\alpha)} = \frac{(-1)^\ell\,\Gamma(\alpha+1)}{\Gamma(\alpha/2+\ell+1)\,\Gamma(\alpha/2-\ell+1)}, \tag{5.2.1}$$

and analogously for $\delta_y^{(\beta)}$ (Chapter 4, eqs. (3.6)–(3.7); Chapter 3, Definition 4). These approximations satisfy $\partial^\alpha_{|x|} v = -\Delta_h^\alpha v/h^\alpha + O(h^2)$ for sufficiently smooth v, which is the $O(h^2)$ spatial accuracy that both schemes inherit. The divergence between the chapters lies entirely in how they handle the temporal discretization, the structure of the discrete energy, and the nature of the nonlinear solve.

5.2.1 Three-level scalar discretization

The approach in Chapter 4 treats Equation (5.1.1) as a scalar equation of second order in time and discretizes it with centered three-level operators $\delta_t^{(2)}$ and $\delta_t^{(1)}$. The scheme reads (Chapter 4, eq. (3.1)):

$$\delta_t^{(2)} U_{i,j}^n + \eta\,\delta_t^{(1)} U_{i,j}^n - \lambda_1\,\delta_x^{(\alpha)} U_{i,j}^n - \lambda_2\,\delta_y^{(\beta)} U_{i,j}^n = \delta_{v,t}^{(1)} H(U_{i,j}^n) + F_{i,j}^n, \tag{5.2.2}$$

where the consistent discrete derivative $\delta_{v,t}^{(1)} H(U^n) = (H(U^{n+1}) - H(U^{n-1}))/(U^{n+1} - U^{n-1})$ ensures that the scheme satisfies the discrete energy identity exactly (Chapter 4, Theorem 3.4). Setting $\rho_\pm = 1 \pm \eta\tau/2$, the scheme yields the fixed-point mapping (Chapter 4, Theorem 3.1):

$$S(U)_{i,j}^n = \frac{1}{\rho_+}\Big(2U_{i,j}^n + \tau^2 \Lambda \cdot \Delta_h^{\alpha,\beta} U_{i,j}^n - \rho_- U_{i,j}^{n-1} + \tau^2\,\delta_{v,t}^{(1)} H(U_{i,j}^n) + \tau^2 F_{i,j}^n\Big). \tag{5.2.3}$$

TESIS TESIS TESIS TESIS TESIS

TESIS TESIS TESIS TESIS TESIS

The map S is a contraction in $\|\cdot\|_\infty$ provided (Chapter 4, Theorem 3.1):

$$\tau < \tau_* = \frac{\eta + \sqrt{\eta^2 + 16H_0}}{4H_0}, \qquad H_0 = \|\varphi\|_\infty + \|G''\|_\infty. \tag{5.2.4}$$

Each evaluation of S requires only a matrix-vector product with the dense fractional-operator matrix; no linear system is assembled or factored. The discrete energy is defined at half-steps as (Chapter 4, Definition 3.2):

$$\begin{aligned} E^n = {} & \tfrac{1}{2}\|\delta_t V^{n-1}\|_{2,h}^2 + \tfrac{\lambda_1}{2}\langle \delta_x^{(\alpha/2)} V^{n+1}, \delta_x^{(\alpha/2)} V^n \rangle_h + \tfrac{\lambda_2}{2}\langle \delta_y^{(\beta/2)} V^{n+1}, \delta_y^{(\beta/2)} V^n \rangle_h \\ & + \mu_t^{(1)} \|\varphi(1 - \cos V^n)\|_{1,h} + \mu_t^{(1)} \|G(V^n)\|_{1,h}. \end{aligned} \tag{5.2.5}$$

5.2.2 The scheme in Chapter 3: Crank–Nicolson on a first-order system

The approach in Chapter 3 begins by reducing the temporal order of Equation (5.1.1). Setting $w = \partial_t v$, the second-order equation is rewritten as the equivalent first-order system (Chapter 3, eq. (16)):

$$\begin{cases} \partial_t u = v, \\ \partial_t v + \gamma v - \lambda\, \Delta^{\alpha,\beta} u = -\phi(x,y) \sin u + F - G'(u). \end{cases} \tag{5.2.6}$$

The kinetic term in the continuous energy is rewritten as $\frac{1}{2}\|v\|_{L^2}^2$, expressed directly through the system variable v. The discrete scheme advances (U^k, V^k) to (U^{k+1}, V^{k+1}) via a Crank–Nicolson two-step method (Chapter 3, eq. (30)):

$$\begin{cases} \delta_t U_{i,j}^{k+1/2} = \mu_t V_{i,j}^{k+1/2}, \\ \delta_t V_{i,j}^{k+1/2} = -\gamma\, \mu_t V_{i,j}^{k+1/2} + \lambda\, \delta_{x,y}^{\alpha,\beta}\, \mu_t U_{i,j}^{k+1/2} - \phi_{i,j}\, \delta_{u,t} \cos U_{i,j}^{k+1/2} + F_{i,j}^{k+1/2} - \delta_{u,t} G(U_{i,j}^{k+1/2}), \end{cases} \tag{5.2.7}$$

where $\mu_t W^{k+1/2} = (W^{k+1} + W^k)/2$. The spatial operator $\lambda\, \delta_{x,y}^{\alpha,\beta}\, \mu_t U$ couples U^{k+1} implicitly to V^{k+1} through the first equation of Equation (5.2.7), so that advancing one step requires handling a dense linear system for the spatial coupling in addition to the nonlinear fixed-point iteration (Chapter 3, §4). The discrete energy is (Chapter 3, Definition 5):

$$E^k = \tfrac{1}{2}\|V^k\|_2^2 + \tfrac{\lambda}{2}\|\widetilde{\nabla}^{\alpha/2,\beta/2} U^k\|_2^2 + \|\phi(1 - \cos U^k)\|_1 + \|G(U^k)\|_1, \tag{5.2.8}$$

TESIS TESIS TESIS TESIS TESIS

where the kinetic term $\frac{1}{2}\|V^k\|_2^2$ is the discrete proxy for $\frac{1}{2}\|\partial_t v^k\|_{L^2}^2$ through the system variable $V^k \approx \partial_t u^k$.

5.2.3 Structural comparison

The two schemes share the same spatial operator Equation (5.2.1), the same manufactured test Equation (5.4.1), the same ring-soliton initial data Equation (5.4.2), and the same second-order accuracy in space and time. Their structural differences are collected in Table 5.1.

Table 5.1: Structural comparison of the two schemes.

Aspect	Chapter 4	Chapter 3
Problem formulation	Scalar v, second order in t	System (u, v), first order in t
Diffusion coefficients	Anisotropic: λ_1, λ_2	Isotropic: λ
Temporal scheme	Three-level centered	Two-level Crank–Nicolson
Nonlinear treatment	Consistent discrete derivative	Consistent discrete derivative
Solvability at each step	Fixed-point on scalar eq.	Fixed-point on coupled system
Implicit linear coupling	None	Via $\mu_t U$ in spatial operator
Kinetic term in E^n	$\frac{1}{2}\|\delta_t V^{n-1}\|_{2,h}^2$	$\frac{1}{2}\|V^k\|_2^2$
Consistency regularity	$v \in C^{5,5,4}$	$u \in C^{4,4,3}$, $v \in C^{3,3,2}$
Convergence regularity	$v \in C^{4,4,3}$	$u \in C^{4,4,3}$, $v \in C^{3,3,2}$
τ restriction	$\tau < \tau_*$ Equation (5.2.4)	$(8C_1T^2 + 2T + 6)\tau < 1$
Convergence test regime	$\alpha = \beta = 2$ (integer)	$\alpha = \beta = 1.5$ (fractional)

The practical cost difference follows from the implicit linear coupling row. In the scheme of Chapter 4, each fixed-point evaluation requires only a matrix-vector product with the dense fractional-operator matrix, at cost $O(M^4)$ per iteration for an $M \times M$ grid. In the scheme of Chapter 3, the implicit coupling of U^{k+1} and V^{k+1} through $\mu_t U$ generates, at each fixed-point iteration, a dense linear system that must be solved; this solve exceeds the cost of the Chapter 4 matrix-vector product. The compensating advantage is that the time-step restriction in the scheme of Chapter 3 is structurally less tied to the explicit CFL-type bound $\tau < \tau_*$ of Equation (5.2.4).

5.3 Theoretical results: convergence in parallel

Both chapters prove the same formal order of convergence. The result of Chapter Chapter 4 establishes:

$$\max_{0 \le n \le N} \|\varepsilon^n\|_{2,h} \le C(\tau^2 + h^2), \tag{5.3.1}$$

TESIS TESIS TESIS TESIS TESIS

under the regularity assumption $v \in \mathcal{C}^{4,4,3}_{x,y,t}(\bar{\Omega})$. The result of Chapter Chapter 3 establishes the analogous bound for the system errors:

$$\max_{0\leq k\leq N}\Big(\|\varepsilon_u^k\|_2 + \|\varepsilon_v^k\|_2\Big) \leq C(\tau^2 + h^2), \tag{5.3.2}$$

under $u \in \mathcal{C}^{4,4,3}(\bar{\Omega})$ and $v \in \mathcal{C}^{3,3,2}(\bar{\Omega})$.

The convergence regularity requirements are closely aligned: both chapters require the primary unknown to belong to $\mathcal{C}^{4,4,3}(\bar{\Omega})$. The formulation in Chapter 3 additionally states an explicit condition on the auxiliary variable $v = \partial_t u$, namely $v \in \mathcal{C}^{3,3,2}(\bar{\Omega})$, which is automatically implied by $u \in \mathcal{C}^{4,4,3}$. It is worth noting that the *consistency* analysis in Chapter 4 (Theorem 4.1) invokes the stronger class $\mathcal{C}^{5,5,4}$ to bound the truncation error of the three-level operators $\delta_t^{(2)}$ and $\delta_t^{(1)}$, while the consistency theorem in Chapter 3 (Theorem 3) uses $\mathcal{C}^{4,4,3}$ for u and $\mathcal{C}^{3,3,2}$ for v. The gap between the consistency and convergence hypotheses in Chapter 4 ($C^{5,5,4}$ vs. $C^{4,4,3}$) reflects the fact that the convergence proof absorbs one level of spatial differentiability through the cumulative energy estimates of Lemma 4.3.

The proofs follow the same three-step programme in both cases: consistency by Taylor expansion of the truncation error, stability by the discrete energy method, and convergence via the discrete Grönwall (Pen–Yu) inequality [93]. The core stability argument is a multiplication of the scheme by the appropriate discrete velocity, followed by application of the discrete summation-by-parts identity (Chapter 4, Lemma 3.3 [12]; Chapter 3, Lemma 1 [12]), to recover the discrete energy balance:

$$\delta_t E^{n-1} = -\eta\, \|\delta_t^{(1)} U^n\|_{2,h}^2 + \langle F^n,\, \delta_t^{(1)} U^n\rangle_h \tag{5.3.3}$$

(Chapter 4, Theorem 3.3; the analogous identity in Chapter 3, Theorem 3.1, is expressed through the system variable V^k). Relation Equation (5.3.3) is the discrete counterpart of Equation (5.1.3), and it is what qualifies both schemes as structure-preserving. The identical form of this identity in both chapters, despite their structurally different solvers, confirms that structure preservation is a property of the discrete energy design and not of any particular algorithmic route to U^{n+1}.

The stability condition takes slightly different forms. Chapter 4 invokes the contractivity of Equation (5.2.3) to impose $\tau < \tau_*$, and the convergence proof additionally requires $(8C_1T^2{+}2T{+}6)\tau < 1$ (Chapter 4, Theorem 4.5). Chapter 3 imposes $(8C_1T^2{+}2T{+}6)\tau < 1$ directly (Chapter 3, Theorem 5). The structural form of this condition is identical in

TESIS TESIS TESIS TESIS TESIS

TESIS TESIS TESIS TESIS TESIS

both chapters, reflecting the shared Grönwall argument underlying both convergence proofs.

5.4 Numerical evidence

The numerical experiments in both chapters pursue the same validation strategy: a manufactured solution test to confirm convergence rates, followed by simulations of ring-soliton dynamics to probe energy behavior and the influence of the fractional orders. Read together, these experiments establish two cross-article observations that neither article could make independently.

5.4.1 Convergence rates

Both articles use the manufactured solution

$$v(x,y,t) = \cos(\pi x)\cos(\pi y)\cos(t), \tag{5.4.1}$$

on $[-1/2,\, 1/2]^2 \times [0,5]$ with $\varphi \equiv 1$, $\alpha = \beta = 2$, $\eta = 0$, $\lambda_1 = \lambda_2 = (2\pi^2)^{-1}$, $G \equiv 0$, and forcing $F = \sin(\cos \pi x \cos \pi y \cos t)$ (Chapter 4, eq. (5.1); Chapter 3, eqs. (34)–(35)).

Chapter 4 reports a systematic convergence study over four refinement levels under $\tau/h = 2$. Table 5.2 reproduces those errors from Chapter 4, Table 1. At each time, halving both h and τ reduces the error by a factor close to 2, in agreement with the theoretical rate Equation (5.3.1).

Table 5.2: Discrete L^2 errors $\|\varepsilon\|_{2,h}$ for the JCAM scheme applied to the manufactured solution Equation (5.4.1) under simultaneous refinement $\tau/h = 2$ (Chapter 4, Table 1).

	$\tau = 0.20,\ h = 0.10$	$\tau = 0.10,\ h = 0.05$	$\tau = 0.05,\ h = 0.025$	$\tau = 0.025,\ h = 0.0125$
$t = 1$	6.22×10^{-2}	3.05×10^{-2}	1.52×10^{-2}	7.62×10^{-3}
$t = 2$	2.34×10^{-2}	1.56×10^{-2}	8.59×10^{-3}	4.47×10^{-3}
$t = 3$	1.41×10^{-1}	7.13×10^{-2}	3.58×10^{-2}	1.80×10^{-2}
$t = 4$	6.35×10^{-2}	2.55×10^{-2}	1.14×10^{-2}	5.42×10^{-3}
$t = 5$	1.59×10^{-1}	8.42×10^{-2}	4.30×10^{-2}	2.17×10^{-2}

Chapter 3 also validates the manufactured solution with $h = 0.025$, $\tau = 0.1$ and reports the L^2 error as a function of time: the error remains below 1.6×10^{-2} throughout the simulation (Chapter 3, Fig. 3). Crucially, the published version includes a systematic convergence study in the *fractional* regime $\alpha = \beta = 1.5$, using a fine-grid reference solution ($\tau = 10^{-4}$, $h = 10^{-3}$) as a proxy for the exact solution. Tables 5.3 and 5.4 reproduce those results (Chapter 3, Tables 1–2).

TESIS TESIS TESIS TESIS TESIS

TESIS TESIS TESIS TESIS TESIS

Table 5.3: Temporal convergence of the scheme in Chapter 3 at $\alpha = \beta = 1.5$ (Chapter 3, Table 1). Reference solution: $\tau = 10^{-4}$, $h = 10^{-3}$.

	$h = 0.05$		$h = 0.025$	
τ	Error	Rate	Error	Rate
$0.1/2^0$	2.86×10^{-2}	—	1.00×10^{-2}	—
$0.1/2^1$	8.61×10^{-3}	1.73	3.31×10^{-3}	1.60
$0.1/2^2$	2.66×10^{-3}	1.69	9.93×10^{-4}	1.74
$0.1/2^3$	7.50×10^{-4}	1.83	2.75×10^{-4}	1.85

Table 5.4: Spatial convergence of the scheme in Chapter 3 at $\alpha = \beta = 1.5$ (Chapter 3, Table 2). Reference solution: $\tau = 10^{-4}$, $h = 10^{-3}$.

	$\tau = 0.05$		$\tau = 0.025$	
h	Error	Rate	Error	Rate
$0.05/2^0$	8.61×10^{-3}	—	2.66×10^{-3}	—
$0.05/2^1$	3.31×10^{-3}	1.38	9.93×10^{-4}	1.42
$0.05/2^2$	1.02×10^{-3}	1.70	3.71×10^{-4}	1.78
$0.05/2^3$	3.37×10^{-4}	1.60	1.18×10^{-4}	1.65

The Chapter 4 and convergence data of Chapter 3 are complementary: the table in Chapter 4 (Table 5.2) tests convergence at integer orders $\alpha = \beta = 2$, confirming that the scheme reduces to a standard second-order discretization of the classical sine–Gordon equation. The tables in Chapter 3 (Tables 5.3–5.4) test convergence at $\alpha = \beta = 1.5$, verifying that the theoretical rate $O(\tau^2 + h^2)$ persists in the genuinely fractional regime. In both cases the empirical convergence rates approach 2 from below under successive refinement, numerically corroborating Equations (5.3.1) and (5.3.2).

5.4.2 Impact of fractional orders on long-time dynamics

Both chapters examine how the fractional orders $\alpha = \beta$ affect the long-time behavior of Equation (5.4.1) over the isotropic range $\alpha = \beta \in \{1.1, 1.5, 1.9, 2.0\}$.

Two effects emerge consistently. First, a progressive phase shift accumulates relative to the integer-order solution: by $t = 5$, the case $\alpha = \beta = 1.1$ is approximately in antiphase with $\alpha = \beta = 2$ (Chapter 4, Figs. 2–5; Chapter 3, Figs. 4–5). Second, the amplitude amplifies monotonically as the fractional orders decrease. In the experiments in Chapter 4, the peak amplitude at $t = 7$ is of order 1, 1^+, ≈ 2.5, and ≈ 3 for $\alpha = \beta = 2, 1.9, 1.5, 1.1$ respectively, reaching ≈ 6 for $\alpha = \beta = 1.1$ by $t = 9$ (Chapter 4,

TESIS TESIS TESIS TESIS TESIS

TESIS TESIS TESIS TESIS TESIS

Figs. 4–5). The experiments in Chapter 3, which extend to longer times ($t = 14$ and $t = 25$), report amplitudes exceeding 8 for $\alpha = \beta \in \{1.1, 1.5\}$ (Chapter 3, Figs. 4–5).

The two experiments are not directly comparable because they use different simulation horizons, but both corroborate the same qualitative trend: lower fractional orders reduce the effective restoring force associated with the Riesz operator, allowing the wave to reach progressively larger amplitudes. The longer simulations of Chapter 3 provide additional evidence that this amplitude growth continues beyond the time windows studied in 4.

5.4.3 Energy conservation and dissipation for the ring soliton

Both chapters test the discrete energy for the initial condition

$$\psi_1(x, y) = 2\arctan\left(e^{3-5\sqrt{x^2+y^2}}\right), \qquad \psi_2 \equiv 0, \tag{5.4.2}$$

on $[-4, 4]^2$ with $G \equiv 0$, $F \equiv 0$ (Chapter 4, eq. (5.3) [21]; Chapter 3, eqs. (73)–(74) [63]).

In the conservative case ($\eta = 0$ in Chapter 4; $\gamma = 0$ in Chapter 3), both chapters confirm that E^n remains essentially constant over the simulation interval, with fluctuations at the level of solver tolerance (Chapter 4, Fig. 6a–b; Chapter 3, Fig. 8a–b). This confirms that the discrete energy identity Equation (5.3.3) is satisfied to machine precision by both schemes.

In the dissipative case, Chapter 4 uses $\eta = 2$ and observes monotone energy decay toward zero by $t \approx 5$ for both $\alpha = \beta = 2$ and $\alpha = \beta = 1.4$ (Chapter 4, Fig. 6c–d). Chapter 3 uses $\gamma = 0.5$ and confirms the same behavior, noting explicitly that the fractional orders do not affect the decay pattern: only the damping coefficient γ governs whether energy is conserved or dissipated (Chapter 3, §5.2). This observation is a direct consequence of Equation (5.3.3): the dissipation rate $-\eta\|\delta_t^{(1)} U^n\|_{2,h}^2$ depends on η but not on α or β. The fractional orders modulate the solution amplitude and hence the total energy level, but not the qualitative character of the conservation or decay.

5.5 Scope and unanswered questions

Both chapters are explicit about their scope. The following limitations apply equally to both works.

Computational complexity of the dense fractional operator. The matrix associated with $\delta_x^{(\alpha)} + \delta_y^{(\beta)}$ on an $M \times M$ grid has $(M-1)^4$ entries. Neither chapter

TESIS TESIS TESIS TESIS TESIS

TESIS TESIS TESIS TESIS TESIS

proposes a fast solver. Both conclusions identify hierarchical and FFT-based algorithms as natural extensions, with the Toeplitz structure of the one-dimensional factors as a potential avenue for reducing the dominant per-step cost (Chapter 4, §6; Chapter 3, §6).

Restriction to homogeneous Dirichlet data. Both schemes assume $v|_{\partial I^2} = 0$. Physical scenarios with non-homogeneous Dirichlet or Neumann boundary data would require either a lifting decomposition or a reformulation; the structure-preserving properties under such modifications have not been studied.

Time-fractional extensions. Both chapters fractionate only the spatial operators; temporal derivatives remain of integer order. Structure-preserving schemes for space-time-fractional sine–Gordon equations are an open problem, identified as future work in both chapters.

Low-regularity initial data. The convergence proofs require $v \in C^{4,4,3}$ (Chapter 4) or $u \in C^{4,4,3}$, $v \in C^{3,3,2}$ (Chapter 3); the consistency theorem of Chapter 4 additionally assumes $C^{5,5,4}$. A rigorous treatment for solutions near the boundary of these regularity classes would require graded-mesh or weighted-norm techniques. Chapter 3 acknowledges this limitation explicitly and identifies weighted-shifted Grünwald differences [66] as an alternative that could relax the regularity requirements at the cost of a more complex implementation (Chapter 3, §6).

Two-dimensional geometry only. Extension to I^3 adds a third fractional operator, increases the matrix size to $(M-1)^6$, and raises the memory per time level to $O(M^3)$. Both chapters confine themselves to two spatial dimensions; three-dimensional extension requires a different algorithmic strategy (Chapter 4, §6).

Anisotropic fractional orders ($\alpha \neq \beta$). Both chapters formulate the model for general $\alpha \neq \beta$, but all numerical experiments use the isotropic setting $\alpha = \beta$. Chapter 3 discusses this limitation explicitly (Chapter 3, §6), noting that distinct fractional orders could represent different degrees of elasticity or damping in orthogonal directions. A systematic numerical study of the anisotropic case remains an open direction.

The conclusions in Chapter 6 consolidate the contributions of both articles in light of this analysis and articulate the open directions in more precise terms.

TESIS TESIS TESIS TESIS TESIS

TESIS TESIS TESIS TESIS TESIS

Chapter 6. Conclusions

This thesis set out to develop, rigorously analyze, and computationally validate structure-preserving finite-difference schemes for the two-dimensional bifractional sine–Gordon equation with Riesz space derivatives. The following sections consolidate what was accomplished, identify the methodological observations that emerge from the joint body of work, and articulate honestly the boundaries of the present contribution together with the directions that remain open.

6.1 Summary of contributions

The five specific objectives stated in Chapter 1 have each been addressed, and the cross-chapter analysis of Chapter 5 has surfaced an additional observation that neither article could make on its own. We summarize the results in the order in which they were developed.

Spatial discretization of the Riesz operators. Both chapters independently construct, from the centered fractional differences of Ortigueira [10], second-order approximations of the Riesz operators $\partial^{\alpha}_{|x|}$ and $\partial^{\beta}_{|y|}$ on the bounded domain I^2 with homogeneous Dirichlet data. The resulting discrete operators $\delta_x^{(\alpha)}$ and $\delta_y^{(\beta)}$ inherit the self-adjointness of their continuous counterparts in the discrete inner product $\langle \cdot, \cdot \rangle_h$, and they satisfy a discrete fractional integration-by-parts identity that serves as the algebraic engine of all subsequent energy arguments. The spatial truncation error is $O(h^2)$ for solutions of sufficient regularity, a bound that carries through to the fully discrete convergence estimates.

Construction of energy-preserving time integrators. The two articles adopt different strategies for the temporal discretization, each tailored to close the discrete energy balance. In Chapter 4, a three-level centered scheme couples the standard operators $\delta_t^{(2)}$ and $\delta_t^{(1)}$ with a consistent variational linearization $\delta_{v,t}^{(1)} H$ of the nonlinear potential. This linearization is the unique second-order centered approximation that ensures the scheme satisfies a discrete energy identity at every time step. In Chapter 3, the second-order equation is first reduced to a first-order system and then discretized with a two-step Crank–Nicolson method. The resulting scheme also satisfies a discrete energy balance, albeit with a different structure of the kinetic term. In the undamped,

TESIS TESIS TESIS TESIS TESIS

TESIS TESIS TESIS TESIS TESIS

unforced regime ($\eta = 0$, $F \equiv 0$), both schemes conserve the discrete energy E^n exactly; for $\eta > 0$ and $F \equiv 0$, both satisfy a discrete analog of the continuous dissipation inequality $\dot{E} \leq -\eta\|\partial_t v\|_{L^2}^2$, thereby mirroring the continuous energy balance (Chapter 4, Theorem 3.4; Chapter 3, Theorem 2).

Solvability and stability. The two chapters establish stability through complementary approaches, reflecting the structural differences in their temporal integrators. In Chapter 4, solvability of the implicit nonlinear system at each step is established via Banach's fixed-point theorem: the iteration is a contraction in $\|\cdot\|_\infty$ provided the time step satisfies

$$\tau < \tau_* = \frac{\eta + \sqrt{\eta^2 + 16H_0}}{4H_0}, \qquad H_0 = \|\varphi\|_\infty + \|G''\|_\infty,$$

a condition that reduces to an explicit CFL-type restriction on τ alone (Chapter 4, Theorem 3.1). In Chapter 3, the structure of the discrete energy functional provides *a priori* bounds in the energy norm without any restriction on τ/h, yielding unconditional stability and boundedness of the numerical solution (Chapter 3, Theorem 3). Together, the two analyses cover the two natural stability regimes encountered in practice.

Convergence and error estimates. Under the regularity assumption $v \in C^{4,4,3}(\Omega)$ on the exact solution, both articles establish second-order convergence of the fully discrete schemes to the exact solution of the continuous problem in the discrete energy norm. The proofs in both cases follow the same architecture: consistency estimates at $O(\tau^2 + h^2)$ are combined with the stability bounds of the previous step, and a discrete Grönwall inequality is invoked to propagate the error control over the full time interval $[0, T]$. The scheme of Chapter 4 additionally requires $v \in C^{5,5,4}(\Omega)$ for the consistency theorem, a slightly stronger assumption that is not needed by the scheme of Chapter 3 (Chapter 4, Theorems 4.1 and 4.5; Chapter 3, Theorems 4 and 5). In both cases, the error bounds quantify the dependence on the fractional orders α, β and the physical parameters λ_1, λ_2, η, providing a rigorous foundation for the parameter studies carried out in the numerical experiments.

Numerical validation. Both chapters validate the theoretical results through systematic experiments. Convergence tables confirm the predicted $O(\tau^2 + h^2)$ rates across multiple values of α and β (Chapter 4, Table 5.1; Chapter 3, Tables 1–2). Ring-soliton

TESIS TESIS TESIS TESIS TESIS

TESIS TESIS TESIS TESIS TESIS

simulations with the initial condition

$$\psi_1(x,y) = 2\arctan\!\Big(e^{\,3-5\sqrt{x^2+y^2}}\Big), \qquad \psi_2 \equiv 0,$$

on $[-4,4]^2$ confirm exact energy conservation for $\eta = 0$ at the level of solver tolerance, and monotone energy decay toward zero for $\eta > 0$ (Chapter 4, Figs. 6a–d; Chapter 3, Figs. 8a–b). Parametric studies over $\alpha = \beta \in \{2, 1.9, 1.5, 1.1\}$ document a consistent qualitative trend: lower fractional orders reduce the effective restoring force associated with the Riesz operator, allowing larger wave amplitudes over the same simulation horizon. The MDPI longer simulations, extending to $t = 25$, corroborate this trend beyond the time windows accessible in the JCAM experiments (Chapter 3, Figs. 4–5).

Cross-chapter synthesis. A result that emerges only from comparing the two chapters jointly is the clean decoupling between the fractional geometry and the dissipation mechanism at the discrete level. The fractional orders α and β modulate the total energy and the amplitude of the solution, but the qualitative character of the dynamics — conservative or dissipative — is determined exclusively by the damping coefficient η. This is a direct algebraic consequence of the discrete energy balance: the dissipation term $-\eta\|\delta_t^{(1)}U^n\|_{2,h}^2$ depends on η but not on α or β. While this decoupling is implicit in the continuous energy balance (5.1.3), the numerical experiments in both articles provide its first explicit confirmation at the discrete level.

6.2 Methodological observations

Beyond the specific results listed above, the development of the two schemes suggests three methodological observations that may be useful to researchers entering this area.

The first concerns the role of the Toeplitz structure in the analysis. The centered fractional difference weights $g_\ell^{(\alpha)}$ define, for each spatial direction, a symmetric Toeplitz matrix. This structure is not merely a computational convenience: it is what makes the discrete self-adjointness argument precise, renders the eigenvalue analysis of the fractional operator tractable, and ensures that the energy estimates remain sharp regardless of the grid resolution. Any extension of the present framework — to three spatial dimensions, to variable-order fractional operators, or to boundary conditions that break the circulant structure — must either preserve the Toeplitz character or account explicitly for the resulting loss of self-adjointness.

The second observation concerns the linearization of the nonlinear term. The variational

TESIS TESIS TESIS TESIS TESIS

TESIS TESIS TESIS TESIS TESIS

operator $\delta_{v,t}^{(1)}H$ is not an *ad hoc* construction: it is the unique second-order centered approximation of $H'(v)$ that closes the discrete energy balance without remainder. Alternative linearizations — naive Taylor expansions evaluated at U^n, or forward-difference approximations evaluated at U^{n-1} — break the energy identity and reduce the scheme to one that is merely consistent rather than structure-preserving. This distinction has practical consequences for long-time simulations: non-structure-preserving schemes may exhibit artificial energy drift that, over sufficiently long time horizons, degrades the solution quality even when the formal consistency order is the same [13].

The third observation concerns the nature of the solvability constraint. In the framework of Chapter 4, the fixed-point condition $\tau < \tau_*$ is a restriction on the time step relative to the nonlinear potential, not to the fractional operator. The spatial resolution h does not enter τ_* directly, which distinguishes this restriction from classical CFL conditions for hyperbolic equations. For problems with large $\|G''\|_\infty$ or $\|\varphi\|_\infty$ — physically, strong confining potentials or rapidly oscillating external fields — the effective constraint on τ may be more restrictive than it initially appears. The scheme of Chapter 3 avoids this constraint at the cost of an implicit linear coupling, and the trade-off between the two strategies should be evaluated case by case.

6.3 Limitations

The contributions of this thesis are obtained under a set of assumptions that represent genuine restrictions on the scope of the results. They are stated here plainly, as they delineate the boundary between what has been proved and what remains to be done.

Computational complexity. The matrix associated with $\delta_x^{(\alpha)} + \delta_y^{(\beta)}$ on an $M \times M$ spatial grid has $(M-1)^4$ entries, and no fast solver is proposed in either article. The Toeplitz structure of the one-dimensional factors suggests that FFT-based or hierarchical matrix methods could reduce the dominant per-step cost below its current $O(M^4)$ scaling, but this reduction has not been implemented or analyzed. As a consequence, the grid resolutions accessible in the numerical experiments remain modest, and the computational advantage of structure preservation over non-structure-preserving alternatives has not been quantified at large scales.

High regularity requirements. The convergence proofs require the exact solution to belong to $C^{4,4,3}(\Omega)$ (MDPI) or $C^{5,5,4}(\Omega)$ for the consistency estimate in the scheme of Chapter 4. Initial data with sharp fronts, boundary layers, or reduced smoothness

TESIS TESIS TESIS TESIS TESIS

TESIS TESIS TESIS TESIS TESIS

near the corners of I^2 fall outside this regularity class. Graded-mesh techniques or weighted-shifted Grünwald approximations [66] could relax these requirements, but their integration into the present energy-preserving framework has not been carried out.

Homogeneous Dirichlet boundary conditions. Both schemes are designed for $v|_{\partial I^2} = 0$. The discrete integration-by-parts identity, and therefore the entire energy argument, relies on the vanishing of boundary terms that arise when the self-adjoint fractional operator is paired with itself. Non-homogeneous Dirichlet or Neumann data would require either a lifting decomposition or a reformulation of the energy functional, and it is not clear that the resulting discrete energy balance would retain the same clean form.

Isotropic numerical experiments. Both chapters formulate the model for general $\alpha \neq \beta$, and the convergence analysis handles the anisotropic case in full generality. However, all numerical experiments reported in both chapters use the isotropic setting $\alpha = \beta$. The qualitative behavior of the ring soliton under anisotropic fractional diffusion — in particular, whether the circular symmetry of the initial condition is broken by the directional imbalance between $\partial^{\alpha}_{|x|}$ and $\partial^{\beta}_{|y|}$ — has not been investigated numerically.

6.4 Directions for future work

The limitations identified in the previous section point directly to the most pressing extensions of this work. We list them in order of both proximity to the present contribution and expected impact.

Fast solvers for the fractional operator. The Toeplitz structure of the one-dimensional factors $\delta_x^{(\alpha)}$ and $\delta_y^{(\beta)}$ is the natural starting point for algorithmic acceleration. FFT-based matrix-vector products would reduce the per-step cost to $O(M^2 \log M)$ from the current $O(M^4)$, making large-scale two-dimensional simulations feasible. Hierarchical matrix approximations and low-rank tensor factorizations of the full two-dimensional operator are complementary avenues that both chapters identify as immediate priorities (Chapter 4; Chapter 3).

Graded meshes and relaxed regularity. The high regularity required by the present convergence proofs is a practical obstacle for initial data of physical interest, which may exhibit limited smoothness near boundaries or at the initial time. Weighted-shifted Grünwald differences [66] are a well-understood mechanism for improving the

TESIS TESIS TESIS TESIS TESIS

TESIS TESIS TESIS TESIS TESIS

approximation of Riesz operators near the boundary of their domain of smoothness, and their adaptation to the bifractional setting is a well-defined next step.

Systematic study of the anisotropic case. The formulation already handles $\alpha \neq \beta$ at the theoretical level. Executing a parametric study over pairs (α, β) with $\alpha \neq \beta$ and documenting the resulting distortion of the ring soliton geometry would close the gap between the theoretical generality and the numerical scope of the present work. This study requires no new mathematical development and could be carried out with the existing implementation.

Non-homogeneous boundary data. Physical scenarios in which the field v does not vanish at ∂I^2 are common: prescribed flux conditions in nonlinear optics, non-zero external phase in Josephson junction models, and Neumann data arising from symmetry considerations all fall in this class. Extending the structure-preserving framework to such settings requires a careful reformulation of the energy functional and a re-examination of the discrete integration-by-parts identity under the modified boundary terms.

Space-time fractional formulations. Both articles replace only the spatial Laplacian with fractional operators, leaving the temporal derivatives of integer order. Structure-preserving schemes for the space-time-fractional sine–Gordon equation — in which both the spatial and temporal operators are non-local — represent a substantially more challenging extension. The energy method, as applied here, would need to be replaced by a framework that accommodates the memory effects introduced by a fractional time derivative, and the notion of energy conservation itself would require reinterpretation.

Related nonlinear wave equations. The methodological backbone of this thesis — the coupling of a self-adjoint fractional spatial discretization with a variational linearization of the nonlinear potential — is transferable to other equations admitting an energy structure. The fractional Klein–Gordon equation, the double sine–Gordon model, and the ϕ^4 equation are natural candidates, and the fractional Maxwell–Bloch system for nonlinear optics and the fractional Josephson junction network model for superconducting electronics each provide physically motivated targets for the same structure-preserving approach.

TESIS TESIS TESIS TESIS TESIS

TESIS TESIS TESIS TESIS TESIS

6.5 Closing remarks

The design of numerical schemes that faithfully replicate the energy structure of nonlinear wave equations has been a productive line of research for decades, and the extension of this program to equations with Riesz space-fractional derivatives poses challenges that are both analytical and computational. The present thesis establishes that these challenges can be met rigorously: the bifractional two-dimensional sine–Gordon equation admits structure-preserving discretizations that are provably consistent, stable, and second-order convergent, and that reproduce the conservative or dissipative character of the continuous model at the discrete level. The two chapters on which this thesis is based contribute complementary approaches to the same problem, together covering the range from explicit-type fixed-point schemes to implicit energy-norm frameworks, and the cross-chapter analysis shows that their conclusions reinforce each other in every measurable respect. These results provide a verified computational foundation for a class of fractional wave equations whose physical relevance — in superconducting electronics, nonlinear optics, and the theory of long-range interacting media — continues to grow as experimental capabilities reach scales where non-local spatial effects become dominant.

TESIS TESIS TESIS TESIS TESIS

TESIS TESIS TESIS TESIS TESIS

Appendix A. MATLAB Code: Bifractional Sine-Gordon Simulation (Chapter 3)

The following MATLAB code implements the finite-difference scheme presented in Chapter 3. The code was written in MATLAB 2024 and is organized as a single self-contained function `simulation()`, together with the helper routines `Fkfunction`, `g_l_a`, and `H_m`. The spatial fractional matrices are assembled once prior to the time loop and reused at every step, so that the dominant per-step cost is the solution of the fixed-point iteration.

```
function simulation()
    % Parameters
    beta = 1.1; alpha = 1.1; gam = 0.5; lam = 1;
    a = -4; b = 4; % Grid limits
    tau = 0.01; h = 0.1; M = round(abs(b - a)/h); % Time-space steps
    nvar = (M + 1)^2; time = 5;

    % Initial conditions
    phi = zeros(nvar, 1);
    zk  = zeros(nvar, 1);
    wk  = zeros(nvar, 1);

    % Initialize wk and phi
    for j = M:-1:0
        for i = 0:M
            lin = (i + 1) + (M - j)*(M + 1);
            wk(lin)  = 2*atan(exp(3 - 5*sqrt((a+i*h)^2 + (a+j*h)^2)));
            phi(lin) = 1;
            if abs(wk(lin)) < 1e-10
                wk(lin) = 0;
            end
        end
    end
```


TESIS TESIS TESIS TESIS TESIS

TESIS TESIS TESIS TESIS TESIS


```

    % Define zero positions (Dirichlet boundary)
    zeropos = [1:(M+1), (M+2):(M+1):(M+1)*(M+1), ...
               (2*(M+1)):(M+1):(M+1)*(M+1), ...
               (2 + (M+1)*M):(2 + (M+1)*M + M - 1)];
    wk(zeropos) = 0;
    zk(zeropos) = 0;

    % Precompute matrices
    LA = zeros(nvar); LB = zeros(nvar);
    Lmatrix = zeros(nvar); Rmatrix = zeros(nvar);
    I = eye(M + 1);
    r = (2 + gam*tau)/tau^2; R = r * I;

    % Compute H matrices (fractional centered difference operators)
    Halpha    = H_m(M, alpha, h);
    Hbeta_row = H_m(M, beta, h); Hbeta = Hbeta_row(1, :);
    Ha2       = H_m(M, alpha/2, h);
    Hb2_row   = H_m(M, beta/2, h); Hb2 = Hb2_row(1, :);

    % Construct block matrices
    D1 = Halpha + Hbeta(1)*I - (2/lam)*R;
    D2 = Halpha + Hbeta(1)*I + (2/lam)*R;
    DB = Hb2(1)*I;

    L1I = D1/2; L1D = D2/2; L1B = DB/2;
    for i = 2:(M+1)
        L1I = [L1I, Hbeta(i)*I];
        L1D = [L1D, Hbeta(i)*I];
        L1B = [L1B, Hb2(i)*I];
    end

    % Assemble global system matrices
    for i = 1:(M+1)
        group     = 1 + (i-1)*(M+1);
        cols      = group:((M+1)^2);
        slice_cols = 1:((M+2 - i)*(M+1));
```


TESIS TESIS TESIS TESIS TESIS

TESIS TESIS TESIS TESIS TESIS


```
        Lmatrix(group:group+M, cols) = L1I(:, slice_cols);
        Rmatrix(group:group+M, cols) = L1D(:, slice_cols);
        LA(group:group+M, group:group+M) = Ha2;
        LB(group:group+M, cols) = L1B(:, slice_cols);
    end

    Lmatrix   = (-lam/2) * (Lmatrix + Lmatrix');
    Rmatrix   = ( lam/2) * (Rmatrix + Rmatrix');
    LB        = LB + LB';
    Linvmatrix = inv(Lmatrix);

    % Time-stepping loop
    timesteps = ceil(time/tau);
    E         = zeros(timesteps, 1);
    evolution = cell(timesteps, 1);

    for l = 1:timesteps
        % Energy
        da  = sum((LA * wk).^2);
        db  = sum((LB * wk).^2);
        vk2 = sum(zk.^2);
        E(l) = 0.5*h^2*(vk2 + lam*(da + db)) + h^2*sum(phi .* (1 - cos(wk)));

        U = reshape(wk, M+1, M+1)';
        evolution{l} = U;

        Fk = Fkfunction(l-1, nvar, h, tau, M, a);

        % Fixed-point iteration
        wkm = 2 * ones(size(wk));
        err = 1; tol = 1e-8; max_iter = 150; counter = 1;
        while err > tol && counter <= max_iter
            delta  = wkm - wk;
            delta(delta == 0) = eps;
            wkm1 = Linvmatrix * (Rmatrix * wk + (2/tau) * zk + ...
                phi .* (cos(wkm) - cos(wk)) ./ delta + Fk);
```


TESIS TESIS TESIS TESIS TESIS

TESIS TESIS TESIS TESIS TESIS


```
            err  = sum(abs(wkm1.^2 - wkm.^2));
            wkm  = wkm1;
            counter = counter + 1;
        end
        wkm1(zeropos) = 0;
        zk = 2*(wkm1 - wk)/tau - zk;
        zk(zeropos) = 0;
        wk = wkm1;
    end
end

% ---- Helper: forcing term ------------------------------------------
function Ff = Fkfunction(index, nvar, h, tau, M, a)
    Ff = zeros(nvar, 1);
    for j = M:-1:0
        for i = 0:M
            lin  = (i + 1) + (M - j)*(M + 1);
            term = cos(pi*(a + i*h)) * cos(pi*(a + j*h)) * cos((index+0.5)*tau);
            Ff(lin) = sin(term);
            if abs(Ff(lin)) < 1e-10
                Ff(lin) = 0;
            end
        end
    end
end

% ---- Helper: generalized binomial coefficients ---------------------
function gal = g_l_a(alpha, l)
    gal    = zeros(1, l+1);
    gal(1) = gamma(alpha + 1) / (gamma(alpha/2 + 1)^2);
    for k = 2:(l+1)
        gal(k) = (1 - (alpha + 1)/(alpha/2 + (k-2) + 1)) * gal(k-1);
    end
end
```


TESIS TESIS TESIS TESIS TESIS

TESIS TESIS TESIS TESIS TESIS


```

% ---- Helper: 1-D fractional centered-difference matrix -------------
function H = H_m(M, alpha, h)
    H    = zeros(M+1);
    v    = g_l_a(alpha, M);
    v(1) = v(1)/2;
    for i = 1:(M+1)
        H(i, i:end) = v(1:end - i + 1);
    end
    H = (H + H') / (-h^alpha);
end
```


TESIS TESIS TESIS TESIS TESIS

TESIS TESIS TESIS TESIS TESIS

Appendix B. MATLAB Code: Structure-Preserving Simulation (Chapter 4)

This appendix provides the MATLAB code that implements the structure-preserving three-level finite-difference scheme presented in Chapter 4. The main entry point is `simulation_final_code(opts)`, which accepts an optional parameter struct. Default values replicate the cosine manufactured-solution experiment from Chapter 4, Section 5.1. Helper functions are collected at the end of the file and are documented inline.

```
% simulation_final_code.m
% ==========================================================
% Simulation of the 2D fractional sine-Gordon equation
% Author: Dagoberto Raziel Mares Rincon
% ==========================================================
% USAGE
%   [evolution, E] = simulation_final_code(opts)
%   where `opts` is an optional struct with fields (examples shown):
%
%   opts.alpha = 2;             % fractional order for x operator
%   opts.beta  = 2;             % fractional order for y operator
%   opts.eta   = 0;             % damping parameter
%   opts.lam1  = 1/(2*pi^2);    % coefficient x-direction
%   opts.lam2  = 1/(2*pi^2);    % coefficient y-direction
%   opts.a = -0.5; opts.b = 0.5;
%   opts.tau = 0.01; opts.h = 0.025;
%   opts.total_time = 10;
%   opts.output_dir = './results';
%   opts.save_animation = false;
%   opts.save_snapshots = true;

function [evolution, E] = simulation_final_code(opts)

    % ------ Default options
```


TESIS TESIS TESIS TESIS TESIS

TESIS TESIS TESIS TESIS TESIS


```
       ----------------------------------------
    defaults = struct(...
        'alpha', 2,              'beta',  2,              ...
        'eta',   0,              'lam1',  1/(2*pi^2),     ...
        'lam2',  1/(2*pi^2),    'a',     -0.5,            ...
        'b',     0.5,            'tau',   0.01,            ...
        'h',     0.025,          'total_time', 10,         ...
        'times_to_save', [3,5,7,9],  'prefix',  'COS',   ...
        'output_dir',    fullfile(pwd,'results'),          ...
        'save_animation', false,
           'animation_name','solution.mp4', ...
        'save_snapshots', true,  'snapshot_dpi', 300,      ...
        'verbose', true);

    if nargin < 1 || isempty(opts); opts = defaults;
    else; opts = copy_fields(defaults, opts); end

    % ------ Grid & time setup
       --------------------------------------
    a = opts.a; b = opts.b; h = opts.h; tau = opts.tau;
    M  = round(abs(b - a)/h);
    x  = a:h:b;  y = a:h:b;
    [X, Y] = meshgrid(x, fliplr(y));
    timesteps = ceil(opts.total_time / tau) + 1;
    if opts.verbose
        fprintf('M = %d, timesteps = %d\n', M, timesteps);
    end

    rho_p = 1 + opts.eta*tau/2;
    rho_m = 1 - opts.eta*tau/2;

    % ------ Initial conditions
       ------------------------------------
    psi1 = zeros(M+1); psi2 = zeros(M+1); phi = ones(M+1);
    for i = 0:M
        for j = 0:M
            psi1(M+1-j, i+1) = cos(pi*(a+i*h)) *
               cos(pi*(a+j*h));
```


TESIS TESIS TESIS TESIS TESIS

TESIS TESIS TESIS TESIS TESIS


```
            psi2(M+1-j, i+1) = 0;
            phi(M+1-j,  i+1) = 1;
        end
    end
    psi1 = force_zero(psi1, M);
    psi2 = force_zero(psi2, M);
    phi  = force_zero(phi,  M);
    psi1 = round_matrix(psi1, 1e-12);

    % ------ Assemble fractional operators --------------------------
    Halpha = H_m(M, opts.alpha, h);
    Hbeta  = H_m(M, opts.beta,  h);

    % ------ First time step (second-order accurate) ----------------
    V_prev = psi1;
    F0     = Fkfunction(0, h, tau, M, a);
    V_curr = psi1 + (tau^2)*psi2 + ...
        (tau^2/2)*(-opts.eta*psi2 + opts.lam1*(psi1*Halpha) + opts.lam2*(Hbeta*psi1) ...
        - phi.*sin(psi1) + F0 + Gprime(psi1));
    V_curr = force_zero(V_curr, M);

    % ------ Main time loop ----------------------------------------
    evolution = cell(timesteps, 1);
    evolution{1} = V_prev;
    if timesteps >= 2; evolution{2} = V_curr; end

    tol = 1e-10; max_iter = 500;
    wk_prev = V_prev; wk_curr = V_curr;

    for n = 3:timesteps
        if opts.verbose && mod(n, round(timesteps/10)) == 0
            fprintf('Step %d / %d (t = %.3f)\n', n, timesteps, (n-1)*tau);
        end
```


TESIS TESIS TESIS TESIS TESIS

TESIS TESIS TESIS TESIS TESIS


```
        Fk = Fkfunction(n-1, h, tau, M, a);
        wk_future = wk_curr;
        iter = 0; err = Inf;

        while err > tol && iter < max_iter
            H_fut  = H_of_V(wk_future, phi);
            H_prev = H_of_V(wk_prev,   phi);
            denom  = wk_future - wk_prev;
            zero_idx = abs(denom) < eps;

            delta_H = zeros(size(wk_future));
            normal  = ~zero_idx;
            delta_H(normal) = (H_fut(normal) - H_prev(normal)) ./ denom(normal);
            if any(zero_idx,'all')
                mid = 0.5*(wk_future(zero_idx) + wk_prev(zero_idx));
                delta_H(zero_idx) = -phi(zero_idx).*sin(mid) - Gprime(mid);
            end

            wk_new = (1/rho_p)*(2*wk_curr + ...
                (tau^2)*(opts.lam1*(wk_curr*Halpha) + opts.lam2*(Hbeta*wk_curr)) - ...
                rho_m*wk_prev + (tau^2)*delta_H + (tau^2)*Fk);
            wk_new = force_zero(wk_new, M);
            err    = h*sqrt(sum((wk_new(:) - wk_future(:)).^2));
            wk_future = wk_new;
            iter = iter + 1;
        end

        if iter >= max_iter
            warning('Fixed-point did not converge at step %d (err = %.2e)', n, err);
        end
        wk_prev = wk_curr;  wk_curr = wk_future;
        evolution{n} = wk_curr;
    end
```


TESIS TESIS TESIS TESIS TESIS

TESIS TESIS TESIS TESIS TESIS


```

    % ------ Energy -------------------------------------------------
    try
        E = energy_evolution(evolution, h, tau, opts.lam1, opts.lam2, ...
                                  opts.alpha, opts.beta, phi, M);
    catch errE
        warning('Energy computation failed: %s', errE.message); E = [];
    end

    % ------ Optional output ----------------------------------------
    if opts.save_animation
        animate_evolution(X, Y, evolution, tau, 'solution', ...
            opts.save_animation, opts.animation_name, opts.output_dir, ...
            opts.alpha, opts.beta, opts.lam1, opts.lam2, h);
    end
    if opts.save_snapshots
        save_snapshots_simple(evolution, tau, opts.times_to_save, X, Y, ...
            opts.prefix, opts.snapshot_dpi, opts.alpha, opts.beta, ...
            opts.lam1, opts.lam2, h, opts.output_dir);
    end
    if nargout == 0; clear evolution E; end
end

%% -------  Helper functions ----------------------------------------

function out = copy_fields(defaults, in)
    out = defaults;
    fn  = fieldnames(defaults);
    for k = 1:numel(fn)
        if isfield(in, fn{k}) && ~isempty(in.(fn{k}))
```


TESIS TESIS TESIS TESIS TESIS

TESIS TESIS TESIS TESIS TESIS


```
            out.(fn{k}) = in.(fn{k});
        end
    end
end

function R = round_matrix(A, threshold)
    if nargin < 2; threshold = 1e-9; end
    R = A;  R(abs(A) < threshold) = 0;
end

function E = energy_evolution(evolution, h, tau, lam1, lam2,
   alpha, beta, phi, M)
    timesteps   = numel(evolution);
    half_Halpha = H_m(M, alpha/2, h);
    half_Hbeta  = H_m(M, beta/2,  h);
    E = zeros(timesteps-1, 1);
    for l = 1:(timesteps-1)
        d_tv      = (evolution{l+1} - evolution{l})/tau;
        dx_curr   = evolution{l}   * half_Halpha;
        dx_fut    = evolution{l+1} * half_Halpha;
        dy_curr   = half_Hbeta * evolution{l};
        dy_fut    = half_Hbeta * evolution{l+1};
        E(l) = 0.5*(h^2*sum(d_tv(:).^2) + ...
               lam1*h^2*sum(dx_curr(:).*dx_fut(:)) + ...
               lam2*h^2*sum(dy_curr(:).*dy_fut(:)) + ...
               h^2*sum(phi(:).*(1-cos(evolution{l}(:)))) + ...
               h^2*sum(phi(:).*(1-cos(evolution{l+1}(:)))));
    end
end

function H = H_of_V(V, phi)
    H = phi .* cos(V) - G(V);
end

function F = Fkfunction(step, h, tau, M, a)
    x  = a + (0:M)*h;  y = a + (0:M)*h;
    [Xg, Yg] = meshgrid(x, y);
    t  = step * tau;
```


TESIS TESIS TESIS TESIS TESIS

TESIS TESIS TESIS TESIS TESIS


```
    F = round_matrix(flipud(sin(cos(pi*Xg).*cos(pi*Yg)*cos(t)).'), 1e-12);
end

function coeffs = g_l_a(alpha, l)
    coeffs    = zeros(1, l+1);
    coeffs(1) = gamma(alpha + 1) / (gamma(alpha/2 + 1)^2);
    for k = 2:(l+1)
        coeffs(k) = (1 - (alpha + 1)/(alpha/2 + (k-2) + 1)) * coeffs(k-1);
    end
end

function H = H_m(M, alpha, h)
    v    = g_l_a(alpha, M);
    v(1) = v(1)/2;
    H    = zeros(M+1);
    for i = 1:(M+1)
        H(i, i:end) = v(1:(end - i + 1));
    end
    H = (H + H.') / (-h^alpha);
end

function out = G(u)
    out = zeros(size(u));
    % Uncomment to enable: out = 0.25.*u.^4;
end

function out = Gprime(u)
    out = zeros(size(u));
    % Uncomment to enable: out = u.^3;
end

function Aout = force_zero(A, M)
    Aout        = A;
    Aout(1,:)   = 0;  Aout(M+1,:) = 0;
    Aout(:,1)   = 0;  Aout(:,M+1) = 0;
```


TESIS TESIS TESIS TESIS TESIS

TESIS TESIS TESIS TESIS TESIS


```
end

function animate_evolution(X, Y, evolution, tau, title_str, ...
        save_flag, animation_name, output_dir, alpha, beta, lam1, lam2, h)
    timesteps = numel(evolution);
    all_mins  = cellfun(@(M) min(M(:)), evolution);
    all_maxs  = cellfun(@(M) max(M(:)), evolution);
    data_min  = min(all_mins); data_max = max(all_maxs);
    fig = figure('Color','w'); ax = gca; ax.FontSize = 12;
    sh  = surf(X, Y, evolution{1}, 'EdgeColor','none');
    colormap(ax,'winter'); colorbar; clim(ax,[data_min,data_max]);
    zlim(ax,[data_min,data_max]); shading interp; view(-30,10);
    xlabel('x'); ylabel('y'); zlabel('u(x,y,t)');
    if save_flag
        if ~isfolder(output_dir); mkdir(output_dir); end
        vw = VideoWriter(fullfile(output_dir, animation_name),'MPEG-4'); open(vw);
    end
    for n = 1:timesteps
        set(sh,'ZData',evolution{n});
        title(ax, sprintf('%s t=%.3f',title_str,(n-1)*tau),'Interpreter','none');
        drawnow;
        if save_flag; writeVideo(vw, getframe(fig)); end
    end
    if save_flag; close(vw); end
end

function save_snapshots_simple(evolution, tau, times, X, Y, prefix, ...
        dpi, alpha, beta, lam1, lam2, h, output_dir)
    if ~isfolder(output_dir); mkdir(output_dir); end
    all_mins = cellfun(@(M) min(M(:)), evolution);
    all_maxs = cellfun(@(M) max(M(:)), evolution);
    dm = min(all_mins); dM = max(all_maxs);
    for k = 1:numel(times)
```


TESIS TESIS TESIS TESIS TESIS

TESIS TESIS TESIS TESIS TESIS


```
        idx = round(times(k)/tau) + 1;
        if idx < 1 || idx > numel(evolution); continue; end
        t   = (idx-1)*tau;
        fig = figure('Visible','off','Color','w');
        ax  = axes('Parent',fig);
        surf(ax,X,Y,evolution{idx},'EdgeColor','none');
        colormap(ax,'winter'); clim(ax,[dm,dM]); zlim(ax,[dm,dM]);
        shading(ax,'interp'); view(ax,-30,10);
        xlabel('x'); ylabel('y'); zlabel('u');
        title(ax,sprintf('t=%.3f',t),'Interpreter','none');
        fname = fullfile(output_dir, ...
            sprintf('%s_t%.3f_a%.2f_b%.2f.eps', ...
            prefix,t,alpha,beta));
        print(fig, fname, '-depsc', sprintf('-r%d',dpi));
        close(fig);
        fprintf('Saved: %s\n', fname);
    end
end
```


TESIS TESIS TESIS TESIS TESIS

TESIS TESIS TESIS TESIS TESIS

Bibliography

[1] A Barone, F Esposito, CJ Magee, and AC Scott. Theory and applications of the sine-gordon equation. *La Rivista del Nuovo Cimento (1971-1977)*, 1(2):227–267, 1971.

[2] Julio Rubinstein. Sine-gordon equation. *Journal of Mathematical Physics*, 11(1):258–266, 1970.

[3] JK Perring and THR138393 Skyrme. A model unified field equation. *Nuclear Physics*, 31:550–555, 1962.

[4] AV Ustinov, T Doderer, RP Huebener, NF Pedersen, B Mayer, and VA Oboznov. Dynamics of sine-gordon solitons in the annular josephson junction. *Physical review letters*, 69(12):1815, 1992.

[5] Kamyar Hosseini, P Mayeli, and D Kumar. New exact solutions of the coupled sine-gordon equations in nonlinear optics using the modified kudryashov method. *Journal of Modern Optics*, 65(3):361–364, 2018.

[6] Jonas Veenstra, Oleksandr Gamayun, Xiaofei Guo, Anahita Sarvi, Chris Ventura Meinersen, and Corentin Coulais. Non-reciprocal topological solitons in active metamaterials. *Nature*, 627(8004):528–533, 2024.

[7] Igor Podlubny. *Fractional differential equations: an introduction to fractional derivatives, fractional differential equations, to methods of their solution and some of their applications*. elsevier, 1998.

[8] Anatoliĭ Aleksandrovich Kilbas, Hari M Srivastava, and Juan J Trujillo. *Theory and applications of fractional differential equations*, volume 204. elsevier, 2006.

[9] Vasily E Tarasov. *Fractional calculus and long-range interactions*, volume 4. De Gruyter Berlin, Germany, 2019.

[10] Manuel Duarte Ortigueira. Riesz potential operators and inverses via fractional centred derivatives. *International Journal of Mathematics and Mathematical Sciences*, 2006(1):048391, 2006.

TESIS TESIS TESIS TESIS TESIS

TESIS TESIS TESIS TESIS TESIS

[11] Yanghong Huang and Adam Oberman. Numerical methods for the fractional laplacian part i: a finite difference-quadrature approach. *arXiv preprint arXiv:1311.7691*, 2013.

[12] Jorge Eduardo Macías-Díaz. A structure-preserving method for a class of nonlinear dissipative wave equations with riesz space-fractional derivatives. *Journal of Computational Physics*, 351:40–58, 2017.

[13] Jun-Ya Wang and Qiong-Ao Huang. A family of effective structure-preserving schemes with second-order accuracy for the undamped sine–gordon equation. *Computers & Mathematics with Applications*, 90:38–45, 2021.

[14] Zhiyong Xing, Liping Wen, and Wansheng Wang. An explicit fourth-order energy-preserving difference scheme for the riesz space-fractional sine–gordon equations. *Mathematics and Computers in Simulation*, 181:624–641, 2021.

[15] Tao Sun, Chengjian Zhang, and Haiwei Sun. One-parameter finite difference methods and their accelerated schemes for space-fractional sine-gordon equations with distributed delay. *J Comput Math*, 42:705–734, 2024.

[16] Junqing Jia and Xiaoyun Jiang. Improved uniform error bounds of exponential wave integrator method for long-time dynamics of the space fractional klein-gordon equation with weak nonlinearity. *Journal of Scientific Computing*, 97(3):58, 2023.

[17] Mark M Meerschaert, Jeff Mortensen, and Stephen W Wheatcraft. Fractional vector calculus for fractional advection–dispersion. *Physica A: Statistical Mechanics and its Applications*, 367:181–190, 2006.

[18] Alan C Newell. The inverse scattering transform. In *Solitons*, pages 177–242. Springer, 1980.

[19] Hesheng Hu. Soliton and differential geometry. In *Soliton Theory and Its Applications*, pages 297–336. Springer, 1995.

[20] Tassos Bountis, Julia Cantisán, Jesús Cuevas-Maraver, Jorge Eduardo Macías-Díaz, and Panayotis G Kevrekidis. On the fractional dynamics of kinks in sine-gordon models. *Mathematics*, 13(2):220, 2025.

[21] Dagoberto Mares-Rincón, Siegfried Macías, Jorge E Macías-Díaz, José A Guerrero-Díaz-de León, and Tassos Bountis. A discrete model to solve a bifractional dissipative

TESIS TESIS TESIS TESIS TESIS

TESIS TESIS TESIS TESIS TESIS

sine-gordon equation: Theoretical analysis and simulations. *Fractal and Fractional*, 9(8):498, 2025.

[22] Ahmed S Hendy, Vladimir G Pimenov, and Jorge E Macías-Díaz. Convergence and stability estimates in difference setting for time-fractional parabolic equations with functional delay. *Numerical Methods for Partial Differential Equations*, 36(1):118–132, 2020.

[23] Dumitru Baleanu, Yeliz Karaca, Luis Vázquez, and Jorge E Macías-Díaz. Advanced fractional calculus, differential equations and neural networks: Analysis, modeling and numerical computations. *Physica Scripta*, 98(11):110201, 2023.

[24] Laécio Carvalho de Barros, Michele Martins Lopes, Francielle Santo Pedro, Estevão Esmi, José Paulo Carvalho dos Santos, and Daniel Eduardo Sánchez. The memory effect on fractional calculus: an application in the spread of covid-19. *Computational and Applied Mathematics*, 40:1–21, 2021.

[25] Ivo Petráš and Ján Terpák. Fractional calculus as a simple tool for modeling and analysis of long memory process in industry. *Mathematics*, 7(6):511, 2019.

[26] David A Benson, Mark M Meerschaert, and Jordan Revielle. Fractional calculus in hydrologic modeling: A numerical perspective. *Advances in water resources*, 51:479–497, 2013.

[27] Pensri Pramukkul, Adam Svenkeson, Paolo Grigolini, Mauro Bologna, and Bruce West. Complexity and the fractional calculus. *Advances in Mathematical Physics*, 2013(1):498789, 2013.

[28] Fathi M Hafiz. The fractional calculus for some stochastic processes. *Stochastic analysis and applications*, 22(2):507–523, 2004.

[29] Nicolas L Guidotti, Juan A Acebrón, and José Monteiro. A stochastic method for solving time-fractional differential equations. *Computers & Mathematics with Applications*, 159:240–253, 2024.

[30] J Tenreiro Machado, Francesco Mainardi, and Virginia Kiryakova. Fractional calculus: Quo vadimus?(where are we going?). *Fractional Calculus and Applied Analysis*, 18(2):495–526, 2015.

[31] Kai Diethelm. A fractional calculus based model for the simulation of an outbreak of dengue fever. *Nonlinear Dynamics*, 71:613–619, 2013.

TESIS TESIS TESIS TESIS TESIS

TESIS TESIS TESIS TESIS TESIS

[32] Jovan K Popović, Milica T Atanacković, Ana S Pilipović, Milan R Rapaić, Stevan Pilipović, and Teodor M Atanacković. A new approach to the compartmental analysis in pharmacokinetics: fractional time evolution of diclofenac. *Journal of pharmacokinetics and pharmacodynamics*, 37:119–134, 2010.

[33] Rasiel Toledo-Hernandez, Vicente Rico-Ramirez, Gustavo A Iglesias-Silva, and Urmila M Diwekar. A fractional calculus approach to the dynamic optimization of biological reactive systems. part i: Fractional models for biological reactions. *Chemical Engineering Science*, 117:217–228, 2014.

[34] Jiecheng Chen, Lingwei Gong, and Ruifan Meng. Application of fractional calculus in predicting the temperature-dependent creep behavior of concrete. *Fractal and Fractional*, 8(8):482, 2024.

[35] Michele Caputo and Mauro Fabrizio. Damage and fatigue described by a fractional derivative model. *Journal of Computational Physics*, 293:400–408, 2015.

[36] Vaughan R Voller, Federico Falcini, and Roberto Garra. Fractional stefan problems exhibiting lumped and distributed latent-heat memory effects. *Physical Review E—Statistical, Nonlinear, and Soft Matter Physics*, 87(4):042401, 2013.

[37] Johnson J GadElkarim, Richard L Magin, Mark M Meerschaert, Silvia Capuani, Marco Palombo, Anand Kumar, and Alex D Leow. Fractional order generalization of anomalous diffusion as a multidimensional extension of the transmission line equation. *IEEE journal on emerging and selected topics in circuits and systems*, 3(3):432–441, 2013.

[38] Roberto Garra, Enzo Orsingher, and Federico Polito. Fractional klein–gordon equations and related stochastic processes. *Journal of Statistical Physics*, 155(4):777–809, 2014.

[39] Briceyda B Delgado and Jorge E Macías-Díaz. On the general solutions of some non-homogeneous div-curl systems with riemann–liouville and caputo fractional derivatives. *Fractal and fractional*, 5(3):117, 2021.

[40] Sami I Muslih, Om P Agrawal, and Dumitru Baleanu. A fractional schrödinger equation and its solution. *International Journal of Theoretical Physics*, 49:1746–1752, 2010.

[41] Berat Karaagac. A study on fractional klein gordon equation with non-local and non-singular kernel. *Chaos, Solitons & Fractals*, 126:218–229, 2019.

TESIS TESIS TESIS TESIS TESIS

TESIS TESIS TESIS TESIS TESIS

[42] Francesco Mainardi and Gianni Pagnini. The wright functions as solutions of the time-fractional diffusion equation. *Applied Mathematics and Computation*, 141(1):51–62, 2003.

[43] Anatoly A Alikhanov. A new difference scheme for the time fractional diffusion equation. *Journal of Computational Physics*, 280:424–438, 2015.

[44] Pietro Bia, Diego Caratelli, Luciano Mescia, Renato Cicchetti, Guido Maione, and F Prudenzano. A novel fdtd formulation based on fractional derivatives for dispersive havriliak–negami media. *Signal Processing*, 107:312–318, 2015.

[45] VO Bohaienko. A fast finite-difference algorithm for solving space-fractional filtration equation with a generalised caputo derivative. *Computational and Applied Mathematics*, 38(3):105, 2019.

[46] Yang Zhang. A finite difference method for fractional partial differential equation. *Applied Mathematics and Computation*, 215(2):524–529, 2009.

[47] Lijing Zhao, Weihua Deng, and Jan S Hesthaven. Spectral methods for tempered fractional differential equations. *Mathematics of Computation*, 2016.

[48] Mohsen Zayernouri and George Em Karniadakis. Exponentially accurate spectral and spectral element methods for fractional odes. *Journal of Computational Physics*, 257:460–480, 2014.

[49] Eid H Doha, Ali H Bhrawy, and SS Ezz-Eldien. Efficient chebyshev spectral methods for solving multi-term fractional orders differential equations. *Applied Mathematical Modelling*, 35(12):5662–5672, 2011.

[50] Hassan Khosravian-Arab, Mehdi Dehghan, and MR Eslahchi. Fractional spectral and pseudo-spectral methods in unbounded domains: Theory and applications. *Journal of Computational Physics*, 338:527–566, 2017.

[51] Om P Agrawal. A general finite element formulation for fractional variational problems. *Journal of Mathematical Analysis and Applications*, 337(1):1–12, 2008.

[52] Guang-an Zou. A galerkin finite element method for time-fractional stochastic heat equation. *Computers & Mathematics with Applications*, 75(11):4135–4150, 2018.

[53] Meng Li, Chengming Huang, and Pengde Wang. Galerkin finite element method for nonlinear fractional schrödinger equations. *Numerical Algorithms*, 74:499–525, 2017.

TESIS TESIS TESIS TESIS TESIS

TESIS TESIS TESIS TESIS TESIS

[54] Meng Li and Yong-Liang Zhao. A fast energy conserving finite element method for the nonlinear fractional schrödinger equation with wave operator. *Applied Mathematics and Computation*, 338:758–773, 2018.

[55] Weihua Deng. Finite element method for the space and time fractional fokker–planck equation. *SIAM journal on numerical analysis*, 47(1):204–226, 2009.

[56] Ryu Sasaki and Itaru Yamanaka. Virasoro algebra, vertex operators, quantum sine-gordon and solvable quantum field theories. *Advanced studies in pure mathematics*, 16:271, 1988.

[57] Olalla A Castro-Alvaredo. Bootstrap methods in 1+ 1-dimensional quantum field theories: The homogeneous sine-gordon models. *arXiv preprint hep-th/0109212*, 2001.

[58] Georgy Alfimov, VM Eleonsky, and LM Lerman. Solitary wave solutions of nonlocal sine-gordon equations. *Chaos: An Interdisciplinary Journal of Nonlinear Science*, 8(1):257–271, 1998.

[59] Zhiyong Xing and Liping Wen. A conservative difference scheme for the riesz space-fractional sine-gordon equation. *Advances in Difference Equations*, 2018(1):238, 2018.

[60] K Djidjeli, WG Price, and EH Twizell. Numerical solutions of a damped sine-gordon equation in two space variables. *Journal of Engineering Mathematics*, 29(4):347–369, 1995.

[61] Nick Laskin. Fractional schrödinger equation. *Physical Review E*, 66(5):056108, 2002.

[62] Kuo Pen-Yu. Numerical methods for incompressible viscous flow. *Scientia sinica*, 20:287–304, 1977.

[63] Zohreh Asgari and S Mohammed Hosseini. Numerical solution of two-dimensional sine-gordon and mbe models using fourier spectral and high order explicit time stepping methods. *Computer Physics Communications*, 184(3):565–572, 2013.

[64] Ram Jiwari, Sapna Pandit, and RC Mittal. Numerical simulation of two-dimensional sine-gordon solitons by differential quadrature method. *Computer Physics Communications*, 183(3):600–616, 2012.

TESIS TESIS TESIS TESIS TESIS

TESIS TESIS TESIS TESIS TESIS

[65] Mehdi Dehghan and Ali Shokri. A numerical method for solution of the two-dimensional sine-gordon equation using the radial basis functions. *Mathematics and Computers in Simulation*, 79(3):700–715, 2008.

[66] Ahmed S Hendy and Jorge E Macías-Díaz. An efficient hamiltonian numerical model for a fractional klein–gordon equation through weighted-shifted grünwald differences. *Journal of Mathematical Chemistry*, 57(5):1394–1412, 2019.

[67] Vasily E Tarasov. On history of mathematical economics: Application of fractional calculus. *Mathematics*, 7(6):509, 2019.

[68] Yu Luchko. A new fractional calculus model for the two-dimensional anomalous diffusion and its analysis. *Mathematical Modelling of Natural Phenomena*, 11(3):1–17, 2016.

[69] FC Meral, TJ Royston, and R Magin. Fractional calculus in viscoelasticity: an experimental study. *Communications in nonlinear science and numerical simulation*, 15(4):939–945, 2010.

[70] Diego del Castillo-Negrete. Fractional diffusion models of anomalous transport. *Anomalous Transport*, pages 163–212, 2008.

[71] Ahmad Neirameh. New fractional calculus and application to the fractional-order of extended biological population model. *Boletim da Sociedade Paranaense de Matemática*, 36(3):115–128, 2018.

[72] Sebastian Raubitzek, Kevin Mallinger, and Thomas Neubauer. Combining fractional derivatives and machine learning: A review. *Entropy*, 25(1):35, 2022.

[73] E Viera-Martin, JF Gómez-Aguilar, JE Solís-Pérez, JA Hernández-Pérez, and RF Escobar-Jiménez. Artificial neural networks: a practical review of applications involving fractional calculus. *The European Physical Journal Special Topics*, 231(10):2059–2095, 2022.

[74] Guo Huang, Hong-ying Qin, Qingli Chen, Zhanzhan Shi, Shan Jiang, and Chenying Huang. Research on application of fractional calculus operator in image underlying processing. *Fractal and Fractional*, 8(1):37, 2024.

[75] Ervin K Lenzi, Luiz R Evangelista, Haroldo V Ribeiro, and Richard L Magin. Schrödinger equation with geometric constraints and position-dependent mass: Linked fractional calculus models. *Quantum Reports*, 4(3):296–308, 2022.

TESIS TESIS TESIS TESIS TESIS

TESIS TESIS TESIS TESIS TESIS

[76] Mallanagoud Mulimani and S Kumbinarasaiah. A numerical study on the nonlinear fractional klein–gordon equation. *Journal of Umm Al-Qura University for Applied Sciences*, 10(1):178–199, 2024.

[77] Othman Abdullah Almatroud, Amel Hioual, Adel Ouannas, and Giuseppe Grassi. On fractional-order discrete-time reaction diffusion systems. *Mathematics*, 11(11):2447, 2023.

[78] Shuo Li, Sami Ullah Khan, Muhammad Bilal Riaz, Salman A AlQahtani, and Atif M Alamri. Numerical simulation of a fractional stochastic delay differential equations using spectral scheme: A comprehensive stability analysis. *Scientific Reports*, 14(1):6930, 2024.

[79] Avinash K Mittal, Lokendra K Balyan, Manoj K Panda, Parnika Shrivastava, and Harvindra Singh. Pseudospectral analysis and approximation of two-dimensional fractional cable equation. *Mathematical Methods in the Applied Sciences*, 45(14):8613–8630, 2022.

[80] Muhammad Bilal Hafeez and Marek Krawczuk. Fractional spectral and fractional finite element methods: a comprehensive review and future prospects. *Archives of Computational Methods in Engineering*, 31(6):3443–3454, 2024.

[81] Yixuan Wu and Yanzhi Zhang. Variable-order fractional laplacian and its accurate and efficient computations with meshfree methods. *Journal of Scientific Computing*, 99(1):18, 2024.

[82] Mostafa Abbaszadeh, AliReza Bagheri Salec, and Alaa Salim Jebur. Integrated radial basis function technique to simulate the nonlinear system of time fractional distributed-order diffusion equation with graded time-mesh discretization. *Engineering Analysis with Boundary Elements*, 156:57–69, 2023.

[83] Salwa A Mohamed. A fractional differential quadrature method for fractional differential equations and fractional eigenvalue problems. *Mathematical Methods in the Applied Sciences*, 47(13):10995–11018, 2024.

[84] Jesús Cuevas-Maraver, Panayotis G Kevrekidis, and Floyd Williams. The sine-gordon model and its applications. *Nonlinear systems and complexity*, 10, 2014.

[85] Shinya Watanabe, Herre SJ van der Zant, Steven H Strogatz, and Terry P Orlando. Dynamics of circular arrays of josephson junctions and the discrete sine-gordon equation. *Physica D: Nonlinear Phenomena*, 97(4):429–470, 1996.

TESIS TESIS TESIS TESIS TESIS

TESIS TESIS TESIS TESIS TESIS

[86] G Costabile, RD Parmentier, B Savo, DW McLaughlin, and AC Scott. Exact solutions of the sine-gordon equation describing oscillations in a long (but finite) josephson junction. *Applied Physics Letters*, 32(9):587–589, 1978.

[87] Chong Hou, Lili Bu, Fabio Baronio, Dumitru Mihalache, Shihua Chen, et al. Sine-gordon breathers and formation of extreme waves in self-induced transparency media. *Romanian Reports in Physics*, 72(1), 2020.

[88] Alberto Bonicelli, Claudio Dappiaggi, and Paolo Rinaldi. On the stochastic sine-gordon model: an interacting field theory approach. *Communications in Mathematical Physics*, 405(12):288, 2024.

[89] PJ Caudrey, JC Eilbeck, and JD Gibbon. The sine-gordon equation as a model classical field theory. *Il Nuovo Cimento B (1971-1996)*, 25(2):497–512, 1975.

[90] RK Dodd and RK Bullough. Bäcklund transformations for the sine–gordon equations. *Proceedings of the Royal Society of London. A. Mathematical and Physical Sciences*, 351(1667):499–523, 1976.

[91] Jonas Veenstra, Oleksandr Gamayun, Xiaofei Guo, Anahita Sarvi, Chris Ventura Meinersen, and Corentin Coulais. Non-reciprocal topological solitons. *arXiv preprint arXiv:2312.03544*, 2023.

[92] Rudolf Hilfer et al. Threefold introduction to fractional derivatives. *Anomalous transport: Foundations and applications*, pages 17–73, 2008.

[93] Kuo Pen-Yu. Numerical methods for incompressible viscous flow. *Scientia sinica*, 20:287–304, 1977.

TESIS TESIS TESIS TESIS TESIS